Techno-economical evaluation of domestic water heating technologies

C.W. Botes

orcid.org/0000-0003-1153-4457

Dissertation accepted in fulfilment of the requirements for the degree *Master of Engineering in Mechanical Engineering* at the North-West University

Supervisor: Dr. Willem van Niekerk

Co-supervisor: Prof. Martin van Eldik

Graduation: June 2021

Student number: 24927554

ACKNOWLEDGEMENTS

Firstly, I would like to acknowledge my supervisors, Dr. Willem van Niekerk and Prof. Martin van Eldik. Thank you for your exceptional guidance, never ending wisdom and patience. Thank you for always walking the extra mile while leading me through my dissertation. Thank you for all the experience and life lesson learned along the way.

Secondly, I would like to acknowledge my father Henk, my mother Ida and my brother Jaco. Mom and Dad, without you this would not have been possible. Thank you for always believing in me and supporting me, not only through my dissertation, but during all my years of study. During hard times, I would always call my Mom and she would calmly say: "it's okay, just try again tomorrow." I will never be able to thank Mom enough for those words. Jaco, thank you for your exceptional example as an older brother. Thank you for pushing me further than I would have ever been able to myself. I love you all.

Lastly, I would like to acknowledge my best friend Heinie. Thank you for being someone I can discuss anything with, without fear of judgement. Thank you for all your advice and support. Thank you for every cup of coffee on the porch, every braai and every Left for Dead game. You will forever be roommate number 1.

ABSTRACT

Water heating accounts for up to 40% of the total energy consumption in an average residential household. With the drastic rise in electricity prices over the last decade, the use of renewable and alternative methods of water heating has become all the more attractive and cost effective over the years. There is a number of different renewable and alternative domestic water heating technologies available to consumers, but it is unclear which technology is the most cost effective.

In this study, four different domestic water heating technologies were evaluated, namely: (a) solar photovoltaic, (b) solar thermal, (c) heat pump and (d) gas water heating. These water heating technologies were compared against the baseline electric resistance water heater. The technologies were compared in terms of their ability to supply hot water when required and the cost effectiveness in doing so.

In order to determine the cost effectiveness of the four technologies, a system level mathematical model was developed for each water heating technology. The models made use of data from a climatic design year and a normalised hot water consumption profile. The solar photovoltaic model includes an experimentally validated simulation model. The photovoltaic simulation model uses solar radiation data to determine the power output of a PV module, based on its characteristics. The solar thermal and heat pump water heating mathematical models respectively incorporates system specifications provided by reputable suppliers. The gas water heating model was verified against experimental work which determined the water heater efficiency. In order to ensure the supply of hot water, a conventional hot water cylinder with an electric resistance heater was included in each model. A retrofit approach was assumed from a cost perspective. In order to calculate the installation cost, it was thus assumed that the hot water cylinder was already installed and only the cost of adding the specific technology was considered. Quotations were requested from reputable South African suppliers in order to determine the capital cost of each retrofitted water heating system. Significant differences were noted in the capital cost given by various suppliers for the same technology.

For each water heating technology, the yearly amount of electrical energy required from the utility grid was determined. By comparing the different technologies to a conventional hot water cylinder with a resistive element, supplying the same amount of hot water, the following was calculated: (i) simple payback period, (ii) annual operational costs, (iii) annual savings and (iv) the percentage grid input saved by each technology.

For the case study it was found that the flat plate solar thermal water heater has the shortest payback period of 3.8 years, followed by the heat pump at 4.7 years. The solar photovoltaic

system also had a payback period of 4.7 years and the evacuated tube solar thermal water heater has the longest payback period of 4.8 years. Gas water heating had no payback period. The annual operational costs of the heat pump water heater were the lowest at R2879 per household, followed by solar photovoltaic at R2922, evacuated tube solar thermal at R3327, flat plate solar thermal at R3357 and gas water heating at R8674. Gas water heating was found to be more expensive than the baseline electric resistance water heater at R7933.

It was also found that in terms of the amount of grid input saved, gas water heating as applied in this study, outperformed the other water heating technologies with a total yearly grid input saved of 99.7%. This is followed by the heat pump at 63.7%, solar photovoltaic at 63.2% and the evacuated tube and flat plate solar thermal respectively at 58.1% and 57.7% grid input saved.

The following was found in terms of the ability of each water heating technology to provide hot water. The solar driven technologies alone cannot provide hot water during early morning hours. The hot water availability of a heat pump water heater equals that of the conventional hot water cylinder with electric resistive heating, although both are grid dependent. Lastly, gas water heating can supply hot water at all times.

From this study the following conclusions were reached. Firstly, if the lowest initial capital investment is the decisive factor, a flat plate solar thermal water heater is the best solution. Flat plate solar thermal is also the best solution if the shortest payback period is the decisive factor. Secondly, if the annual operational costs of water heating are considered the decisive factor, a heat pump water heater is the best solution, followed very closely by a solar photovoltaic system. Both of these water heating technologies delivered the lowest annual operational costs, generating the highest annual savings relative to the baseline. Lastly, gas water heating saved the greatest percentage of grid input required by the baseline. The most effective grid independent water heating solution would be the conventional tankless application of gas water heating.

It is important to note that the following conclusions can only be drawn on the specific water heating systems evaluated in this study. For example, it was concluded that the flat plate solar thermal water heater had the shortest payback period. Although this is true for the specific systems evaluated in this study, the finding cannot be generalized for all solar thermal water heaters.

Keywords: domestic water heating; solar photovoltaic: solar thermal; heat pump; gas; simulation, mathematical modelling, performance, operational costs, payback period.

TABLE OF CONTENTS

LIST OF FIGURES

LIST OF TABLES

LIST OF EQUATIONS

LIST OF ABBREVIATIONS

AC	Alternating current
ANN	Artificial neural network
COP	Coefficient of performance
DC	Direct current
EES	Engineering Equation Solver
EF	Energy factor
EWH	Electric water heating
GWH	Gas water heating
HPWH	Heat pump water heating
IBT	Inclining block rate tariff
IV	Current-voltage
LPG	Liquefied petroleum gas
MPP	Maximum power point
MPPT	Maximum power point tracking
NERSA	National Energy Regulator of South Africa
PV	Photovoltaic / Power-voltage
PVWH	Photovoltaic water heating
REIPPPP	Renewable Energy Independent Power Producer Procurement Programme
SPP	Simple payback period
STC	Standard test conditions
STWH	Solar thermal water heating

LIST OF SYMBOLS

β	Tilt angle
δ	Declination angle of the sun
ΔT_{AUX}	Change in temperature due to the auxiliary grid input
ΔT_{LOSS}	Change in temperature due to the standing loss
$\Delta T_{\dot{m}}$	Change in temperature due to consumption
ΔT_{PV}	Change in temperature due to the input of the PV generated energy
ΔT_{U}	Change in temperature due to the input of the useful thermal energy
$\frac{dI}{dV}_{SC}$	Slope of the curve at short circuit
$\frac{dI}{dV}_{OC}$	Slope of the curve at open circuit
η	Efficiency
ϕ	Latitude
ω	Hour angle of the sun
A_{AC}	AC ampere in PV experiment
A_{c}	Aperture area of solar collector
A_{DC}	DC ampere in PV experiment
c_{p}	Specific heat of water
E_{AUX}	Heating capacity of electric water heater
$E_{COMBUSTION}$	Thermal energy generated by the combustion of the fuel gas in the GWH experiment
E_{ENVIR}	Heat lost to the environment in the GWH experiment
E_{ET}	Evacuated tube auxiliary grid energy required

E_{EWH}	EWH grid energy required
E_{FP}	Flat plate auxiliary grid energy required
E_{GRID}	Energy supplied by utility grid in PV experiment
E_{GWH}	GWH auxiliary grid energy required
E_{HP}	Electrical energy utilized by the heat pump water heater
E_{HPWH}	HPWH auxiliary grid energy required
E_{IN}	Sum of energy supplied to system in PV experiment
E_{LOSS}	Energy lost in PV experiment
$E_{OFF-GAS}$	Heat lost in the off-gas of the combustion process in the GWH experiment
E_{OUT}	Sum of energy delivered by system in PV experiment
E_{PUMP}	Electrical energy utilized by the circulation pump
E_{PV}	Energy supplied by PV system in PV experiment / Electrical energy generated by the PV array in mathematical model
E_{PVWH}	PVWH auxiliary grid energy required
$E_{REQUIRED}$	Yearly electrical energy required by GWH circulation pump
E_{WATER}	Energy transferred to the water in PV & GWH experiment
G	Solar irradiance
G_{NOM}	Solar irradiance at STC
G_{VAR}	Arbitrary solar irradiance
HHV	Higher heating value
H_P	Enthalpy of the products
H_R	Enthalpy of the reactants
i	Current hour / Step value

I	External current
I_0	Reserve saturation current
i-1	Previous hour
I_{AC}	Current drawn by air-supply fan in GWH experiment
I_D	Diode current
I_{INT}	Intersect current
I_{MP}	Maximum power current
I_{PV}	Photogenerated current / Photocurrent
I_{REST}	Portion of external current equation
I_{SC}	Short circuit current
I_{SC_STC}	Short circuit current at STC
I_{SH}	Shunt current
k	Boltzmann constant
K_I	Current temperature coefficient
K_V	Voltage temperature coefficient
L	Flow rate of hot water in PV experiment
$\dot{m}$	Water flow rate recorded in GWH experiment
m_{gas}	Amount of fuel gas
mS_{water}	Hot water consumption during summer months
mW_{water}	Hot water consumption during winter months
n	Day of the year / Diode ideality factor
N_S	Number of cells connected in series
P_{cp}	Nominal pump power

P_{FAN}	Power used by the air-supply fan
P_{INT}	Intersect power
P_M	Maximum power
P_{SI}	Simulated power generated by the PV array
q	Electron charge
$Q_{COMBUSTION}$	Thermal energy generated by the combustion of the fuel gas
Q_{INPUT}	Thermal combustion energy that must be delivered in order to heat the water and compensate for the standing loss in GWH
Q_{LOSS}	Standing loss of electric water heater
$Q_{OFF\text{-}GAS}$	Heat lost in the off-gas of the combustion process
$Q_{REQUIRED}$	Yearly Auxiliary / electrical grid energy required
Q_U	Useful thermal energy generated by the solar collector
Q_{WATER}	Thermal energy required to heat the water
R	Resistance / Load
R_b	Ratio of radiation on a tilted surface to that of a horizontal surface
$R_{capital}$	Capital cost of the retrofitted system, including installation and VAT
R_{EWH}	Yearly EWH operational costs
R_{GWH}	Yearly GWH operational costs
R_{HPWH}	Yearly HPWH operational costs
R_{kWh}	Cost of electricity
R_{LPG}	Cost of LPG
R_{PVWH}	Yearly PVWH operational costs
R_S	Series resistance

R_{saved}	Annual savings of each water heating technology relative to the baseline
R_{SH}	Shunt resistance
R_{STWH}	Yearly STWH operational costs
SI	Solar irradiance
ST	Local solar time
T	Cell temperature
T_a / Ta	Ambient temperature
Tc_{in}	Temperature of solar collector inlet water
Tc_{out}	Temperature of solar collector outlet water
T_{ENVIR}	Environmental temperature in PV experiment
T_{IN}	Cold water temperature in PV experiment
T_{inlet}	Inlet water temperature
T_m	Average solar collector temperature
T_{NOM}	Cell temperature at STC
T_{OUT}	Hot water temperature in PV experiment
Tt	Average tank temperature
Tt_0	Initial tank temperature
Tt_i	Tank temperature at hour i
Tt_{i-1}	Tank temperature at hour i-1
V	External voltage
V_{AC}	Single-phase utility voltage
V_D	Diode voltage
V_{DC}	DC Volts supplied by PV in PV experiment

Vi	Volume consumed/added to tank at hour i
V_{INT}	Intersect voltage
V_{MP}	Maximum power voltage
V_{OC}	Open circuit voltage
V_{OC_STC}	Open circuit voltage at STC
Vt	Volume of water storage tank
V_T	Thermal voltage
X	Solar collector efficiency factor

LIST OF UNITS

A	Ampere
°	Angular degrees
m^3	Cubic meter
°C	Degrees Celsius
h	Hour
K	Kelvin
kg	Kilogram
kJ	Kilojoule
kW	Kilowatt
kWh	Kilowatt hour
L	Litre
MJ	Megajoule
m^2	Meter squared
min	Minute
Ω	Ohm
%	Percentage
R	Rand
V	Voltage
W	Watt

CHAPTER 1 – INTRODUCTION

1.1 Background

South Africa experienced the first of a series of power outages and load-shedding between November 2007 and January 2008. This was due to a shortage in generating capacity at Eskom, the national supplier of electricity (Deloitte Consulting Pty (Ltd), 2017:15).

In the late 1970's, Eskom overinvested in a massive capacity expansion programme, which led to a substantial surplus in supply (Deloitte Consulting Pty (Ltd), 2017:39). The surplus motivated a temporary standstill in future capacity expansion programmes and caused the below real cost pricing of electricity in order to stimulate demand. The price of electricity in South Africa has always been influenced by the political priorities of the government and the price thereof seldom reflected the true economic cost of supply. Electricity was being sold at a cost that did not reflect the marginal cost of supply and which did not include capital maintenance cost. The government had also been subsidizing the cost of electricity since the 1980's. The price of electricity therefore gradually declined to artificially low levels between 1983 and 2000, stabilized in 2001 to be among the lowest in the world (Deloitte Consulting Pty (Ltd), 2017:39).

As the electricity tariff remained relatively stable between 2001 and 2008, the total consumption of the residential sector rose from 16% in 1993 to 20% in 2013 (Deloitte Consulting Pty (Ltd), 2017:20). This was mainly due to the household electrification programme launched by the Department of Energy and Eskom, which added 5.7 million residential grid connections between 1994 and 2013 (Deloitte Consulting Pty (Ltd), 2017:20).

A steady rise in consumption coupled with a temporary standstill in capacity expansion, led to a capacity shortage that had been threatening to emerge for some time. In 2002, the reserve margin of generation capacity was at 25% (NERSA, 2008:3). It reached 16% in 2006 and in 2008 it was only at 8-10% of peak demand (NERSA, 2008:3). After lengthy political delay, the go-ahead was given for an investment programme to increase power generation capacity in 2008 (Deloitte Consulting Pty (Ltd), 2017:39). Eskom was however unable to finance the new programme due to historical low tariffs and inadequate revenue (Deloitte Consulting Pty (Ltd), 2017:15). In order to help finance the new programme, the National Energy Regulator of South Africa (NERSA) approved an increase of annual tariffs. Between 2008 and 2013, electricity prices more than doubled in real terms, rising by 114% (Deloitte Consulting Pty (Ltd), 2017:39).

In order to alleviate the demand for power on the national grid, Eskom introduced a number of renewable water heating rebate programmes. These programmes included: the solar home system programme in 1999, the national solar water heating rebate programme in 2010 and the residential heat pump rebate programme in 2011. The Renewable Energy Independent Power Producer Procurement Programme (REIPPPP) was also introduced in 2011 to strengthen the national grid supply with alternative renewable generated energy, which included large scale solar photovoltaic power generation (Jain & Jain, 2017:723).

Water heating accounts for up to 40% of the total energy consumption in an average residential household (Hohne et al., 2019:1). The resistance electric water heater is the most commonly used heater in South Africa due to their high system efficiency and easy implementation (Hohne et al., 2019:2). A water heating system that is only dependent on grid electricity is vulnerable to load shedding and is getting more expensive to operate with the current trends in electricity tariffs. The use of renewable and alternative methods of water heating has thus become more attractive and cost effective over the years. These methods include: solar photovoltaic, solar thermal, heat pump and gas water heating. Solar photovoltaic and solar thermal water heating uses renewable irradiation energy. Although a heat pump water heater is powered by electricity, it is still classified as renewable due the fact that it extracts the majority of its useful thermal energy from the ambient air (Tangwe et al., 2014:204). Gas water heating is an alternative method, as it is primarily achieved using liquefied petroleum gas and is not renewable.

The renewable water heating technologies are all dependent on solar irradiation. Figure 1.1 below details the daily global horizontal irradiation in South Africa.

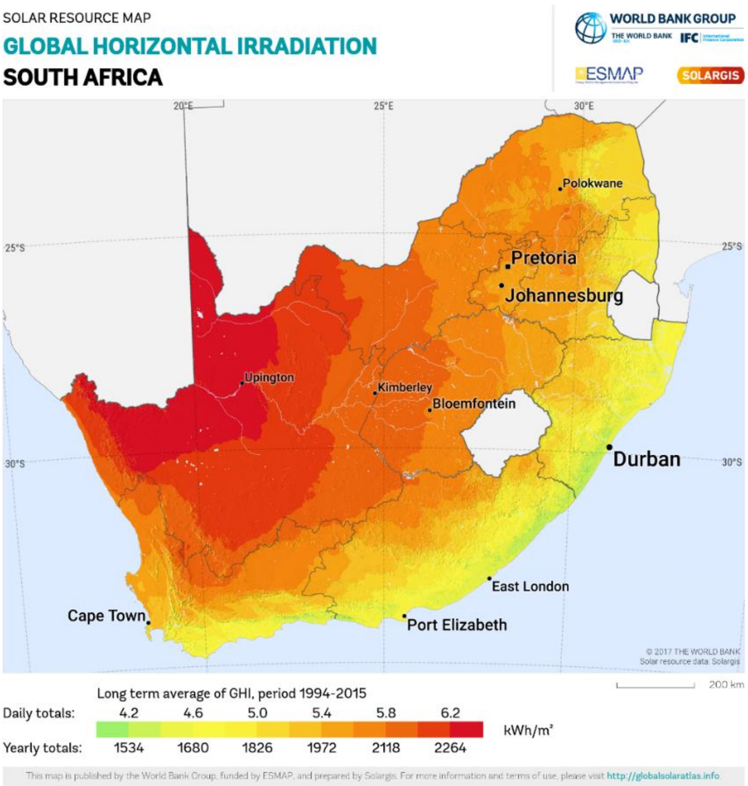

Figure 1.1: Global horizontal irradiation of South Africa (© 2019 The World Bank, Source: Global Solar Atlas 2.0, Solar resource data: Solargis)

The solar recourse map indicates that South Africa has an abundance of solar irradiation, with a daily global horizontal irradiation average raging between 4.2-6.2kWh/m^2 (Solargis, 2019). This correlates to a global irradiation average of 220W/m^2 in South Africa, compared to approximately 150W/m^2 in the United States and 100W/m^2 in Europe (Department of Renewable Energy, 2020). There is thus great potential for solar dependent renewable water heating technologies in South Africa.

1.2 Problem statement

There is a number of alternative and renewable domestic water heating technologies available and it is unclear which technology is the most cost effective when being compared on an equal footing. The cost effectiveness, as well as the ability to supply hot water when required, of the different technologies has not been systematically investigated for South African conditions.

1.3 Purpose of the study

The purpose of the study is to develop a mathematical model that will compare the cost effectiveness of the chosen domestic water heating technologies, in providing hot water when required, over a typical climatic year.

1.4 Scope

The study will focus on four domestic water heating technologies, namely: (a) solar photovoltaic, (b) solar thermal, (c) heat pump and (d) gas water heating. Each application will incorporate a standard hot water cylinder with a conventional electric resistance heater, which will act as a backup heater and hot water storage unit. This will ensure that hot water (in the case of solar technologies) is at least available early in the mornings before sunrise and late in the afternoon at sunset if the renewable energies prove insufficient. The water storage unit also ensures that system losses are equal for each water heating system. Also, in the case of gas water heating, it became clear from literature that the efficiency of gas water heating is significantly lower when small amounts of hot water is consumed at a time. This is due to transient heating effects. Therefore, a hot water cylinder was included to ensure that the gas water heater could run for longer periods of time. The water heating systems will be compared in terms of their cost effectiveness over a typical climatic year in Johannesburg, South Africa. The comparison will be done for a residential household containing four people.

Each water heating technology will be individually discussed. Solar photovoltaic water heating will be studied in noticeably more detail when compared to the other technologies. The reason therefore will be motivated in its introduction. Each chapter will entail a literature study and mathematical model of its respective technology. Solar photovoltaic and gas water heating will be experimentally tested. System specifications will be obtained from reputable suppliers respectively for solar thermal and heat pump water heating. The system size required for each technology will be applied as proposed by the supplier. Model input data will consist of data from a typical climatic design year and a normalised hot water consumption profile. The consumption profile will also not be optimized for each technology. The same input parameters will be applied to each technology, ensuring comparison on an equal footing. The techno-economical study will be concluded with a side-by-side comparison of the simple payback period, annual operational costs, annual savings and performance of each water heating technology relative to the baseline.

1.5 Method

The method section will discuss the approach followed in the literature study and development of the mathematical model of each technology. Similarities between the mathematical models of the different technologies will also be discussed in the modelling approach subsection to follow.

The literature study will be introduced with the working principles of the water heating technology as it is applied in this study. The study will only focus on literature that is most relevant to the given application of the water heating technology. The energy balance method will be applied to mathematically model the water heating technology, represented as a black-box. The black-box model approaches a system in terms of its inputs and outputs, without focussing on its internal components and workings. Modelling will thus be done on a system level and not component level. The mathematical model will be used to predict the performance and annual operational costs of the water heating technology. The photovoltaic water heating chapter will include a solar photovoltaic power generation simulation. Mathematical modelling will be conducted in the Microsoft Excel environment. The solar photovoltaic simulation will be modelled in the MATLAB environment. Lastly, the experimental methods of solar photovoltaic and gas water heating will be discussed in their respective chapters.

1.6 Modelling approach

As stated in the scope, identical input data will be used in the mathematical model of each respective water heating technology. In order to avoid unnecessary repetition per chapter, the input parameters will be listed and discussed in this section. Note that any changes made to this given modelling approach will be discussed in the respective chapter.

1.6.1 Climatic design year data

The climatic design year data chosen was that of Johannesburg, coordinates 26°20’S; 28°04’E (van Deventer, 1971). Johannesburg falls within the intermediate range of irradiation available in South Africa, as was shown in Figure 1.1. A section of the climatic design year data is listed in Table 1.1 below.

Table 1.1: Section of climatic design year data

Month	Day	Hour	Total radiation (W/m^2)	Dry bulb ambient temperature (°C)
3	26	11	690	20.6
3	26	12	700	21.6
3	26	13	870	22.5
3	26	14	880	23.4
3	26	15	650	23.9
3	26	16	530	23.9
3	26	17	290	22.9
3	26	18	90	22.1
3	26	19	10	20.9
3	26	20	0	20.7
3	26	21	0	20
3	26	22	0	19.5
3	26	23	0	17.1
3	26	24	0	17.1
3	27	1	0	14.1
3	27	2	0	13.1

As indicated by the first row of Table 1.1, the data used consists of hourly weather data for the total radiation and the dry bulb ambient temperature. Humidity, wet bulb and wind velocity was also supplied in the data. It is simply not listed in Table 1.1, as it was not applied in this study. The total radiation will be applied as the climatic input for solar photovoltaic and solar thermal water heating. The dry bulb ambient temperature will be applied as the climatic input data for heat pump water heating.

1.6.2 Orientation and tilt angle of the photovoltaic panel and thermal collector

The orientation and tilt angle of a photovoltaic panel and solar collector has a significant effect on the amount of solar irradiation it can absorb (Hohne et al., 2019:4). The general practice is to permanently fix the tilt angle at the optimal angle during winter conditions, ensuring maximum water heating capability in the colder months of the year (Hohne et al., 2019:4). In this study the photovoltaic panel and solar collector will be modelled in a due north orientation, at the latitude of Johannesburg, at a fixed tilt angle equal to the latitude plus 10 degrees. Page-Shipp (1980:2) has referenced this orientation and tilt angle setup as optimal for yearly efficiency.

The total radiation of the climatic design year data was measured on a horizontal surface. The theory on the ratio of radiation on a tilted surface to that of a horizontal surface by Duffie and Beckman (2013:23) was applied in order to determine the total tilted radiation. This ratio R_b for an orientation due north in the southern hemisphere is referenced from Duffie and Beckman (2013:24) as:

$$R_b = \frac{\cos(\phi+\beta)\cos\delta\cos\omega + \sin(\phi+\beta)\sin\delta}{\cos\phi\cos\delta\cos\omega + \sin\phi\sin\delta} \tag{1.1}$$

The angles ϕ, β, δ, and ω refer to geometric relationships between the plane in question, the earth and incoming solar irradiation from the sun (Duffie and Beckman, 2013:12). ϕ represents the latitude, β the tilt angle measured from horizontal, δ the declination and ω the hour angle. The declination is the angle of the sun relative to the equator and is given by Equation (1.2) below.

$$\delta = 23.45\sin\left(\frac{360}{365}(284+n)\right) \tag{1.2}$$

Depending on the day of the year n, the declination angle lies between $-23.45^\circ \leq \delta \leq 23.45^\circ$. The hour angle represents the angular position of the sun, east or west of the local meridian. The hour angle is caused by the rotation of the earth around its polar axis at 15° per hour and is given by Equation (1.3) below (Maleki et al., 2017:3).

$$\omega = 15^{\circ}(12 - ST) \quad (1.3)$$

ST is the local solar time and is dependent on the local standard time, standard local meridian and longitude of the location. The local solar time is only a few minutes different than the standard local time and for the purpose of this study it was assumed to be equal to the standard local time.

The ratio is only applied when the sun is above the horizon, due to unrealistic radiation peaks that occur during sunrise and sunset intervals (Widén & Munkhammar, 2019:35). In order to determine if the sun is above the horizon, the numerator and denominator of Equation (1.1) must both be greater than zero.

1.6.3 Normalised hot water consumption profile

A normalised hot water consumption profile will be applied in the mathematical model of each respective technology. Figure 1.2 below details the daily normalised hot water consumption profile of a typical South African residence.

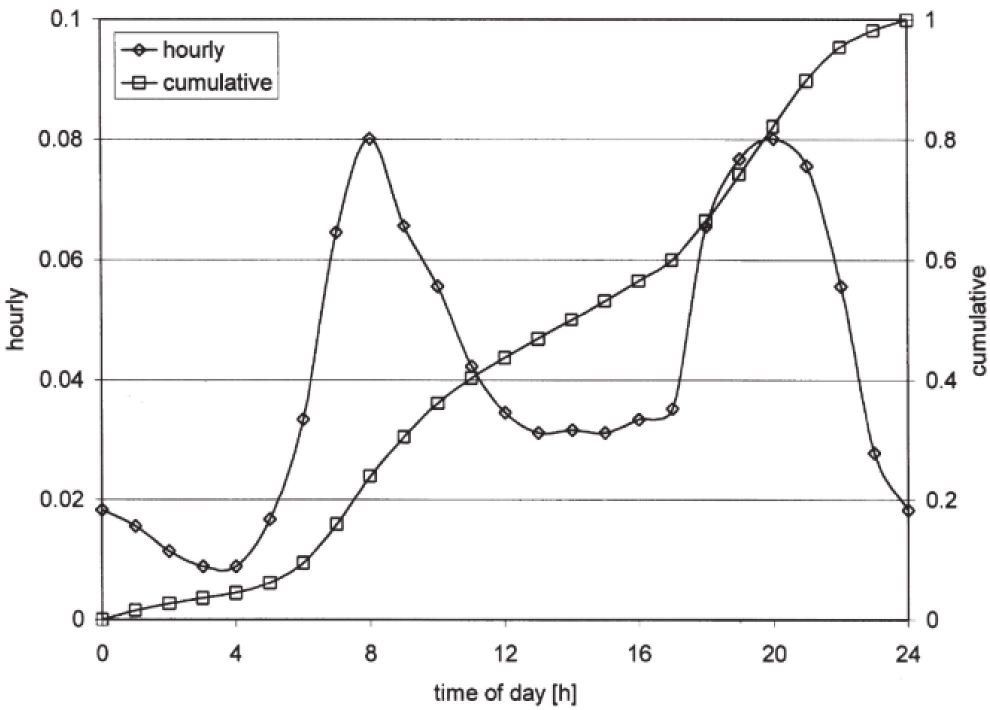

Figure 1.2: Normalised hot water consumption profile (Rousseau & Greyvenstein, 2000:56)

The profile consists of two peaks, around 08h and 20h respectively. The normalised hot water consumption profile will be repeated daily to match the format of the climatic design year data. The normalised consumption profile will be applied to a daily amount of hot water consumed per household, which differs from summer to winter. This will be discussed in Section 1.6.5.

1.6.4 Auxiliary and water storage unit

As stated in the scope, each water heating technology will be modelled with a hot water cylinder equipped with a resistive heater. The 200L KWIKOT Superline 400 Dual electric water heater, model DSG-200-5, will be used in this study (Electrolux SA, 2019). The electric water heater firstly acts as auxiliary electrical heat input, ensuring that sufficient hot water is provided if a technology cannot cope on its own. The electric water heater secondly acts as a water storage unit, ensuring that system losses are equally represented between technologies. Note thus that both the phrases “electric water heater” and “water storage tank” to be used in this dissertation refers to the same thing.

1.6.5 Input parameter values

The input parameter values that will be used in the different mathematical models of the water heating technologies are listed in Table 1.2.

Table 1.2: Mathematical model input parameters of a 4-person household

Parameter	Description	Value	Unit
mS_{water}	Hot water consumption during summer months	180	L/household/day
mW_{water}	Hot water consumption during winter months	260	L/household/day
c_p	Specific heat of water	4.184	kJ/kgK
T_{inlet}	Inlet water temperature	15	°C
Tt_0	Initial tank temperature	55	°C
Vt	Volume of water storage tank	200	L
Q_{LOSS}	Standing loss of electric water heater	1.37	kWh/day
E_{AUX}	Heating capacity of electric water heater	4	kW
R_{kWh}	Cost of electricity	2.20	R/kWh
ϕ	Latitude of Johannesburg	-26.2	°
β	Optimal tilt angle	36.2	°
i	Current hour	-	-
i-1	Previous hour	-	-
Tt_i	Tank temperature at hour i	…	°C
Tt_{i-1}	Tank temperature at hour i-1	…	°C
V_i	Volume consumed/added to tank at hour i	…	L

The hot water consumption for a residential household, housing four occupants, is given two separate values during different months of the year. During the eight warmer months, September through April, the hot water consumption mS_{water} is chosen as 180L at 45L per occupant. During the four months of winter, May through August, the hot water consumption mW_{water} is chosen as 260L at 65L per occupant. Note that the operational costs of the water heating technologies will be given in Rands per household per year. The symbol c_p is the fixed specific heat of water (Borgnakke and Sonntag, 2009). It is assumed that the inlet water temperature T_{inlet} of the water heating systems is 15°C, which is a good average temperature for municipal water feed (Rankin & van Eldik, 2010:5). The initial temperature of the water in the storage tank for all the water heating systems is chosen as 55°C and the volume of the tank Vt is 200 litres. In order to ease modelling conditions, an already heated tank was assumed at the start. It is also assumed that the temperature distribution within the water storage tank is uniform, thus neglecting stratification (Hohne et al., 2019b:274). The maximum and minimum temperatures of the water storage tank differ for the different water heating technologies and will be discussed in their respective chapters. The electric water heater has a B rated energy efficiency, which according to SANS 151 400kPa regulations, accounts for a standing loss of 1.37 kWh/day (Electrolux SA, 2019). As modelling will be done in an hourly format, the hourly standing loss of the electric water heater Q_{LOSS} is equal to 205.5 kJ/hour. The electric water heater has a 4kW element and a maximum heating capacity E_{AUX} of 14400kJ/hour (Electrolux SA, 2019). The cost of electricity depends on the regulations of the local municipality, season, location and the type of consumer. There is also an inclining block rate tariff (IBT) for residential consumers (JB Marks Local Municipality, 2019). The VAT included energy charge of block 4 (>600 kWh) will be applied in this study and the cost of electricity R_{kWh} will thus be taken as R2.20/kWh (JB Marks Local Municipality, 2019). Lastly, the latitude ϕ of Johannesburg is -26.2° and the optimal tilt angle β is the absolute value of the latitude plus 10°.

In terms of modelling notation, i will represent the current hour and i-1 the previous hour. The temperature of the water in the storage tank Tt will be modelled per hour Tt_i and (amongst others) will be dependent on the storage tank temperature of the previous hour Tt_{i-1}. The normalised hot water consumption profile will result in an hourly volume of water consumed V_i, which is also the amount of cold inlet water entering the storage tank during the respective hour. Note that not all variables will be given the i and i-1 notation and unless otherwise indicated, are in terms of the current hour i. This is simply to avoid the unnecessary addition of the notation i in every equation.

CHAPTER 2 – SOLAR PHOTOVOLTAIC WATER HEATING

The goal of this chapter is firstly to develop and test a simulation model that will be able to accurately simulate solar photovoltaic (PV) power generation. Secondly, to develop a mathematical model that will accurately predict the performance and cost of solar photovoltaic water heating (PVWH). There is a number of factors that influence the performance, capital and operational costs of PVWH. This study will mainly focus on the following factors: the efficiency of a solar panel and the array size, which dictates the amount of power that can be generated from solar radiation; the type of application, which dictates the type of PV connection and system components.

The direct application of PV technology for water heating originated from the PVWH system patented by Fanney and Dougherty (1997). PVWH stemmed from solar thermal water heating and is frequently compared to its renewable counterpart. While the comparative study by Dintchev *et al.* (2018) preferred PV above solar thermal, a more recent study by Buckley *et al.* (2020) found that solar thermal water heating was most beneficial. There is a great number of factors that influences the various findings, and the contradictive findings from literature resulted in a bigger focus on understanding PVWH in this study.

Chapter 2 will entail: a literature study, firstly reviewing the working principles of a PVWH system as applied in this study and secondly, focussing on PV modelling; the development and methodology of the PVWH simulation model; the PVWH experiment and results; the validation of the PVWH model by comparison of the simulation and experimental results and finally a discussion of the results.

2.1 Literature study

The PV field of study is vast and hundreds of studies have been done over the years in order to describe the current voltage (IV) characteristics of a PV cell (Laudani et al., 2014:433). The literature section aims to provide only the basic and relevant information required for the purpose of this study.

2.1.1 Working principles of a photovoltaic water heating system

PVWH is the direct application of solar generated PV power to heat water (Fanney & Dougherty, 1997:126).

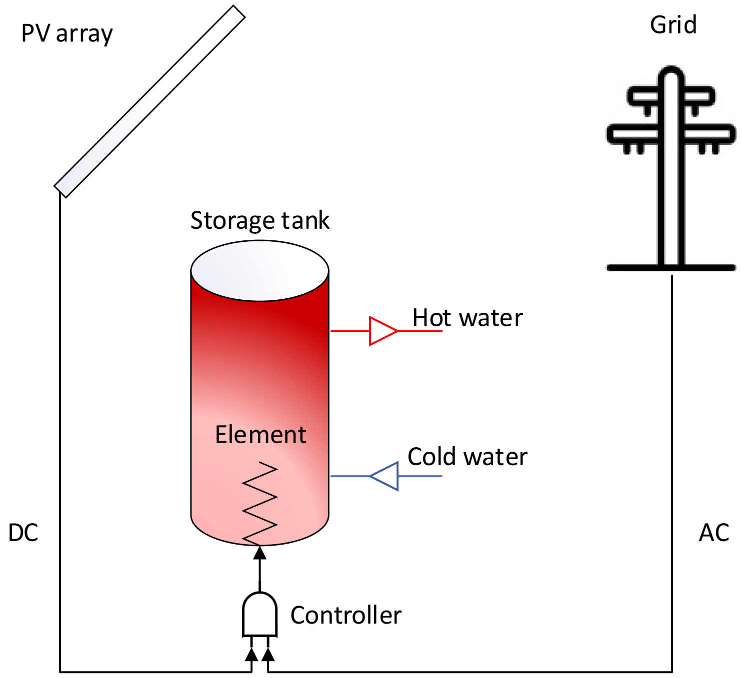

Figure 2.1: PVWH schematic

As illustrated in Figure 2.1, the main components of a PVWH system are the PV array, microprocessor controller and water storage tank. Note that cells are connected to form a module/panel and modules/panels are connected to form an array. A PV array generates direct current (DC), which is connected to the resistive heating element of the water storage tank via the controller. The utility grid, supplying alternating current (AC), is also connected via the controller as auxiliary. A PVWH system is dependent on solar radiation and good weather conditions. During poor weather conditions, grid power ensures the supply of hot water. The type of system application shown in Figure 2.1 is also commonly referred to as a grid tied residential rooftop system without feedback, meaning that any surplus energy goes unused (Kritzinger, 2017:7). The operational characteristics of a PV module is represented by an IV curve, at a given solar irradiance and module temperature (Fanney & Dougherty, 1997:127). Figure 2.2 below represents the IV and load curve of a PVWH system.

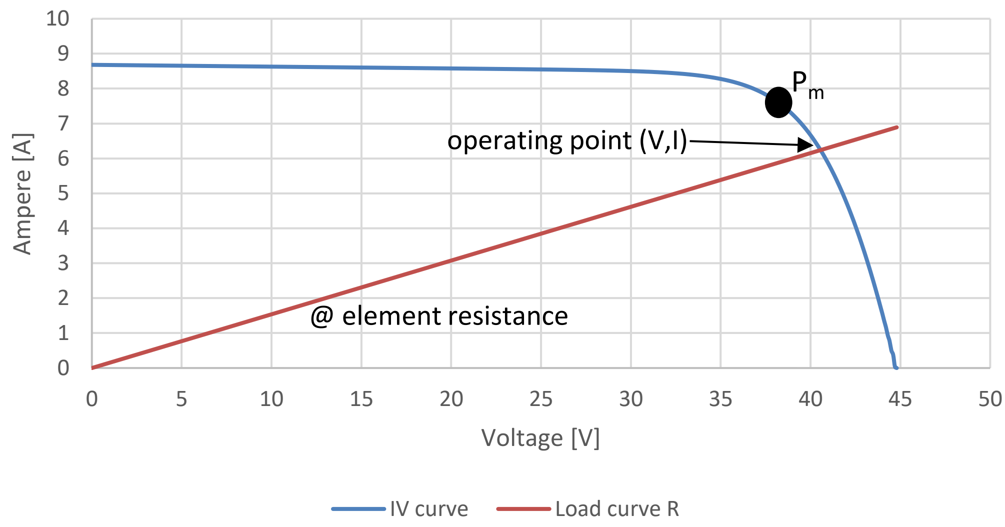

Figure 2.2: IV characteristic curve and load curve

As indicated on Figure 2.2, the operating point is dependent on the load connected and determines the amount of power generated (Fanney & Dougherty, 2001:2). P_m on the IV curve indicates the maximum power point (MPP). An operating point that coincides with the MPP will generate the maximum amount of power (Fanney & Dougherty, 2001:2).

The literature to follow will focus on the modelling of PV in order to simulate and predict the power generated by a system.

2.1.2 Photovoltaic modelling

PV power generation is an expensive investment, due to the high cost of modules (Ishaque et al., 2011a:586). A PV module is thus modelled in order to optimize performance and efficiency, maximize cost effectiveness and to determine its economic feasibility prior to installation (Lo Brano *et al.*, 2010:1358; Ishaque *et al.*, 2011b:1613). Modelling of a PV module entails the estimation of its nonlinear IV characteristic curves by utilizing the equivalent electrical circuit of a PV cell (Ishaque *et al.*, 2011b:1613). Solar radiation and operating cell temperature are the two most crucial parameters that affect the IV characteristics (Salilih & Birhane, 2019:4). PV modelling therefore aims to simulate the characteristics of a module when subjected to changes in the irradiance level and cell temperature (Ishaque et al., 2011a:586).

In order to simulate a PV module, a set of lumped circuit parameters are required. The Shockley theory of an illuminated p-n junction is the starting point of most models (Mares et al., 2015:139). Using the Shockley theorem allows for the equivalent electrical circuit of a PV cell to be described at different levels of complexity, leading to the creation of single and two-diode models (Mares et al., 2015:139). Challenges in modelling arise due to the fact that not all characteristic parameters are provided by manufacturers (Ibrahim & Anani, 2017:69). PV module manufacturers only provide the basic product performance data at a fixed irradiance of 1000W/m^2 and operating cell temperature of 25°C (Lo Brano *et al.*, 2010:1359). The IV characteristic curves are also only provided for fixed standard test conditions (STC) (Lo Brano *et al.*, 2010:1359). In order to extract the unknown characteristic parameters, these models either employ numerical or analytical methods (Ibrahim & Anani, 2017:69). In the following subsections the single and two-diode models, characteristic parameters and the numerical and analytical parameter extraction methods are discussed, concluding with the choice of model for this study.

2.1.2.1 Single- and two-diode models

Single and two-diode models are classified by the number of diodes approximated in the equivalent electrical circuit, as shown in Figure 2.3 below (Ayodele et al., 2016:51).

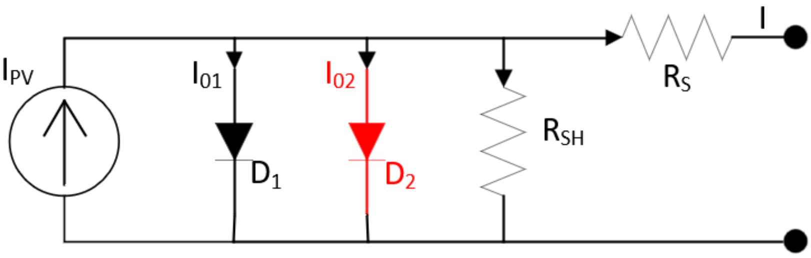

Figure 2.3: Single diode and two-diode (addition of red) equivalent electrical circuit

The number of diodes approximated directly relate to the number of characteristic parameters, mathematical complexity and the accuracy of the model (Ayodele et al., 2016:51). The number of parameters that must be extracted also depend on the mathematical approach applied in the model. Humada *et al.* (2016:495) grouped these models, with their respective mathematical methods, in terms of the number of extracted parameters, ranging from two to five parameters. The two-diode model can have up to seven parameters affecting the shape of the IV curve, taking into consideration the recombination loss in the depletion region of the solar cell (Lo Brano *et al.*, 2010:1360; Ishaque et al., 2011a:586). The modelling of a two-diode cell requires semiconductor parameters which are rarely given by commercial PV datasheets (Ishaque et al., 2011a:587). These parameters are difficult to determine, due to the implicit form and exponential terms of the photogenerated current equation (Lo Brano *et al.*, 2010:1360).

When comparing the single and two-diode models, the two-diode model is superior in accuracy, but requires demanding computational effort (Ishaque et al., 2011a:586). This makes the single diode model more attractive as it requires less computational effort while still being quite accurate (Ishaque et al., 2011a:587). Lo Brano *et al.* (2010:1360) stated that the single diode model is an adequate representation of the IV characteristic curves at STC and must not be rejected. Villalva et al. (2009:1200) and Mares et al. (2015:139) commented that the single diode model is a “good compromise” and “trade-off” between accuracy and simplicity.

2.1.2.2 Parameter characteristics

The equivalent electrical circuit parameters, as shown in Figure 2.3, are the photogenerated current (I_{PV}), reserve saturation current (I_0), diode ideality factor (n), shunt (R_{SH}) and series (R_S) resistances (Cotfas et al., 2013:588). Humada *et al.* (2016) provided a detailed demonstration on the effect of these characteristic parameters on the IV curve. The diode ideality factor and both resistances have significant influence on the IV curve, while most of the mathematical modelling techniques are focused on solving these three parameters.

1. Diode ideality factor

   When modelling the IV characteristics of a PV cell, most inaccuracies are due to the interdependent nature of the diode ideality factor (Lo Brano *et al.*, 2010:1361). A number of two-diode studies consider the diode ideality factors equal to 1 and 2 respectively. Although the assumption is generally accepted, it is not always true (Ishaque et al., 2011a:587). Numerous studies have found that the ideality factor of a single diode lies between 1 and 1.5, depending on various other cell parameters. Villalva et al. (2009:1201) and others modified the diode ideality factor throughout the simulation process in order to improve the IV curve fitting and model accuracy.

2. Resistances

   The shunt and series resistances affect the slope of the IV curve at the short circuit current and the open current voltage respectively (Lo Brano *et al.*, 2010:1360). The shunt and series resistances do not physically exist within the cell (Lo Brano *et al.*, 2010:1360). They are respectively the electrical representation of current leakage and contact resistances found within the semiconductor (Villalva et al., 2009:1201). The IV curves given by manufacturers can be graphically evaluated in order to determine the values of the shunt and series resistances (Lo Brano *et al.*, 2010:1361). Mares et al. (2015:142) stated that the accuracy of the graphical approach is highly dependent on the operating ability of the user. In order to simplify modelling and reduce the number of parameters, authors mainly look to the resistances. The assumptions are sometimes made that the series resistance is so small that is may be neglected and that the shunt resistance is so large that it may be equated to infinity (Villalva et al., 2009:1202; Mares et al., 2015:141).

2.1.2.3 Numerical and analytical parameter extraction methods

There is a vast number of parameter extraction methods found in literature and Cotfas et al. (2013) provided a critical outlining and discussion of 34 different methods. These methods are either numerical or analytical. Numerical methods use an iterative or numerical algorithm in order to solve a set of equations (Ibrahim & Anani, 2017:69). The extraction approach of analytical methods is to make simplifying assumptions and/or approximate parameter values (Ibrahim & Anani, 2017:69).

Ayodele et al. (2016) investigated and compared the most common numeric algorithms used for solving the five-parameter single diode model. It was found by Ayodele et al (2016:59) that no single algorithm is ultimately the best and the usage of different algorithms depends on the focus area of the user as each algorithm is best suited for a given metric. In contrast, Ibrahim and Anani (2017) evaluated six different analytical techniques used for extraction. Although approximations are required to simplify and reduce computational effort, Ibrahim and Anani (2017:78) found that they compete in accuracy with popular numeric algorithms. Most studies utilize a numerical algorithm for the extraction of the parameters, as analytical methods can prove difficult to use due to the implicit non-linear nature of the PV cell (Ayodele et al., 2016:51).

To conclude the literature study, it was decided that the simpler single diode model would prove adequate for the purpose of this study, when comparing different water heating technologies.

2.2 Simulation model development

The PV simulation model is developed and discussed throughout the following four subsections. The ReneSola Virtus II 300W PV module (ReneSola, 2014) was utilized for this study and the system comprises of an array of four modules. Firstly, the methodology of PV modelling is discussed and the characteristic parameter equations are given. Secondly, the unknown characteristic parameters of the PV module are extracted. With all the characteristic parameters known, the IV curves of the PV system are modelled and compared in order to validate the simulation model. The modelling of the IV curves is done in the MATLAB environment. The final subsection concludes the development process with the discussion of the single diode PV simulation model, which is done in the Microsoft Excel environment.

2.2.1 Modelling methodology

The electrical circuit of a single diode PV cell model is illustrated by Figure 2.4 below.

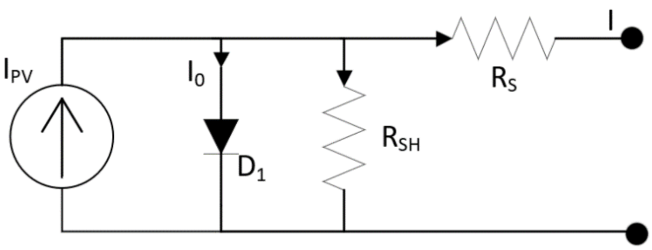

Figure 2.4 Single diode PV cell model

The external current (I) of a single diode PV cell, Equation (2.1),

$$I = I_{PV} - \underbrace{I_0\left[\exp\left(\frac{V_D}{V_T}\right) - 1\right]}_{I_D} - \underbrace{\frac{V_D}{R_{SH}}}_{I_{SH}} \tag{2.1}$$

is equal to the photogenerated current (I_{PV}) minus the currents passing through the diode (I_D) and shunt resistor (I_{SH}). The fully expressed external current of Equation (2.2) is given when substituting the diode voltage (V_D) and thermal voltage (V_T),

$$I = I_{PV} - I_0\left[\exp\left(\frac{q(V + IR_S)}{nN_SkT}\right) - 1\right] - \frac{V + IR_S}{R_{SH}} \tag{2.2}$$

with the diode voltage $V_D = V + IR_S$ and thermal voltage $V_T = \frac{nN_SkT}{q}$.

Since a PV module is approximated by modelling a PV cell, N_S refers to the number of cells connected in series to form the module. V is the external voltage, T is the operating temperature of the cell, k the Boltzmann constant and q the electron charge. The IV curve, again shown in Figure 2.5 below, is the plot of the external current (I) Equation (2.2).

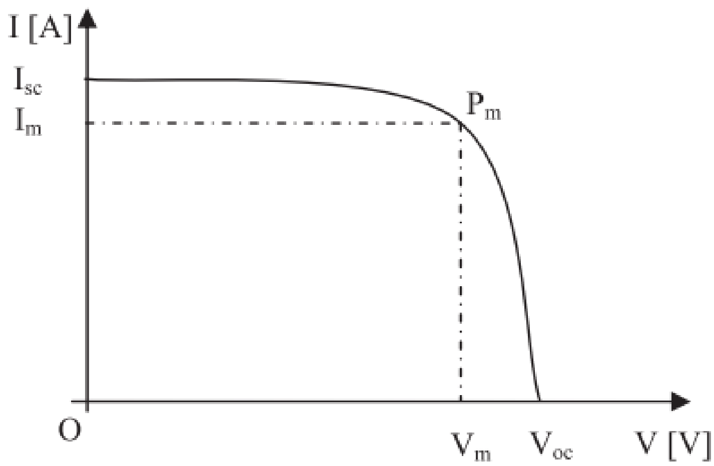

Figure 2.5: IV characteristic curve parameters (Cotfas et al., 2013:589)

The external voltage (V) is swept from zero to maximum voltage and for each voltage increment the external current is calculated. The few coordinates noted on the IV curve are the main parameters supplied by PV datasheets, including temperature coefficients and module efficiency. When the external terminal of the circuit is shorted, maximum current is delivered, the short circuit current (I_{sc}). When the terminal is open, maximum voltage is reached, the open current voltage (V_{oc}). As the external voltage increases and approaches V_{oc}, the external current reduces as the amount of current passing through the diode rapidly increases. The MPP (P_m) is the product of the largest simultaneous current (I_m) and voltage (V_m).

In order to extract the unknown parameters (I_{PV}, I_0, n, R_{SH}, R_S), the given parameters (I_{SC}, V_{OC}, I_M, V_M, P_M) are used to derive their respective expressions (refer to Annexure A Section A.1 for the derivations).

a) Photogenerated current

To attain the expression of the photogenerated current or simply the photocurrent, short circuit conditions are assumed, resulting in $I_{PV} = I_{SC}$. I_{SC} must be evaluated in order to further express I_{PV}. According to Humada *et al.* (2016), I_{SC} depends on the irradiance level, cell area, cell material and the cell temperature. I_{SC} is linearly proportional to irradiance and cell temperature has barely any effect, as the current temperature coefficient K_I is negligibly small. I_{PV} is therefore expressed at any given irradiance and temperature as:

$$I_{PV} = \frac{G}{G_{NOM}}\left(I_{SC\_STC} + K_I \Delta T\right) \tag{2.3}$$

with G the irradiance, G_{NOM} the irradiance at STC (1000W/m^2), I_{SC_STC} the short circuit current at STC and $\Delta T = T - T_{NOM}$ the difference between the actual operating cell temperature T and the cell temperature at STC T_{NOM} (25°C or 298.15K).

b) Reverse saturation current

The reverse saturation current I_0 is attained by simply writing Equation (2.2) as an expression of I_0. Under the open circuit conditions of $V = V_{OC}$, $I = 0$ and with $I_{PV} = I_{SC}$, I_0 is expressed as:

$$I_0 = \frac{I_{SC} - \frac{V_{OC}}{R_{SH}}}{\exp\left(\frac{qV_{OC}}{nN_S kT}\right) - 1} \tag{2.4}$$

c) Shunt resistance

As previously discussed, the shunt resistance R_{SH} effects the slope of the IV curve at the short circuit condition. R_{SH} is thus expressed as the inverse of the slope at short circuit:

$$R_{SH} = -\frac{dV}{dI}_{SC} \tag{2.5}$$

d) Series resistance

Also previously discussed, the series resistance R_S effects the slope of the IV curve at the open circuit condition. R_S is thus expressed as the inverse of the slope at open circuit:

$$R_S = -\frac{dV}{dI}_{OC} - \frac{V_T}{I_{SC}}$$
(2.6)

The expression of the thermal voltage V_T, present in both Equations (2.4) and (2.6), contain the diode ideality factor n, which is still unknown. The parameters n, I_0 and R_S are all interdependent and will be solved simultaneously with a system of non-linear equations.

e) Diode ideality factor

The diode ideality factor n is a measurement of the solar cell material quality and lies in between a value of 1 and 1.5. The effect of n is most dominant at the MPP (Humada *et al.*, 2016). The maximum current is thus expressed in order to supply a third equation containing the diode ideality factor:

$$I_{MP} = I_{SC} - I_0\left[\exp\left(\frac{q(V_{MP} + I_{MP}R_S)}{nN_SkT}\right) - 1\right] - \frac{V_{MP} + I_{MP}R_S}{R_{SH}}$$
(2.7)

Equation (2.7) supplies the final equation needed for the system of three non-linear equations that will be used to solve n, I_0 and R_S simultaneously. These seven equations are all that is needed in order to develop a basic PV model. In the following sections, they are utilized in order to extract the unknown parameters, plot the IV curves and to develop the single diode PV simulation model.

2.2.2 Characteristic parameter extraction

Before modelling of the IV curves and development of the single diode model can begin, all characteristic parameters must be known. This section will summarise the parameters that are known and needed for extraction, the extraction procedure and results thereof.

2.2.2.1 Parameter extraction setup

The ReneSola Virtus II 300W module specifications from its datasheet are listed in Table 2.1 below. The IV curves of the Virtus II module are presented by Figure 2.6 below. Table 2.1 and Figure 2.6 supply the parameters necessary to extract the unknown parameters.

Table 2.1: ReneSola Virtus II 300W module specifications (ReneSola, 2014)

Symbol	Parameter name	Value	Unit
V_{OC}	Open circuit voltage	44.8	V
V_M	Maximum power voltage	36.6	V
I_{SC}	Short circuit current	8.69	A
I_M	Maximum power current	8.2	A
P_M	Maximum power	300	W
N_S	Number of cells in series	72	-

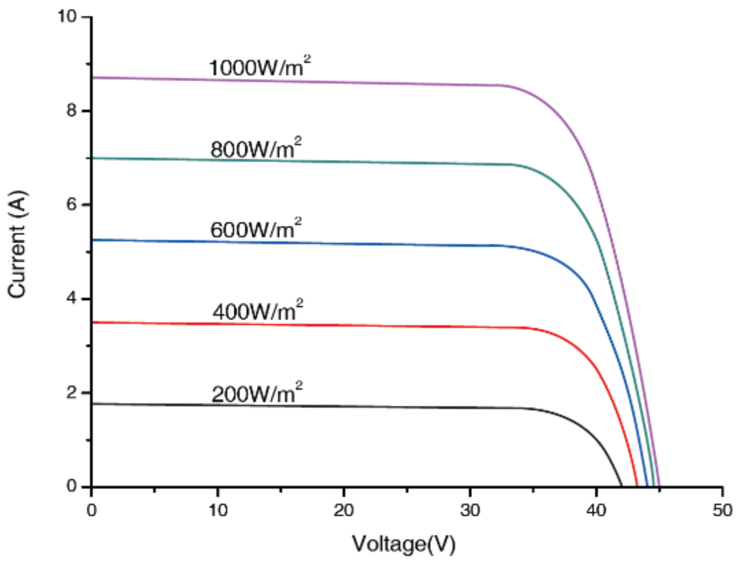

Figure 2.6: ReneSola Virtus II 300W module IV STC characteristic curves (ReneSola, 2014)

2.2.2.2 Parameter extraction procedure

The procedure followed in order to extract the unknown parameters are summarised by the following steps:

1) Determine the photocurrent I_{PV}.

The photocurrent can by directly read from the datasheet as $I_{PV} = I_{SC}$. The effect of the temperature coefficients has been neglected in the PV model as the operating cell temperature is unknown. An assessment was however done on the variation of operating cell temperatures and is available in Annexure A Section A.2.

2) Determine the slopes of the 1000W/m^2 IV curve at short and open circuit.

The values of the slopes were graphically estimated from the given IV curves of Figure 2.6.

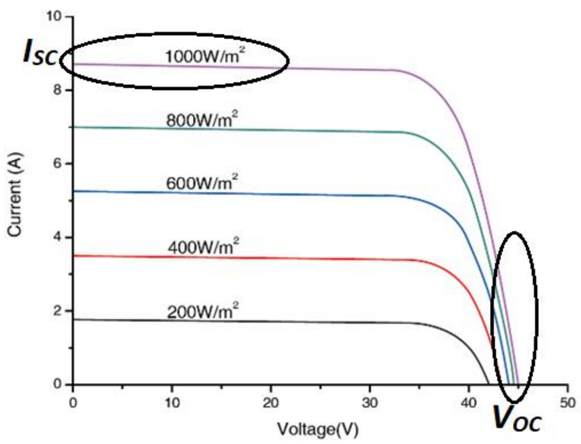

Figure 2.7: Slopes of the 1000W/m^2 IV curve

WebPlotDigitizer was used to extract the data from the indicated curve sections of Figure 2.7. The corresponding plot data was then used to calculate the slopes.

3) Determine the shunt resistance R_{SH}.

The shunt resistance is determined at the short circuit condition by using Equation (2.5).

4) Determine the diode ideality factor n, reverse saturation current I_0 and series resistance R_S.

As previously discussed, n, I_0 and R_S are interdependent and must be solved simultaneously. The set of non-linear equations are Equations (2.4), (2.6) and (2.7). Each equation was expressed as a function equal to zero, represented by Equation (A.1), (A.2) and (A.3) respectively, and solved using the fsolve function in MATLAB (refer to Annexure A Section A.1 point 4).

2.2.2.3 Parameter extraction results

The extracted parameter results are listed in Table 2.2 below.

Table 2.2: Extracted parameter values

Symbol	Parameter name	Value	Unit
I_{PV}	Photogenerated current	8.69	A
$\frac{dI}{dV}_{SC}$	Slope of the curve at short circuit	-0.005164	-
$\frac{dI}{dV}_{OC}$	Slope of the curve at open circuit	-1.514044	-
R_{SH}	Shunt resistance	193.6593	Ω
n	Diode quality factor	1.212065	-
I_O	Reverse saturation current of the diode	1.77E-08	A
R_S	Series resistance	0.189366	Ω

With all the electrical characteristics of the PV module known, the IV curves can be simulated and evaluated. The final step of the single diode model development is discussed thereafter.

2.2.3 Modelling of the IV characteristic curves

Although modelling of the IV curves is just a step in the process of the complete simulation model development, it is discussed as an independent sub-model. This is done not only to lay the groundwork for the final single diode model of the PV system, but to ensure the accuracy of its IV characteristic predictions. The IV curves were modelled in the MATLAB environment. The model setup, methodology of the modelling approach and the results are discussed in this section. In order to validate the model, the actual IV curves of the PV system are extracted and compared.

2.2.3.1 MATLAB modelling of the IV curves

The PV system consists of an array of four Virtus II modules connected in series, which is compensated for by simply increasing the module voltage values fourfold. The PV system input parameters needed for the modelling of the IV curves are listed in Table 2.3 below.

Table 2.3: PV system specifications

Input parameters			
Symbol	Parameter name	Value	Unit
V_{OC}	Open circuit voltage	179.2	V
I_{SC}	Short circuit current	8.69	A
I_{PV}	Photocurrent	8.69	A
V_{MP}	Maximum power voltage	146.6	V
I_{MP}	Maximum power current	8.2	A
N_S	Number of cells connected in series	72	-
G_{NOM}	Solar irradiance at STC	1000	W/m^2
G_{VAR}	Arbitrary solar irradiance	-	W/m^2
G	Solar irradiance for IV curve – 200, 400, 600, 800, 1000		W/m^2
T_{NOM}	Cell temperature at STC	298.15	K
T	Cell temperature	298.15	K
q	Electron charge	1.60218E-19	C
k	Boltzmann constant	1.38065E-23	J/K
I_0	Reverse saturation current	1.77E-08	A
n	Diode quality factor	1.212065856	-
R_S	Series resistance	0.189365673	Ω
R_{SH}	Shunt resistance	193.6592708	Ω
V_T	Thermal voltage	2.242161404	V

In order to simulate the IV curves, the terms of Equation (2.2) were separated and redefined. This was done to simplify the loop procedure applied for the calculation of the external current at each voltage increment. The photocurrent I_{PV} remains constant. The diode current I_D and shunt current I_{SH} are assigned to a new current term dubbed:

$$I_{REST} = \underbrace{I_0\left[\exp\left(\frac{q(V+IR_S)}{nN_s kT}\right)-1\right]}_{I_D} + \underbrace{\frac{V+IR_S}{R_{SH}}}_{I_{SH}} \qquad (2.8)$$

The external current I is assigned an initial, present and future value. The step value i is also introduced. The initial value, i = 1, is set to zero I(1) = 0. The present value (initially zero) of the current I(i) is substituted in the external current value of the I_{REST} equation:

$$I_{REST}(i) = I_0\left[\exp\left(\frac{q\left(V + I(i)R_S\right)}{nN_s kT}\right) - 1\right] + \frac{V + I(i)R_S}{R_{SH}}$$

(2.9)

The future value of the external current is set to I(i+1) and defined as:

$$I(i+1) = I_{PV} - I_{REST}(i)$$

(2.10)

After the future value is calculated the loop is reset by assigning the calculated future value to the present value of the external current i = i+1, meaning that the calculated I(i+1) becomes the new value of I(i) which is again used to calculate I_{REST}(i) to give a new future current value I(i+1) and the process is reiterated until the loop is finished.

The loop is reiterated for each incremental value of the input voltage, ranging from zero to the open circuit voltage of the system. The simulation is also reiterated for each STC value of irradiance.

2.2.3.2 MATLAB results of the IV curves

The result of the MATLAB IV curves simulation is shown in Figure 2.8 below.

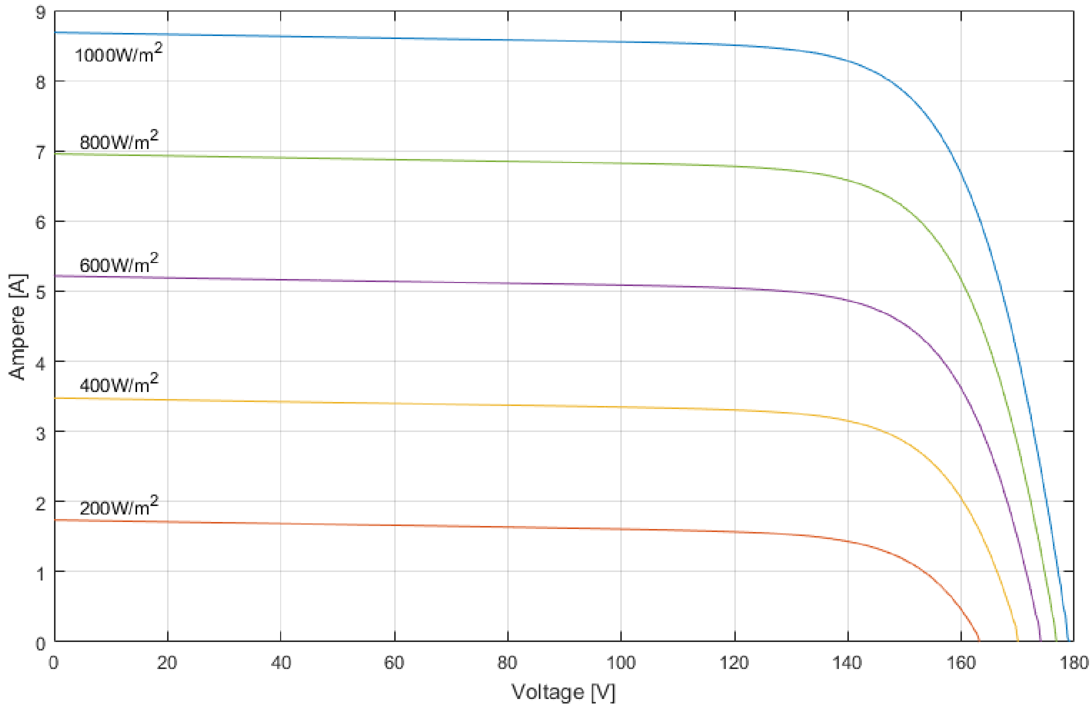

Figure 2.8: MATLAB simulated STC IV characteristic curves

The power voltage (PV) characteristic curves was also plotted by simply multiplying the input voltage with its calculated external current P = VI and is shown in Figure 2.9 below.

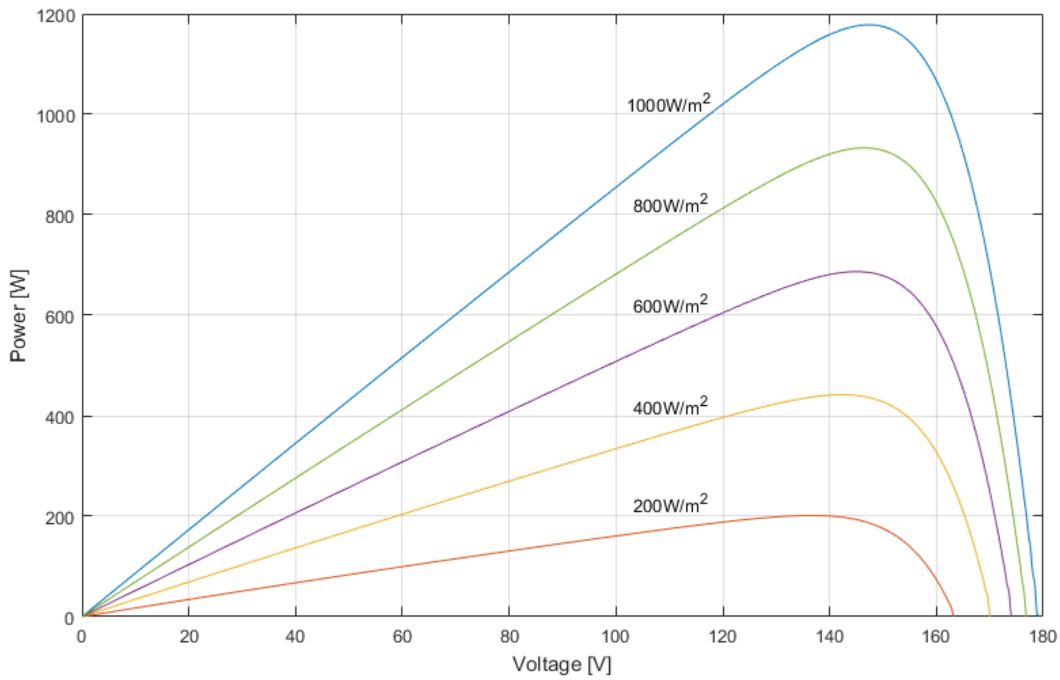

Figure 2.9: MATLAB simulated STC PV characteristic curves

2.2.3.3 IV curves of the PV system

The STC IV curves given by the manufacturer are presented in image format on the PV datasheet. WebPlotDigitizer was utilized in order to extract the plot data from the image. WebPlotDigitizer uses pixel technology and the accuracy thereof is limited to the quality of the image and the number of pixels able to fit on the curves. The WebPlotDigitizer IV plot of the PV system is shown in Figure 2.10 below and should in theory be identical to Figure 2.6, with the exception of the increased voltage.

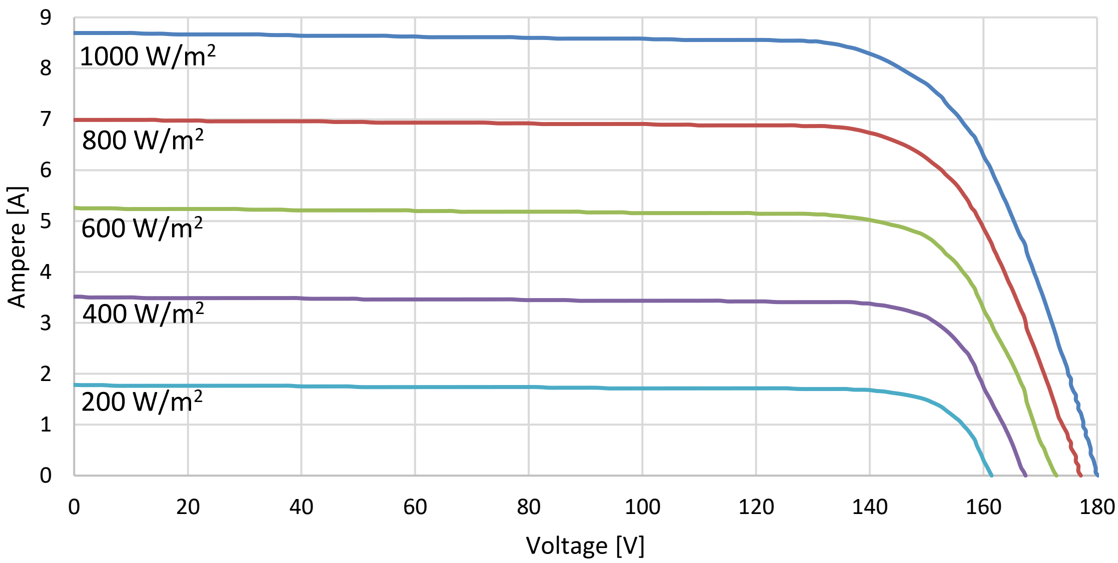

Figure 2.10: WebPlotDigitizer IV characteristic curves of the PV system

Minor fluctuation is observed in the curve plots close to the open voltage region. This is due to the aforementioned limitations of the pixel technology combined with the close proximity of the IV curves at open circuit voltage observed in Figure 2.6.

2.2.3.4 Comparison of the IV curves

The MATLAB modelled and WebPlotDigitizer IV curves were compared in order to validate the MATLAB IV curve model. Figure 2.11 below presents the validation between the WebPlotDigitizer and MATLAB curve plots.

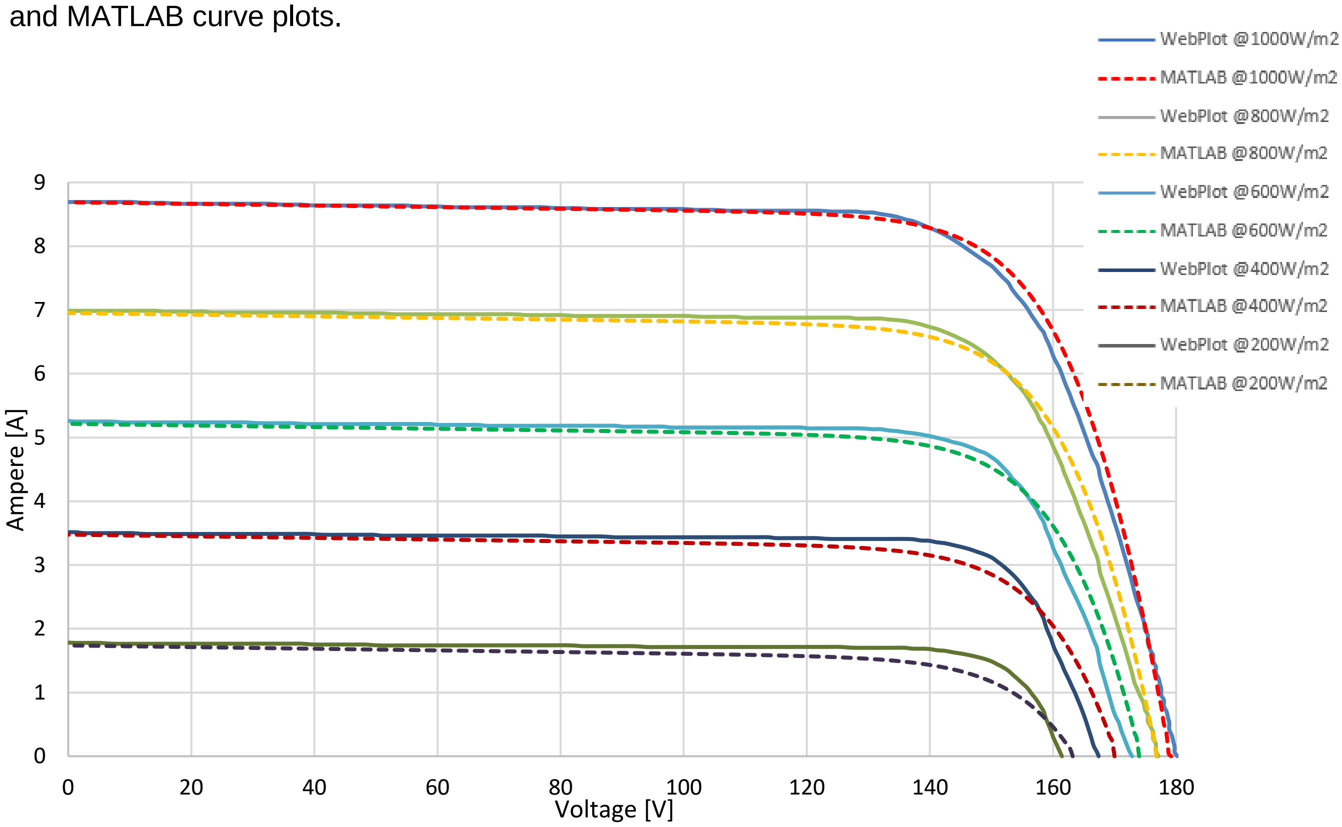

Figure 2.11: WebPlotDigitizer vs MATLAB STC IV characteristic curves

The major difference between the curves are most evident at the MPP region. Along with the previously discussed limitations of WebPlotDigitizer, the increasing error as irradiance lowers is also due to the interdependent nature of the diode ideality factor (Lo Brano *et al.*, 2010:1361). The MATLAB modelled curves may be closer to the true IV curves of the Virtus II module than what WebPlotDigitizer was able to capture. MATLAB has the programming ability to finely plot per very small incrementations, increasing accuracy, whereas WebPlotDigitizer is only capable of capturing data per corresponding pixel. The effectiveness of WebPlotDigitizer for validation may seem questionable, however the 1000W/m^2 WebPlot curve (most accurate comparison) proved essential in ascertaining the resistance values. The validation is also in support of the statement by Mares et al., (2015:141) concerning the accuracy of graphical methods.

2.2.4 The single diode photovoltaic simulation model

The single diode PV simulation model was developed in order to simulate the performance of the PVWH system under any arbitrary irradiance condition. The model was coded in the Microsoft Excel environment. The input parameters of the model are the same as listed in Table 2.3. The procedure of the single diode PV model is identical to the previously discussed MATLAB modelling of the IV curves procedure, with two additional steps.

The only explanatory difference in the procedure thus far is that an array must be generated in MATLAB, thus the introduction of the i and i+1 step values which represented the row elements. The Excel environment is already array based, where the elements i and i+1 simply represent the current and next cell respectively.

The two model additions are 1) the external resistance of the water heating element and 2) the arbitrary irradiance condition.

1) External resistance

The PVWH system utilizes a 26Ω resistive water heating element. In order to include the external resistance, Ohm's law was expressed in terms of the dependent current $I = V / R$. With $R = 26Ω$, $I = V / 26$ and for each voltage increment the current was calculated and plotted to give the load curve R, as shown in Figure 2.12 below.

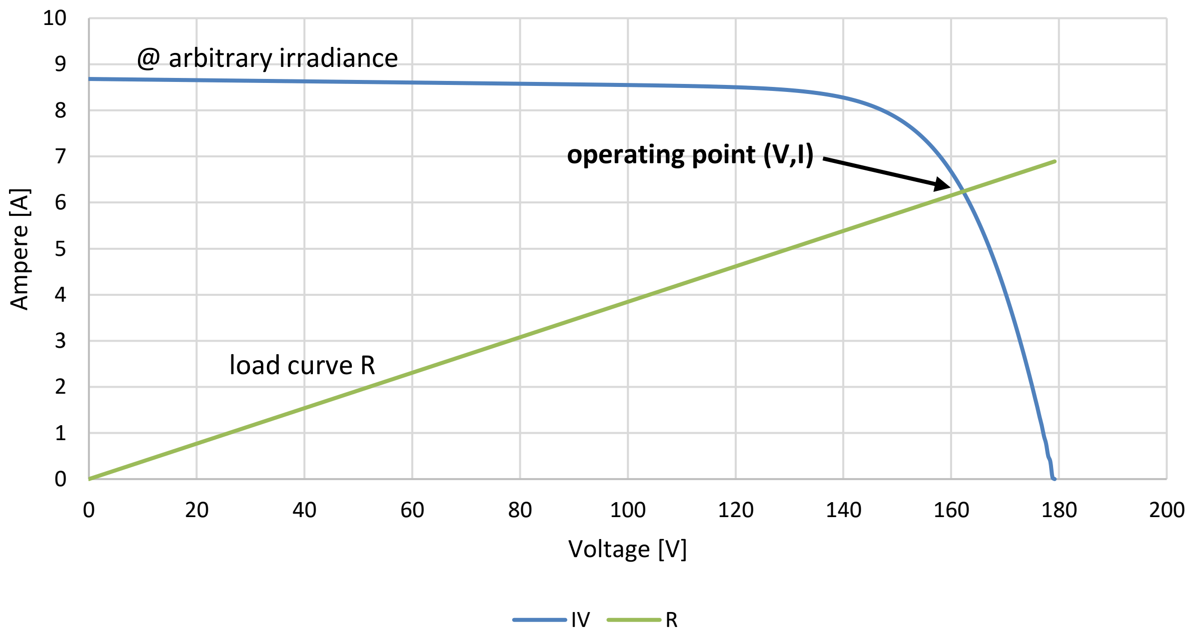

Figure 2.12: Single diode PVWH model IV curve vs load curve R

The load curve R represents all the available operating conditions of the PV system. At any given irradiance the operating point of the system is determined by the intersection between the IV curve and the load curve R, where the point coordinates IV(V, I) = R(V, I) (Salilih & Birhane, 2019). There exist multiple points of intersection where the plot data lines intersect due to the small incrementation of the external voltage. The intersecting point closest to zero must thus be determined.

Firstly, all the intersecting points were determined by taking the absolute values of the difference between the IV and load curve R, given as ABS(IV – R) = IV(V, I) - R(V, I). The smallest intersecting point was determined by using the built in Excel function SMALL. The corresponding voltage and current values were then determined using the MATCH function. Those values were extracted and individually presented by utilizing the INDEX function, which returns selected values from an array. With the operating point extracted from the plot data, the operating power was calculated by simply multiplying the intersecting coordinates P = VI. In conclusion to the addition of the external resistance, the variables listed in Table 2.4 below was added to the model.

Table 2.4: IV & R curve intersect point variables

Symbol	Variable name	Formula	Unit
V_{INT}	Intersect voltage	INDEX(MATCH(SMALL)))	V
I_{INT}	Intersect current	INDEX(MATCH(SMALL)))	A
P_{INT}	Intersect power	$V_{INT} I_{INT}$	W

2) Arbitrary irradiance

Equation (2.3) was simplified into Equation (2.11) below in order to plot the IV curve for any arbitrary irradiance. The parameter G represented the STC irradiances in the MATLAB model, whereas G_{VAR} is introduced as a variable in the Excel model to represent any given condition of irradiance:

$$I_{PV} = \frac{G_{VAR}}{G_{NOM}} I_{SC} \tag{2.11}$$

The value of I_{PV} is recalculated as G_{VAR} variates. Equation (2.10) then recalculates the external current value and the corresponding IV curve is plotted for every G_{VAR}. As the IV curve is updated, the intersect power P_{INT} is recalculated. This was achieved by utilizing the data table function within Excel's What-If Analysis. For further detail on the What-If-Analysis applied and an example of the model procedure, refer to Annexure A Section A.3.

2.3 Photovoltaic water heating experiment

The PVWH experimental section discusses the experimental setup, procedure and the results of the experiment. The experimental results are obtained by processing the recorded data in an energy balance across the PVWH system. The energy balance is then used to validate the experimental setup, assess the energy relationship of the system and to indicate the amount of utility grid energy saved by the system.

2.3.1 Experimental setup

The experiment was conducted on a pre-existing PVWH system at a residential home in Potchefstroom, North-West province, South Africa, housing a family of two, in the summer months of February and March. The experimental setup is shown in Figure 2.13 below.

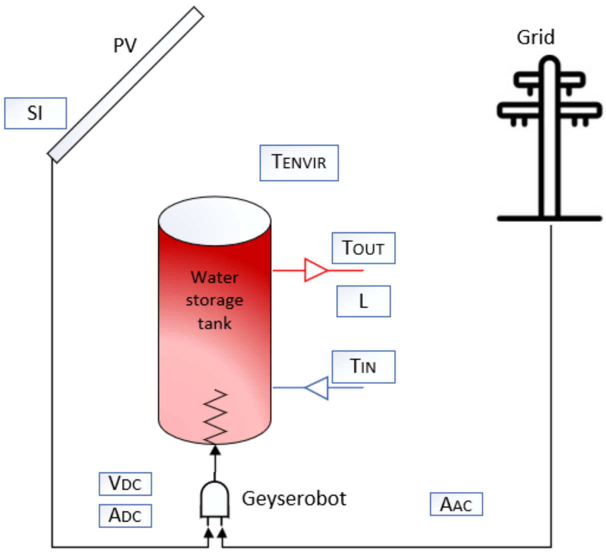

Figure 2.13: PV experimental setup

The PV system and utility grid were connected to a Geyserobot controller box (Geyserobot, 2015), which controlled the power supplied to the electric water heater. Geyserobot is a controlling device specifically designed to function with a residential hot water cylinder equipped with a resistive heater, without the need for expensive modification. Geyserobot utilizes solar PV generated electricity, with grid supplied electricity as backup, in order to heat water. Geyserobot does so by controlling the water temperature in the geyser and prioritizing PV, but can be overwritten by the user to utilize grid electricity. A 150L KWIKOT Superline 400 Dual electric water heater was used (Electrolux SA, 2019). The electric water heater was covered in a fiberglass insulation material to minimize loss of heat to its surrounding environment in the roof.

A dataTaker DT80W Data Logger (dataTaker, 2017) was used to measure, monitor and log all recorded variable data in one-minute intervals. The variables measured in the experimental setup are described in Table 2.5 below, along with the measuring equipment used. The water temperature sensors were installed and insulated close to the inlet and outlet of the electric water heater. The measuring equipment was calibrated before installation.

Table 2.5: PV experimental variables and measuring equipment

Symbol	Variable description	Measuring equipment	Unit
SI	Solar irradiance	SP-215 Pyranometer	W/m^2
A_{DC}	DC Amps supplied by PV	Hall effect sensor	A
V_{DC}	DC Volts supplied by PV	Voltage divider	V
A_{AC}	AC Amps supplied by grid	Current transformer	A
L	Flow rate of hot water	Mechanical pulse output water flow meter	L/min
T_{IN}	Cold water temperature	Type T thermocouple	°C
T_{OUT}	Hot water temperature		°C
T_{ENVIR}	Environmental temperature surrounding electric water heater		°C

2.3.2 Experimental procedure

The operational pattern of the electric water heater and the water draw pattern was completely dependent on the occupants of the residence and subject to unpredictable changes. Whenever available, Geyserobot would utilize PV generated electricity to heat the water in the electric heater to its setpoint temperature of approximately 58°C. The occupants set Geyserobot to utilize grid power to heat water in the early morning hours and again in the evening as necessary.

Once the dataTaker was set to start logging, little user interface was required other than ensuring continued operation and the periodic extraction of recorded data. The recorded data was processed by dividing the data into set intervals over periods of time. An interval is taken over the respective points in time where grid power was utilized and finished heating the water up to setpoint temperature. The intervals were taken over periods of 24, 48, 72 and 96 hours in order to assess any effect of variating interval times. The processed data was used to apply the law of conservation of energy across the PVWH system, as shown by Figure 2.14 below.

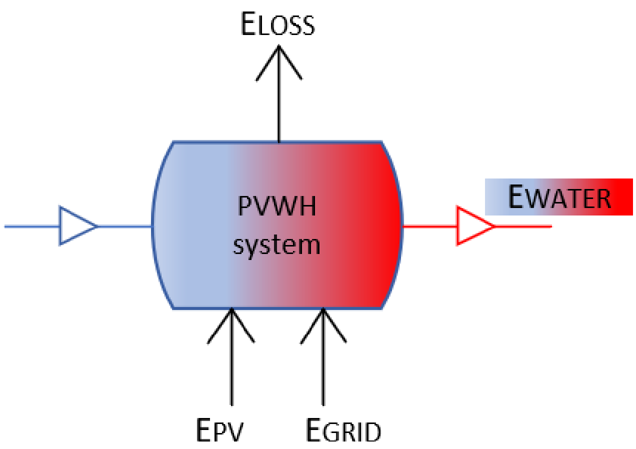

Figure 2.14: PV experimental energy balance

The energy balance across the PVWH system is summarised in Table 2.6:

Table 2.6: PV energy balance

Symbol	Description	Unit
E_{IN} - Sum of energy supplied to system		
E_{PV}	Energy supplied by PV system	kJ
E_{GRID}	Energy supplied by utility grid	kJ
E_{OUT} - Sum of energy delivered by system		
E_{WATER}	Energy transferred to the water	kJ
E_{LOSS}	Energy lost	kJ

Note that the internal energy of the system was neglected as the initial and final temperature over the respective intervals are equal at constant volume.

The following experimental results section summarizes the three main energy balance results of the PVWH system, namely: 1) the energy loss, which serves as an experimental validation against the rated loss of the electric water heater, 2) the linear relationship between the energy input and thermal output of the system, validating the energy balance taken across the system and 3) the amount of utility grid input energy saved by the PVWH system.

2.3.3 Experimental results

1) Energy loss results

The energy balance results of the respective interval cycles are listed in Table 2.7 below.

Table 2.7: PV energy balance results

Cycle	Timeframe	E_{IN} [kJ]	E_{WATER} [kJ]	E_{LOSS} [kWh/day]
24h cycles				
1	09 Febr - 10 Febr	20797.92	17043.08	1.04
2	10 Febr - 11 Febr	17852.15	14739.38	0.86
3	11 Febr - 12 Febr	18171.13	14825.46	0.93
4	26 Febr - 27 Febr	16835.16	13597.69	0.90
5	27 Febr - 28 Febr	16069.45	12928.73	0.87
6	02 March - 03 March	15978.00	12892.51	0.86
48h cycles				
7	16 Febr - 18 Febr	35280.32	29040.36	0.87
8	18 Febr - 20 Febr	33839.27	28475.16	0.75
9	20 Febr - 22 Febr	31870.78	25763.00	0.85
10	22 Febr - 24 Febr	31303.93	25279.88	0.84
11	24 Febr - 26 Febr	35470.86	29342.17	0.85
72h cycles				
12	09 Febr - 12 Febr	56821.20	46607.92	0.95
13	24 Febr - 27 Febr	52306.01	42939.86	0.87
14	01 March - 04 March	56644.73	45831.42	1.00
96h cycles				
15	16 Febr - 20 Febr	69119.59	57515.53	0.81
16	20 Febr - 24 Febr	63174.71	51042.88	0.84
17	27 Febr - 02 March	65459.94	56293.07	0.64
Average system energy loss:				**0.87**

The results from Table 2.7 indicate an average system energy loss of 0.87 kWh/day. The energy balance results were determined as follows. Referring to Table 2.6, E_{IN} is the sum of the energy supplied by the PV system E_{PV} and the energy supplied by the utility grid E_{GRID}. E_{WATER} is the amount of energy transferred into the water and E_{LOSS} is the amount of energy lost. Referring to Table 2.5, E_{PV} is the multiplication of the measured DC amps and volts supplied by the PV system. E_{GRID} is the multiplication of the measured AC amps and the single-phase utility voltage. E_{WATER} is the multiplication of the specific heat of water c_p, flow rate of the hot water L and the temperature difference between the hot water T_{OUT} and cold water T_{IN} temperatures.

A significantly lower loss is found during the experiment due to the aforementioned fact that the electric water heater was covered in a fiberglass insulation material. The fact that the average experimental energy loss with insulation was lower than the rated energy loss without added insulation proves the correctness of the experimental measurements and procedure.

2) Relationship between the energy input and thermal output

The relationship between the energy input and thermal output of the PVWH system is displayed in Figure 2.15 below.

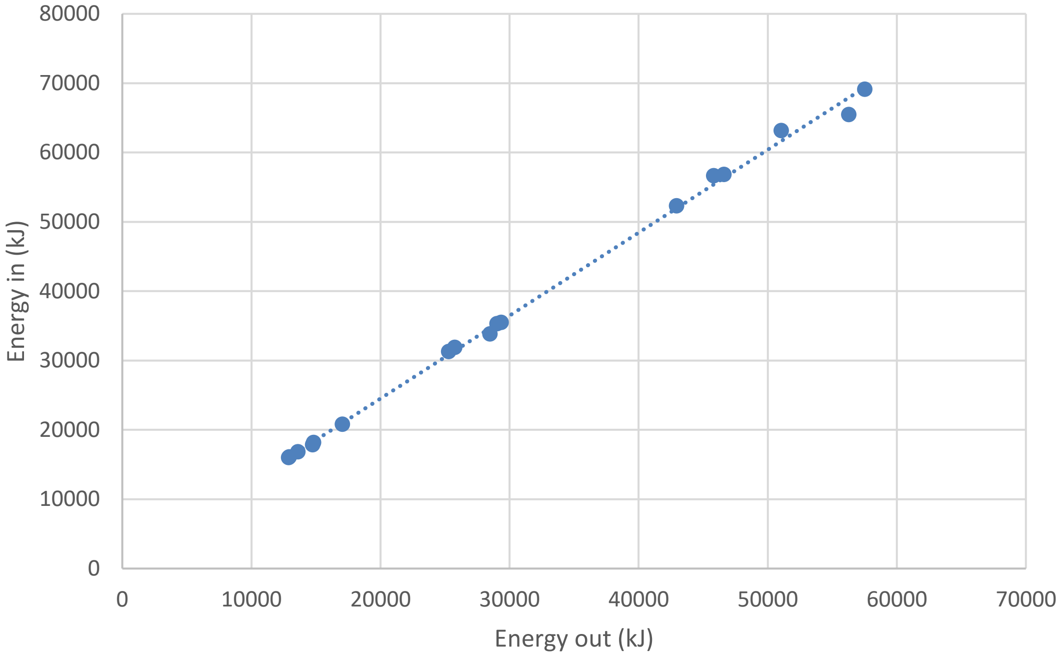

Figure 2.15: Linear relationship of PV system energy

The linearity of the input-output energy relationship serves as a validation of the energy balance taken across the PVWH system. A linear energy input-output relationship allows for the prediction of system performance under different demands. The relationship of the PVWH system presented in Figure 2.15 is however restricted to the timeframe and location in which it was calculated, as irradiance varies throughout the year. The relationship therefore only serves as a validation of the energy balance.

3) Utility grid input power saved

The PVWH system saved on average 65% of the grid input energy required over the respective cycles of the experiment, as shown in Table 2.8 below.

Table 2.8: PV utility grid input saved

Cycle	Timeframe	E_{GRID} [kJ]	E_{PV} [kJ]	Grid input saved
1	09 Febr - 10 Febr	4453.51	16344.42	79%
2	10 Febr - 11 Febr	4605.73	13246.42	74%
3	11 Febr - 12 Febr	5969.76	12201.37	67%
4	26 Febr - 27 Febr	5139.16	11696.00	69%
5	27 Febr - 28 Febr	5148.48	10920.97	68%
6	02 March - 03 March	8517.78	7460.22	47%
7	16 Febr - 18 Febr	11017.60	24262.71	69%
8	18 Febr - 20 Febr	14984.46	18854.81	56%
9	20 Febr - 22 Febr	11678.55	20192.22	63%
10	22 Febr - 24 Febr	10076.53	21227.40	68%
11	24 Febr - 26 Febr	8486.15	26984.70	76%
12	09 Febr - 12 Febr	15029.00	41792.20	74%
13	24 Febr - 27 Febr	13625.31	38680.70	74%
14	01 March - 04 March	18990.37	37654.36	66%
15	16 Febr - 20 Febr	26002.07	43117.52	62%
16	20 Febr - 24 Febr	21755.08	41419.62	66%
17	27 Febr - 02 March	42322.58	23137.37	35%
Average grid input saved:				65%

The percentage grid input saved was assessed by calculating the fraction of PV generated energy supplied in the total energy input per cycle:

$$\%=\frac{E_{PV}}{E_{PV}+E_{GRID}}\times 100 \qquad (2.12)$$

The average percentage is thus a rough estimation of the grid input that would have been required without the PV system. In the next section, the accuracy of the PVWH simulation model is validated. This is done by simulating the amount of PV energy generated and comparing the prediction against the actual experimental result. If found accurate, the PVWH simulation model can be applied to predict the amount of PV energy generated from any arbitrary irradiance.

2.4 Photovoltaic water heating model assessment

Figure 2.16 below presents the compared simulated and experimental results of each respective cycle over the course of the experiment.

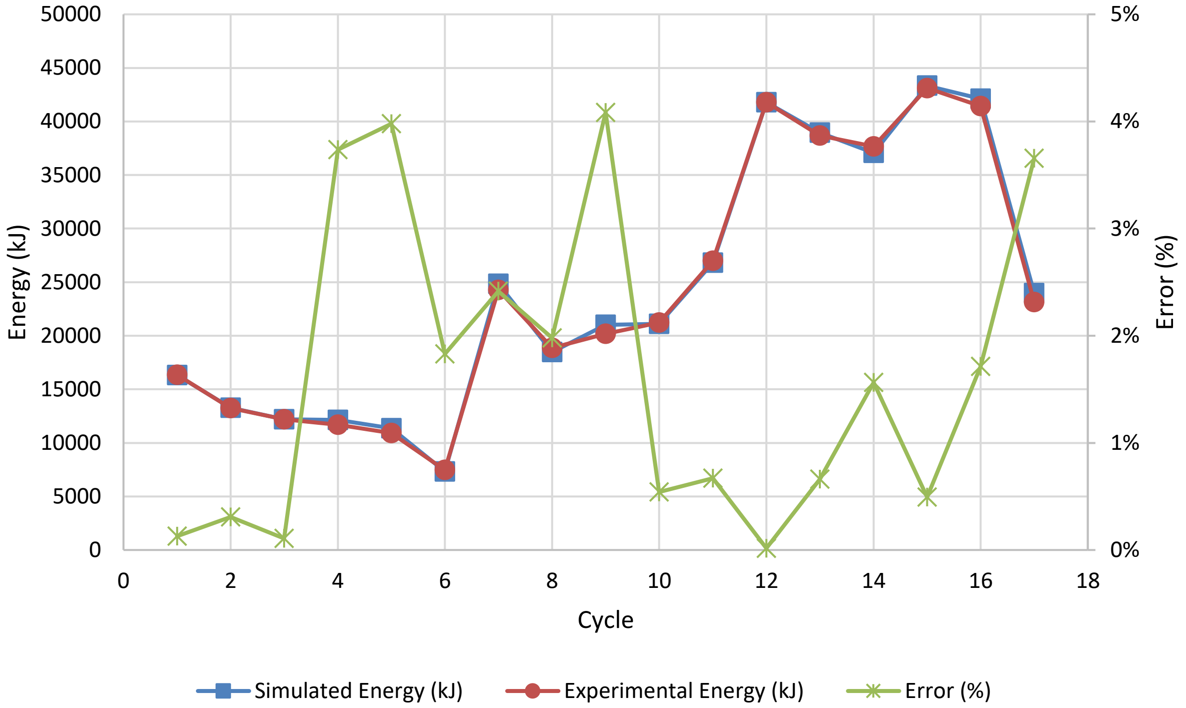

Figure 2.16: PV simulated vs experimental cycle energy results

The PV simulation model accurately predicted the amount of experimental PV generated energy utilized, with an average error of 1.64%, over all the respective cycles. The energy and prediction error values of each respective cycle are also listed in Table 2.9 below.

Table 2.9: PV simulated vs experimental cycle energy results

Cycles	Timeframe	Simulated Energy (kJ)	Experimental Energy (kJ)	Error (%)
1	09 Febr - 10 Febr	16323.51	16344.42	0.1279%
2	10 Febr - 11 Febr	13287.38	13246.42	0.3092%
3	11 Febr - 12 Febr	12188.09	12201.37	0.1088%
4	26 Febr - 27 Febr	12133.17	11695.99	3.7378%
5	27 Febr - 28 Febr	11355.58	10920.97	3.9796%
6	02 March - 03 March	7323.73	7460.22	1.8295%
7	16 Febr - 18 Febr	24848.98	24262.71	2.4163%
8	18 Febr - 20 Febr	18481.86	18854.81	1.9780%
9	20 Febr - 22 Febr	21016.99	20192.22	4.0846%
10	22 Febr - 24 Febr	21112.28	21227.39	0.5423%
11	24 Febr - 26 Febr	26803.64	26984.70	0.6710%
12	09 Febr - 12 Febr	41798.97	41792.20	0.0162%
13	24 Febr - 27 Febr	38936.81	38680.70	0.6621%
14	01 March - 04 March	37065.19	37654.36	1.5647%
15	16 Febr - 20 Febr	43330.84	43117.52	0.4947%
16	20 Febr - 24 Febr	42129.27	41419.62	1.7133%
17	27 Febr - 02 March	23983.14	23137.37	3.6554%

The error ranges from as little as 0.02% to the highest error of 4.08%. When comparing the cycle data of the lowest and highest error, a clear difference in the irradiance profile over the course of the cycle is observed. The cycle with the lowest prediction error had recorded overall high irradiance levels, reaching 1000W/m^2 in each day of the cycle. The highest prediction error was found during a cycle that included a day with a low averaging irradiance profile, peaking at an irradiance of approximately 700W/m^2. Their respective cycle data graphs are available in Annexure A Section A.4. It is thus clear that the inaccuracy of the PVWH model is increased on days with an overall lower level of irradiance. This finding is also in support of the statement by Lo Brano *et al.* (2010:1358), that the single diode model accuracy is dependent on high levels of solar irradiance.

The validation of the developed PV simulation model allows for the accurate prediction of PV generated energy under any arbitrary irradiance condition. An example with discussion of the exact energy prediction made by the model over a heating cycle is available in Annexure A Section A.5.

2.5 Mathematical model development

The setup and methodology of the mathematical model are discussed in this section. The mathematical model will incorporate the simulation model, described in Section 2.2, in order to determine the power generated from the solar irradiation profile of the climatic design year data. The setup, as well as the energy balance, of the mathematical model is illustrated in Figure 2.17 below.

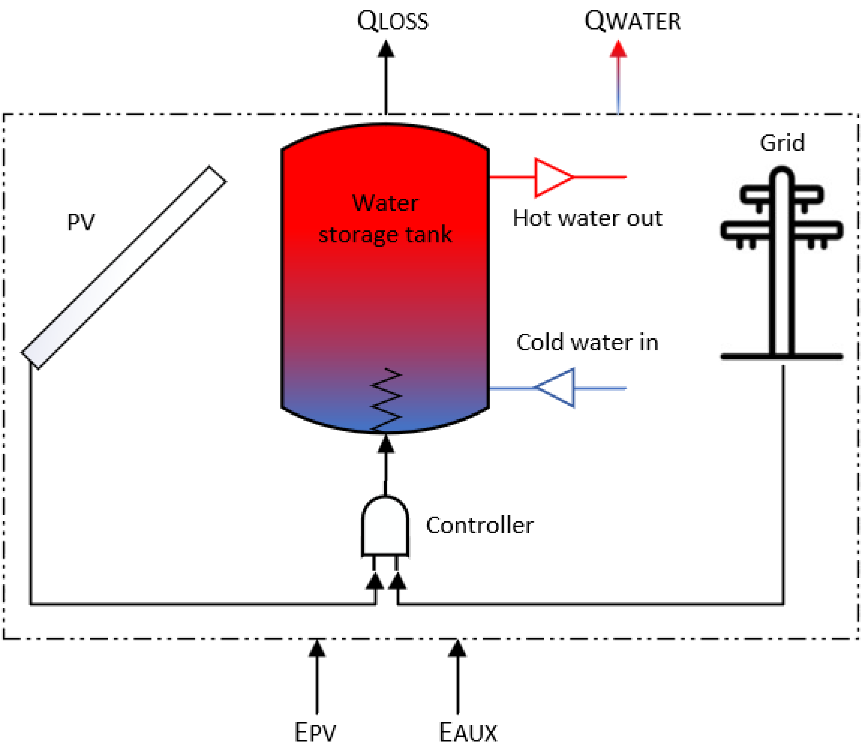

Figure 2.17: PVWH mathematical model setup and energy balance

The setup of the mathematical model is the same as the experimental layout discussed in Section 2.3.1. The energy balance of Figure 2.17 equates to:

$$U_{i-1} + E_{PV} + E_{AUX} = U_i + Q_{WATER} + Q_{LOSS} \quad (2.13)$$

U_{i-1} represents the internal energy of the water storage tank at the previous hour i-1. E_{PV} is the electrical energy generated by the PV array. E_{AUX} is the auxiliary electrical energy supplied by the utility grid and utilized by the electric water heater as backup. U_i represents the internal energy of the water storage tank at the current hour i after heating has occurred through either E_{PV} or E_{AUX} (depending on the time of day). Q_{WATER} represents the change in thermal energy within the water storage tank due to the simultaneous consumption and replenishment of the water storage tank volume. It is thus also the thermal energy required to heat the water. Q_{LOSS} is the standing loss of the water storage tank, indicating the amount of heat lost to the environment surrounding the water storage tank.

In order to predict the operational costs of PVWH, the amount of auxiliary energy supplied by the grid must be determined. The amount of auxiliary energy utilized is dependent on the amount of thermal energy required to heat the water, as well as to compensate for the standing loss of the storage tank, minus the amount of energy generated by the PV array.

In order to determine the amount of auxiliary energy utilized to provide the thermal energy required to heat the water, the temperature of the water in the storage tank must be determined. Equation (2.13) above is thus derived in order to express it in terms of temperatures. Note that the derivation equations that follow will not be given equation numbers, as they are not directly applied in the mathematical model, simply used for explanation purposes.

The derivation of the energy balance follows as:

$$mc_p Tt_{i-1} + E_{PV} + E_{AUX} = mc_p Tt_i + mc_p \left(T_{out} - T_{inlet}\right) + Q_{LOSS}$$

Firstly, each term in Equation (2.13) is fully expressed. Each term has already been explained and is available in Table 1.2. After heating has occurred through either E_{PV} or E_{AUX}, the new internal state of the water storage tank is given by the current hour tank temperature Tt_i. Q_{WATER} is expressed as the change in temperature due to water being consumed at temperature T_{out} and simultaneously being refilled with inlet water at temperature T_{inlet}, given in Table 1.2.

The temperature at which water is consumed T_{out} is equal to the temperature of the water storage tank at the current hour Tt_i. The equation can be further simplified by dividing the mass volume and specific heat product:

$$Tt_{i-1} + \frac{E_{PV}}{mc_p} + \frac{E_{AUX}}{mc_p} = Tt_i + \left(Tt_i - T_{inlet}\right) + \frac{Q_{LOSS}}{mc_p}$$

By doing so, the terms E_{PV}, E_{AUX} and Q_{LOSS} are expressed in terms of their temperature difference:

$$Tt_{i-1} + \Delta T_{PV} + \Delta T_{AUX} = Tt_i + \left(Tt_i - T_{inlet}\right) + \Delta T_{LOSS}$$

Finally, the term (Tt_i - T_{inlet}) is substituted as the change in temperature due to consumption $\Delta T_{\dot{m}}$:

$$Tt_{i-1} + \Delta T_{PV} + \Delta T_{AUX} = Tt_i + \Delta T_{\dot{m}} + \Delta T_{LOSS} \quad \textbf{(2.14)}$$

The temperature of the water in the storage tank is thus dependent on 1) the change in temperature due to the input of the PV generated energy ΔT_{PV}, 2) the change in temperature due to the auxiliary grid input of the electric water heater ΔT_{AUX}, 3) the change in temperature due to consumption $\Delta T_{\dot{m}}$ and 4) the change in temperature due to the standing loss ΔT_{LOSS}. The respective terms of Equations (2.13) and (2.14) are discussed in the following subsection.

2.5.1 PVWH energy balance terms

The PVWH simulation model is used to determine the power generated from the tilted solar irradiation profile, calculated from the horizontal solar irradiation profile given by the climatic design year data. The amount of energy generated by the PV array, E_{PV}, is determined by Equation (2.15) below.

$$E_{PV} = P_{SI} \times \frac{3600}{1000} \tag{2.15}$$

P_{SI} is the power generated by the PV array in watt and simulated per hour, in accordance with the climactic design year data format. As proposed by PowerOptimal, a supplier of solar PV water heating solutions, the retrofit of a PV solar system without maximum power point tracking (MPPT) to an existing 200L electric water heater and with the consumption applied in this study, requires a maximum power output of 1.8kW from the PV array. Mentioned in the introduction of Section 2.2, the PV simulation model was created using four 300W PV panels connected in series, producing an array power output of 1.2kW. To achieve the proposed power output of 1.8kW, the simulation model is simply adapted to include two more PV panels, totalling an array of six panels connected in series. This is achieved by simply multiplying the open circuit voltage V_{OC} of the PV module with six instead of four. Finally, E_{PV} is determined by multiplying P_{SI} by 3.6 in order to determine the amount of energy generated in kJ per hour.

The change in temperature due to the PV generated energy is given by Equation (2.16) below.

$$\Delta T_{PV} = \frac{E_{PV}}{c_p Vt} \tag{2.16}$$

The PV generated energy E_{PV} is divided by the specific heat of water c_p and the volume of the water storage tank Vt. The change in temperature due to the auxiliary electrical grid energy utilized by the electric water heater as backup is given by Equation (2.17) below.

$$\Delta T_{AUX} = \frac{E_{AUX}}{c_p Vt} \tag{2.17}$$

The change in temperature due to consumption and standing loss are respectively given by Equation (2.18) and Equation (2.19) below.

$$\Delta T_{\dot{m}} = Tt_{i-1} - \frac{Tt_{i-1}\left(Vt - V_i\right) + T_{inlet} V_i}{Vt} \tag{2.18}$$

The change in temperature due to consumption is caused by the amount of cold water entering the storage tank to replace the amount consumed. The term Tt_{i-1} $(Vt - V_i)$ represents the volume of water remaining after consumption at the previous tank temperature Tt_{i-1}. Note that although Tt_i was shown in the derivation, Tt_i after consumption in the current hour becomes Tt_{i-1} that will be used for the next hour Tt_i. $T_{inlet}V_i$ represents the amount of water entering the storage tank to replace the consumed amount at the temperature T_{inlet}. By dividing the sum of these terms by the total volume of the storage tank Vt, the new tank temperature is determined and subtracted from the previous tank temperature Tt_{i-1} to give the change in temperature due to consumption.

The change in temperature due to the standing loss, given by Equation (2.19) below, is caused by the transfer of heat from the storage tank to its environment and is assumed constant at the rated loss of the electric water heater.

$$\Delta T_{LOSS} = \frac{Q_{LOSS}}{c_p Vt} \tag{2.19}$$

All terms of Equation (2.19) have already been discussed in Table 1.2.

2.5.2 PVWH control methodology

This section will discuss the control methodology of the PVWH mathematical model. The model contains a number of IF conditions and accompanying equations, which can be referred to in Annexure A Section A.6. The control methodology will discuss the different temperature and energy control methodologies throughout the following points. Lastly, the methodology for the determination of the annual operational costs and simple payback period is discussed.

i. Auxiliary grid input

The auxiliary grid input is controlled by a timer. The timer will activate grid power input roughly two hours before sunrise (4h, 5h) and two hours after sunset (18h, 19h). This is done to ensure the adequate supply of hot water during the peak consumption hours of the day.

ii. Maximum and minimum setpoint temperatures

The maximum temperature of the water storage tank is set to 65°C (Tt_{maxPV}) when utilizing PV generated energy and set to 55°C (Tt_{maxAUX}) when utilizing auxiliary energy. The higher PV setpoint is simply to take advantage of the storage capacity when heating with solar power during limited solar time. The minimum temperature setpoint is 0°C in both cases to ensure that there is no auxiliary backup from the grid during solar time, and that the dependency of PVWH on solar irradiation is rightfully considered.

iii. Solar photovoltaic heat input

During solar time, the temperature of the water in the storage tank is subject to changes caused by consumption, the heat input from the PV generated energy and the standing loss.

The PV generated energy may heat the water up to its maximum PV temperature of 65°C. If no PV energy is generated during solar time, the temperature of the water may continually decline.

iv. Auxiliary heat input

During the timed grid input hours, the auxiliary heat input ensures that the water in the storage tank is heated and maintained at the maximum grid temperature of 55°C. From the auxiliary heat input, the amount of auxiliary electrical energy utilized in order to provide the thermal energy required to heat the water Q_{WATER} can be determined.

v. Annual operation costs and simple payback period

The yearly sum of auxiliary electrical grid energy required in order to provide the thermal energy required to heat the water is given by Equation (2.20) below

$$E_{REQUIRED} = \sum_{1}^{8760} Q_{WATER} \tag{2.20}$$

The amount of electrical grid energy required is thus simply the sum of Q_{WATER} over all 8760 hours of a year. The annual operational costs R_{PVWH} in R/year is given by Equation (2.21) below.

$$R_{PVWH} = \frac{E_{REQUIRED}}{3600} \times R_{kWh} \tag{2.21}$$

R_{PVWH} is thus equal to the yearly amount of electrical grid energy required, divided by 3600 (converting kJ to kWh) and multiplied with the cost of electricity R_{kWh} in R/kWh. Finally, the simple payback period (SPP) is calculated using Equation (2.22) below.

$$SPP = \frac{R_{capital}}{R_{saved}} \tag{2.22}$$

Where $R_{capital}$ is the capital cost of the retrofitted system, including installation and VAT. R_{saved} is the annual savings relative to the annual operational costs of the baseline. The capital cost of a retrofitted system, including installation lies between R22295 and R25572 (including VAT). It is assumed that all water heating systems are bought up front and that there is no financing cost applicable. Quotations were requested from three different suppliers. Geyserobot quoted their 4 kVa Smart PV system with a total surface area of 4.8m^2. PowerOptimal quoted their Elon 100, 1.8kWp PV system. Geyserwise quoted their 200L PV water heating system for low irradiation areas.

Given the input parameters of the mathematical model as listed in Table 1.2 and those explained in this section, the model results are determined and discussed in the next section.

2.6 Results and discussion

The final results are listed in Table 2.10 below.

Table 2.10: PVWH cost results

Symbol	Result	Value	Unit
R_{PVWH}	PVWH operational costs	2922	R/year
R_{EWH}	Baseline EWH operational costs	7933	R/year
R_{SAVED}	Annual savings relative to baseline	5011	R/year

The estimated annual operational costs of PVWH per household is R2922. This does however not include maintenance costs as maintenance on PV panels are assumed neglectable. This is compared to the estimated annual operational costs of the baseline electric water heater R_{EWH} per household of R7933. PVWH thus results in an annual savings of R5011. An average capital cost of R23431 is used to determine the SPP of the PVWH system. The SPP of PVWH, based on the average capital cost and annual savings, is 4.68 years. The SPP can also vary between 4.45 and 5.1 years, based in the capital cost of different suppliers.

In terms of performance, Table 2.11 below indicated the amount of energy required from the grid for PVWH and EWH.

Table 2.11: PVWH grid energy required

Symbol	Result	Value	Unit
E_{PVWH}	PVWH auxiliary grid energy required	1328.12	kWh/year
E_{EWH}	Baseline EWH grid energy required	3605.79	kWh/year

The results indicate that PVWH, as applied in this study, saved 63.17% of the utility grid input required for EWH.

This concludes the PVWH chapter, with the focus now moving to solar thermal water heating. The techno-economical comparison of the different water heating technologies will be presented and discussed in the final chapter.

CHAPTER 3 – SOLAR THERMAL WATER HEATING

The goal of this chapter is to develop a mathematical model that will accurately predict the performance and cost of solar thermal water heating (STWH). A STWH system is mainly categorised by the type of solar collector used, of which there exists four different types (Hohne et al., 2019:4). This study will only focus on flat plate and evacuated tube collectors. The performance, capital and operational costs of STWH vary between the different types of solar collectors and their efficiencies. The efficiency of a solar collector is dependent on environmental and operational conditions, as indicated by its efficiency curve. The efficiency curve and system specifications of both the flat plate and evacuated tube solar collectors will be obtained from reputable suppliers.

Chapter 3 will entail: a literature study focussing on the working principles of a STWH system, the respective solar collectors used and the factors affecting the efficiency of a solar collector; the development of the STWH mathematical model and finally a discussion of the results.

3.1 Literature study

The literature study will discuss the relevant working principles of a solar thermal water heater, the flat plate and the evacuated tube solar collector. Lastly, the different factors affecting the efficiency of a solar collector will be discussed.

3.1.1 Working principles of a solar thermal water heater

A STWH system is mainly categorised by its type of solar collector. A STWH system is further categorised as an active or passive system. An active system uses forced circulation, meaning the fluid is pumped (Hohne et al., 2019:4). A passive system relies on the thermosiphon phenomena for the natural circulation of water (Hohne et al., 2019:4). Active systems are also subdivided as an open (direct) or closed (indirect) loop. An open loop is the direct circulation and heating of the water, whereas a closed loop refers to indirect heating of the water through the use of a working fluid and heat exchanger within the water storage tank (Hohne et al., 2019:4). Note that, as illustrated by Figure 3.1 below, this study will focus on an active, direct flat plate system and an active, indirect evacuated tube system.

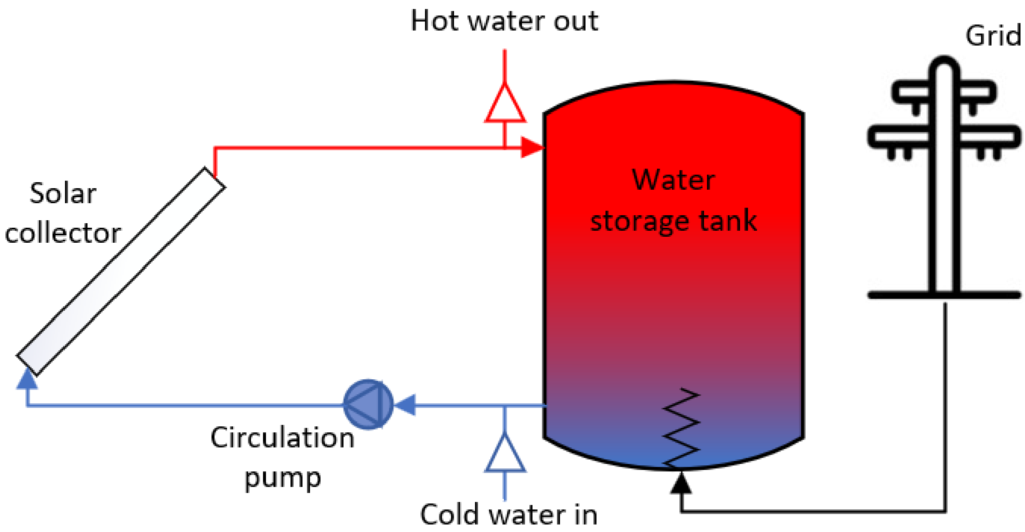

Figure 3.1: STWH cycle schematic

The basic working principle of a solar thermal water heater, as shown in Figure 3.1 above, are as follows. A STWH system consists of a water storage tank, solar collector and circulation pump. Water is pumped from the storage tank, through a solar collector and back into the tank. A solar collector absorbs solar radiation and converts it into thermal energy in order to heat the water circulating through it (Hohne et al., 2019:4). As with PVWH, STWH is also dependent on solar radiation and good weather conditions. During unfavourable condition, utility grid power ensures the supply of hot water as required.

3.1.1.1 Flat plate soar collector

A flat plate solar collector is shown in Figure 3.2 below.

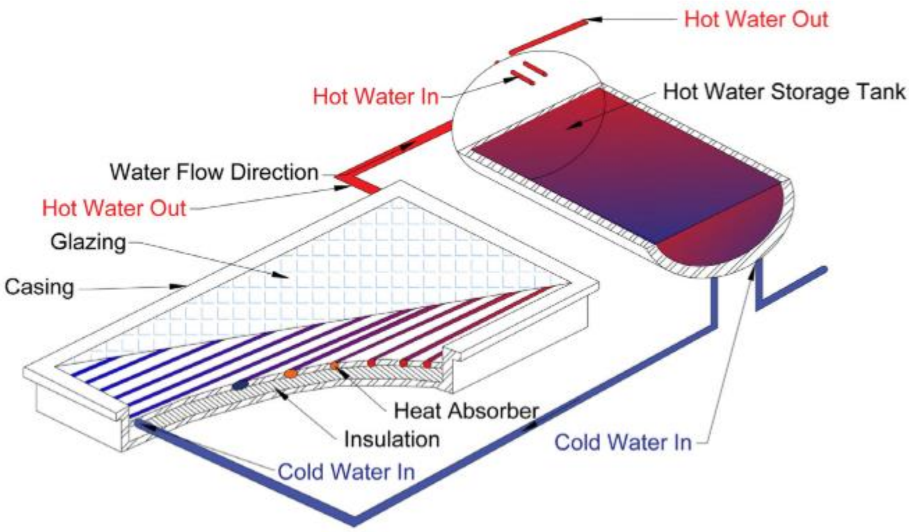

Figure 3.2: Flat plate solar collector (Hohne et al., 2019:5)

A flat plate solar collector consists of an insulated casing, absorber plate, fluid circulation piping and a glazed cover. High frequency solar radiation penetrates the glazed cover and is absorbed by the heat absorbing plate (Hohne et al., 2019:4). The glazed cover prevents the escape of low frequency radiation from the absorber plate (Dobriyal *et al.*, 2020:1653). Along with the insulated casing, the glazed cover also reduces heat loss caused by environmental condition (Dobriyal *et al.*, 2020:1653). The solar radiation is converted into thermal energy by the heat conductive absorber plate and transferred to the water flowing through the collector (Hohne et al., 2019:4). The circulation piping is either an integral part of the absorber plate or simply attached (Dobriyal *et al.*, 2020:1653).

3.1.1.2 Evacuated tube solar collector

An evacuated tube solar collector is shown in Figure 3.3 below.

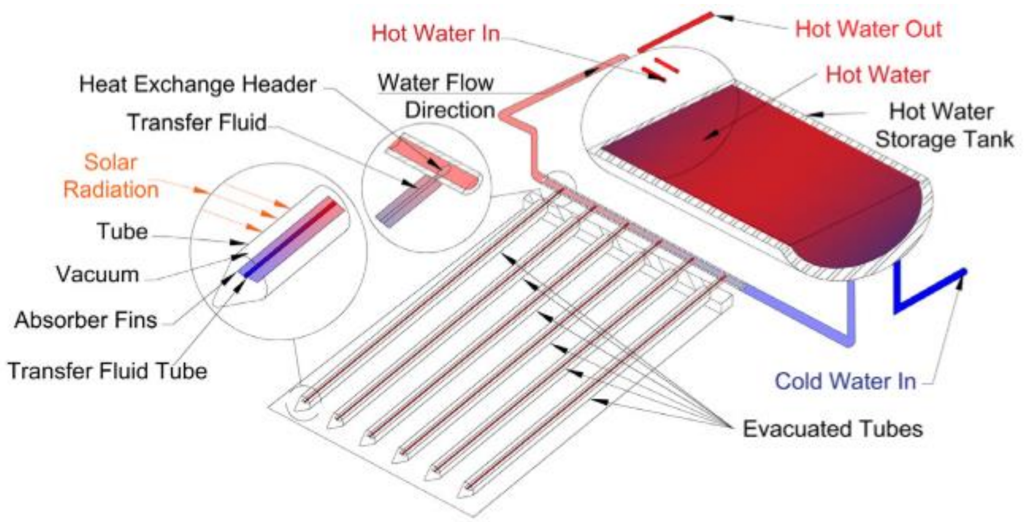

Figure 3.3: Evacuated tube solar collector (Hohne et al., 2019:6)

The evacuated tube solar collector consists of a vacuum insulated glass tube casing, heat absorber, heat pipe containing a working fluid and an insulated manifold. Solar radiation penetrates the outer glass tubing and is absorbed by the absorber plate and heat pipe (Hohne et al., 2019:4). The heat pipe transfers the thermal energy to the working fluid, which evaporates and rises to the heat pipe heat exchanger head (Hohne et al., 2019:4). The heat exchanger head of the heat pipe is held within the manifold (Hohne et al., 2019:4). Water is circulated through the manifold from the water storage tank and the thermal energy is transferred from the heat exchanger head to the water, thus heating the water (Hohne et al., 2019:4). The vapor inside the heat pipe head is condensed and flows back to the bottom of the heat pipe (Hohne et al., 2019:4).

3.1.2 Factors affecting the efficiency of a solar collector

The factors affecting the efficiency of a solar collector can be categorised as: 1) the type of solar collector, 2) environmental and 3) operational conditions (Diez *et al.*, 2019:1320). The factors related to these categories are discussed in the respective subsections that follow. Referring to the type of solar collector, note that there is a vast number of component level design specifications that has an effect on the efficiency of a solar collector (Diez *et al.*, 2019:1323). Shukla *et al.* (2013) presented a detailed summary on the effect of different design specification on the efficiency of a solar collector and also listed the advantages and disadvantages of the different specifications. These component level factors are however only mentioned as they are not relevant to the current study.

3.1.2.1 Type of solar collector

The different working principles of a flat plate and evacuated tube results in a significant difference in solar collector efficiency. Ayompe *et al.* (2011:3377) found that the annual average solar collector efficiency and the system efficiency of an evacuated tube solar collector was respectively 14.6% and 12.4% greater than that of a flat plat solar collector. One of the main reasons an evacuated tube is more efficient, is due to its cylindrical shape which is capable of passively tracking the sun (Mangal *et al.*, 2010:283). Another reason is due to the vacuum insulated glass tube casing of the evacuated tube, which is less susceptible to heat loss caused by environmental conditions (Mangal *et al.*, 2010:279). Although a flat plate solar collector is less efficient, it is still capable of heating water up to a temperature of 80°C (Hohne et al., 2019:4).

3.1.2.2 Environmental conditions

Environmental conditions refer to a) the incident solar radiation per unit area of the solar collector and b) the ambient temperature.

a) Solar radiation

The efficiency is significantly dependent on the amount of solar radiation absorbed and useful thermal energy generated by a solar collector (Ge *et al.*, 2014:2563). The amount of useful thermal energy generated increases as solar radiation increases (Ge *et al.*, 2014:2563). The amount of solar radiation absorbed by a solar collector is also dependent on its placement, orientation and tilt angle, as previously discussed in Chapter 1 Section 1.6 (Hohne et al., 2019:4).

b) Ambient temperature

The efficiency of a solar collector increases as the ambient temperature increases (Ge *et al.*, 2014:2563). This is simply due to less heat being lost to the surrounding environment of the solar collector.

3.1.2.3 Operational conditions

The operational conditions refer to c) the average temperature of the solar collector and d) the water flow rate through the collector.

c) Average solar collector temperature

According to the EN 12975 standard, the average temperature of a solar collector is determined by the average of the inlet and outlet temperatures of the water flowing through the solar collector (Seco-Nicolás et al., 2020:1). In order to evaluate this standard, Seco-Nicolás et al. (2020) experimentally calculated the actual average temperature of a flat plate solar collector absorber plate. Seco-Nicolás et al. (2020) found a 5% difference between the actual average solar collector temperature and the average temperature of the water flowing through it. This led to the conclusion that the EN 12975 standard provided sufficient accuracy for general purpose use (Seco-Nicolás et al., 2020:1).

When analysing the effect of the average water temperature on the efficiency of a solar collector, most studies simply considering the inlet water temperature (Struckmann, 2008; Farahat et al., 2009; Jafarkazemi & Ahmadifard, 2013; Ge *et al.*, 2014). An increase in the inlet water temperature leads to a decrease in the efficiency of a solar collector (Jafarkazemi & Ahmadifard, 2013:62). As the difference between the water and ambient temperature increases, the amount of heat that can be lost to the environment increases, thus lowering the efficiency of the solar collector (Jafarkazemi & Ahmadifard, 2013:61).

d) Water flow rate

The efficiency of a solar collector increases as the flow rate of the water through the collector increases (Diez *et al.*, 2019:1325). A higher flow rate results in a smaller difference between the inlet and outlet temperatures of the water, meaning less heat is transferred from the solar collector to the water (Jafarkazemi & Ahmadifard, 2013:61).

The next section will discuss the development of the mathematical model. The four factors a, b, c and d will be applied in order to determine the efficiency of the respective solar collectors and predict the overall performance of the STWH systems.

3.2 Mathematical model development

This section presents the development of the mathematical model by discussing its setup, assumptions and methodology. The solar collector, circulation pump and the water storage tank are treated as a black-box. The energy balance method is applied on the STWH system, as illustrated in Figure 3.4 below.

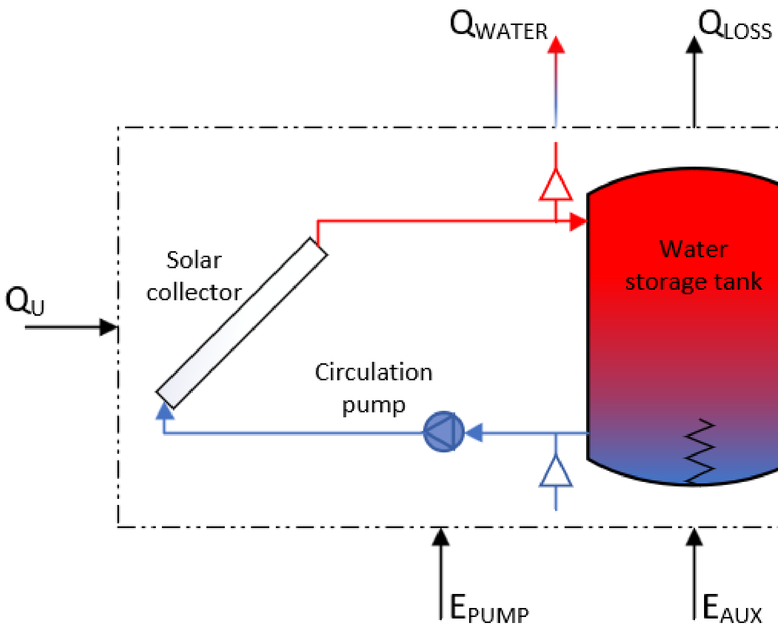

Figure 3.4: STWH mathematical model setup and energy balance

As shown in Figure 3.4 above, cold water enters the storage tank and is continuously circulated through the solar collector via a circulation pump, where it is heated before being pumped back into the storage tank. The resistive heating element of the water storage tank utilized power from the utility grid in order to heat the water if the solar power is insufficient. The energy balance of Figure 3.4 equates to:

$$U_{i-1} + Q_U + E_{PUMP} + E_{AUX} = U_i + Q_{WATER} + Q_{LOSS} \quad (3.1)$$

Similar to the energy balance equation pf the PVWH system, $U_{i\text{-}1}$ represents the internal energy of the water storage tank at the previous hour i-1. Q_U is the useful thermal energy generated by the solar collector. E_{PUMP} is the electrical energy utilized by the circulation pump. E_{AUX} is the auxiliary electrical energy supplied by the utility grid and utilized by the electric water heater as backup. Q_{WATER} represents the change in thermal energy within the water storage tank due to the simultaneous consumption and replenishment of the water storage tank volume. It is thus also the thermal energy required to heat the water. Q_{LOSS} is the standing loss of the water storage tank, indicating the amount of heat lost to the environment surrounding the water storage tank.

In order to predict the operational costs of STWH, the amount of auxiliary energy supplied by the grid must be determined. The amount of auxiliary energy utilized is dependent on the amount of thermal energy required to heat the water, as well as to compensate for the standing loss of the storage tank, minus the amount of useful thermal energy generated by the solar collector.

In order to determine the amount of auxiliary energy utilized to provide the thermal energy required to heat the water, the temperature of the water in the storage tank must be determined. Equation (3.1) is thus derived in the same manner as explained in the Section 2.5, resulting in Equation (3.2) below.

$$Tt_{i-1} + \Delta T_U + \Delta T_{AUX} = Tt_i + \Delta T_{\dot{m}} + \Delta T_{LOSS} \tag{3.2}$$

The temperature of the water in the storage tank at the end of the hour Tt_i is thus dependent on 1) the change in temperature due to the input of the useful thermal energy ΔT_U, 2) the change in temperature due to the auxiliary grid input of the electric water heater ΔT_{AUX}, 3) the change in temperature due to consumption $\Delta T_{\dot{m}}$ and 4) the change in temperature due to the standing loss ΔT_{LOSS}. The respective terms of Equations (3.1) and (3.2) are discussed in the following subsection.

3.2.1 STWH energy balance terms

The amount of useful thermal energy that a solar collector can generate is determined by its efficiency. In order to determine the efficiency of a solar collector, a number of studies employ the Hottel-Whillier-Bliss equation (Struckmann, 2008; Jafarkazemi & Ahmadifard, 2013; Ge *et al.*, 2014; Lee & Baek, 2014; Ranjith & Karim, 2016; Alberto & Ferrer, 2017). In this study however, the efficiency of the solar collectors will be determined directly from their efficiency curves, as obtained from reputable suppliers. The efficiency curve of the flat plate solar collector was obtained from Chromagen and is publicly available (Chromagen, 2020:12). The efficiency curve of the evacuated tube solar collector was requested and obtained from a reputable South African supplier (who wishes to stay anonymous). The flat plate and evacuated tube solar collector efficiency curves are both shown in Figure 3.5 below.

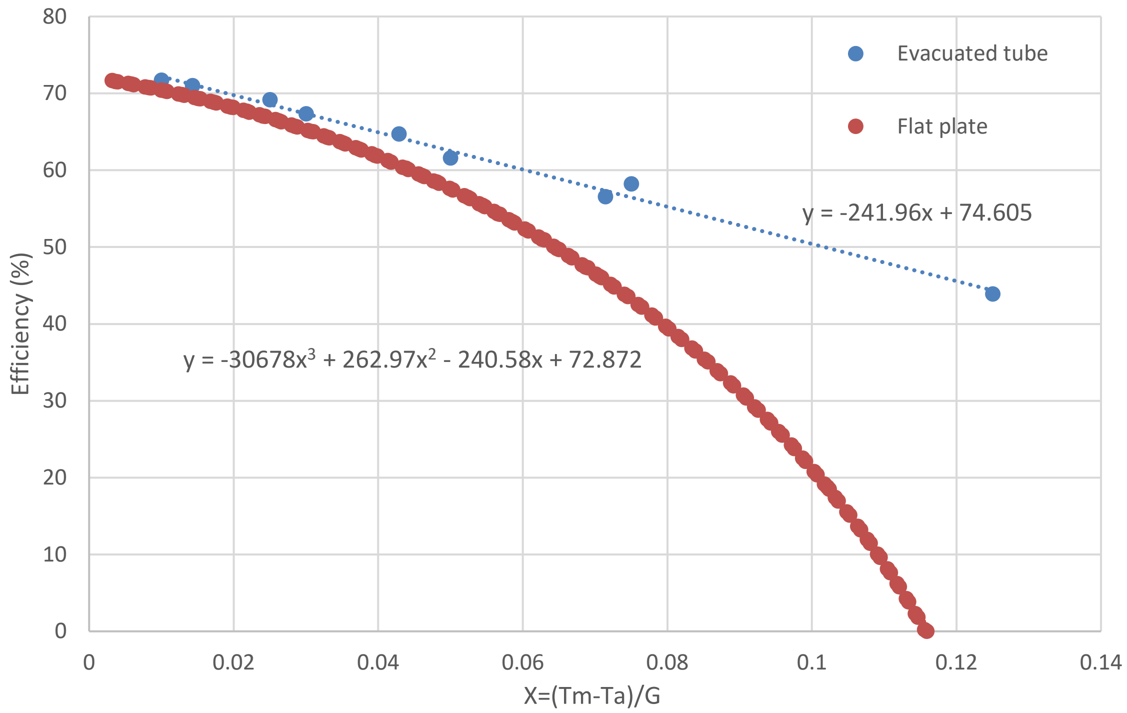

Figure 3.5: Flat plate (red) and evacuated tube (blue) solar collector efficiency curve (Chromagen, 2020:12)

The flat plate solar collector efficiency curve was plotted using WebPlotDigitizer and a 3rd order polynomial trendline was applied in order to determine the curve equation as shown in Figure 3.5 above. The evacuated tube solar collector efficiency curve was plotted from data supplied directly from the supplier. A linear trendline was applied in order to determine the curve equation as shown in Figure 3.5 above. The flat plate and evacuated tube solar collector efficiency curve equations are respectively represented by Equation (3.3) and Equation (3.4) below.

$$\eta = -30678X^3 + 262.97X^2 - 240.58X + 72.872 \quad (3.3)$$

$$\eta = -241.96X + 74.605 \quad (3.4)$$

The factor X is determined by Equation (3.5) below.

$$X = \frac{T_m - T_a}{G} \quad (3.5)$$

T_m is the average solar collector temperature, T_a the ambient temperature and G the solar irradiation. The ambient temperature conditions are given by the climatic design year data, as discussed in Section 1.6.1. The solar irradiation incident on the tilted surface of the solar collector is calculated from the horizontal solar irradiation profile, also given by the climatic design year data. The average solar collector temperature is given by Equation (3.6) below.

$$T_m = \frac{Tc_{in} - Tc_{out}}{2} \tag{3.6}$$

The average solar collector temperature is thus equal to the average of the inlet Tc_{in} and outlet Tc_{out} of the water flowing through the solar collector. While an initial Tc_{in} can be chosen, the outlet temperature Tc_{out} is dependent on the flow rate of the water and the amount of useful thermal energy available, which is also dependent on the efficiency of the solar collector. Several studies aimed to simulate the outlet temperature of the solar collector. Kicsiny (2014) developed a multiple linear regression model and Diez *et al.* (2019) developed an artificial neural network (ANN) model in order to determine the outlet temperature. These simulation methods are however rather complex and time consuming (Kicsiny, 2014:497). Another approach, as followed by Alberto and Ferrer (2017:509), is to simply assume an average daily efficiency based on perfect solar collector conditions.

In this study, the average solar collector temperature T_m will be assumed equal to the tank temperature of the previous hour Tt_{t-1}, changing Equation (3.5) to:

$$X_i = \frac{Tt_{i-1} - T_a}{G} \tag{3.7}$$

Equation (3.7) above thus provides a current hour factor X_i, which is determined by the tank temperature of the previous hour, along with the ambient temperature and solar irradiation of the current hour. In order to support this assumption, it will also be assumed that the flow rate of the water through the collector is relatively high. A high flow rate causes a smaller temperature difference between the inlet and outlet of the solar collector, resulting in an average solar collector temperature that is closer in value to that of the tank temperature. The high flow rate value of the water is assumed to be equal to that required in order to circulate the entire volume of the water storage tank within the modelled hour.

By substituting Equation (3.7) into Equation (3.3) and (3.4), the hourly efficiency of the solar collectors can be determined. The hourly useful thermal energy generated by the solar collectors is given by Equation (3.8) below.

$$Q_U = \eta A_c G \tag{3.8}$$

The product A_cG is the solar irradiation G incident on the aperture area A_c of the solar collector. The aperture areas of the flat plate and evacuated tube solar collector are $2.14m^2$ and $1.86m^2$ respectively. According to suppliers, the specific areas are required when these systems are retrofitted to an existing 200L electric water heater. On its own, the term A_cG thus represents the amount of solar power available to the solar collector. It is multiplied with the efficiency η in order to determine the amount of useful thermal energy generated by the solar collector. Q_U is also multiplied with 3.6 in order to convert it from W to kJ/h. Finally, the change in temperature due to the input of the useful thermal energy ΔT_U can be determined by Equation (3.9) below.

$$\Delta T_U = \frac{Q_U}{c_p Vt} \tag{3.9}$$

The change in temperature due to the useful thermal energy is thus equal to the useful thermal energy divided by the product of the specific heat of water c_p and the volume of the storage tank Vt as listed in Table 1.2. The volume of the storage tank is applied due to the flow rate assumptions made. With the amount of useful thermal energy and its change in temperature known, the amount of auxiliary energy utilized in order to provide the thermal energy required to heat the water can be determined.

3.2.2 STWH control methodology

Note that the control methodology (referring to the timed auxiliary input, minimum and maximum temperatures and heat inputs) of the STWH mathematical model is identical to the PVWH mathematical model discussed in Section 2.5.2. The exact same IF conditions and accompanying equations (refer to Annexure A Section A.6) is applied while simply substituting ΔT_{PV} with ΔT_U. The only addition to the methodology is the determination of the electrical energy utilized by the circulation pump E_{PUMP}.

A 12V DC pump with a nominal power of 7.5W is modelled (GeyserWise, 2020). A temperature differential control circuit is applied in order to determine the pump operation (Hohne et al., 2019b:275):

If there is useful thermal energy:

$$E_{PUMP} = P_{cp} \times \frac{3600}{1000} \tag{3.10}$$

The condition states that if there is a temperature difference within the solar collector, the pump is switched on. This control strategy ensures that the pump is off during the absence of solar irradiation (Hohne et al., 2019b:275). The electrical energy utilized by the circulation pump is equal to the nominal pump power P_{cp} multiplied by 3.6, converting W to kJ/hour. Finally, the yearly sum of auxiliary and pump energy utilized in order to provide the thermal energy required to heat the water $E_{REQUIRED}$ is given by Equation (3.11) below.

$$E_{REQUIRED} = \sum_{1}^{8760} \left(Q_{WATER} + E_{PUMP} \right) \tag{3.11}$$

The amount of electrical energy required is thus simply the sum of Q_{WATER} and E_{PUMP} over all 8760 hours of a year. The annual operational costs R_{STWH} in R/year is given by Equation (3.12) below.

$$R_{STWH} = \frac{E_{REQUIRED}}{3600} \times R_{kWh} \tag{3.12}$$

R_{STWH} is thus equal to the yearly amount of electrical grid energy required, divided by 3600 (converting kJ to kWh) and multiplied with the cost of electricity R_{kWh} in R/kWh. Equation (2.22) is also applied to determine the SPP of both the flat plate and evacuated tube solar thermal water heaters.

The capital cost of a retrofitted system, including installation, for a flat plate solar thermal water heating system lies between R14265 and R20239 (including VAT). The capital cost of a retrofitted system, including installation, for an evacuated tube solar thermal water heating system lies between R18050 and R25740 (including VAT). Quotations were requested from two different suppliers. ITS Solar quoted their 2.4m^2 flat plate collector and 20 pipe evacuated tube collector. NuPower Solar quoted their 200L flat plate system and 24 evacuated tube solar collector.

Given the input parameters of the mathematical model as listed in Table 1.2 and those explained in this section, the model results are determined and discussed in the next section.

3.3 Results and discussion

The final results for the flat plate and evacuated tube solar thermal water heaters are listed in Table 3.1 below.

Table 3.1: STWH cost results

Symbol	Result	Value	Unit
R_{EWH}	Baseline EWH operational costs	7933	R/year
	Flat plate		
R_{STWH}	STWH operational costs	3357	R/year
R_{SAVED}	Flat plate annual savings relative to baseline	4576	R/year
	Evacuated tube		
R_{STWH}	STWH operational costs	3328	R/year
R_{SAVED}	Evacuated tube annual saving relative to baseline	4606	R/year

The estimated annual operational costs of STWH per household when using a flat plate solar collector is R3357. The estimated annual operational costs of STWH per household when using an evacuated tube solar collector is R3328. Relative to the baseline R_{EWH} of R7933, the annual savings for the flat plate and evacuated tube solar collectors are R4576 and R4606 respectively. An average capital cost of R17252 and R21895 is used to respectively determine the SPP for the flat plate and evacuated tube solar collectors.

The SPP for the flat plate and evacuated tube solar collectors, based on the average capital cost, is 3.77 and 4.75 years respectively. The SPP can also vary between 3.12 and 4.42 years for a flat plate solar thermal system. For an evacuated tube solar thermal system, the SPP can vary between 3.92 and 5.59 years. This is based on the capital cost of the different suppliers.

In terms of performance, Table 3.2 below indicated the amount of energy required from the grid for STWH and EWH.

Table 3.2: STWH grid energy required

Symbol	Result	Value	Unit
E_{FP}	Flat plate auxiliary grid energy required	1525.82	kWh/year
E_{ET}	Evacuated tube auxiliary grid energy required	1512.40	kWh/year
E_{EWH}	Baseline EWH grid energy required	3605.79	kWh/year

The results indicate that flat plate and evacuated tube STWH, as applied in this study, respectively saved 57.68% and 58.06% of the utility grid input required for EWH. Although almost insignificant, the difference in annual operational costs and percentage grid input saved, indicate that the evacuated tube solar collector was superior.

This concludes the STWH chapter, with the focus now moving to heat pump water heating. The techno-economical comparison of the different water heating technologies will be presented and discussed in the final chapter.

CHAPTER 4 – HEAT PUMP WATER HEATING

The goal of this chapter is to develop a mathematical model that will accurately predict the performance and cost of heat pump water heating (HPWH). The performance, capital and operational costs vary between heat pump manufacturers with different efficiencies. The efficiency of a heat pump is indicated by its coefficient of performance (COP) (Kakaza & Folly, 2015:469). Instead of experimentally evaluating the COP of a heat pump water heater, findings from the dissertation by Ras (2015) will be used in this study.

Chapter 4 will entail: a literature study focussing on factors affecting the COP of a heat pump water heater, including the experimental findings by Ras (2015); the development of the HPWH mathematical model and finally a discussion of the results.

4.1 Literature study

The literature study will firstly focus on the working principles of a heat pump and the factors that affect the COP thereof. Thereafter the findings of Ras (2015), indicating the difference between the manufacturer rated and the actual in-field performance of a heat pump water heater, will be discussed in detail.

4.1.1 Working principles of a heat pump water heater

The basic working principles of a heat pump water heater is shown in Figure 4.1 below.

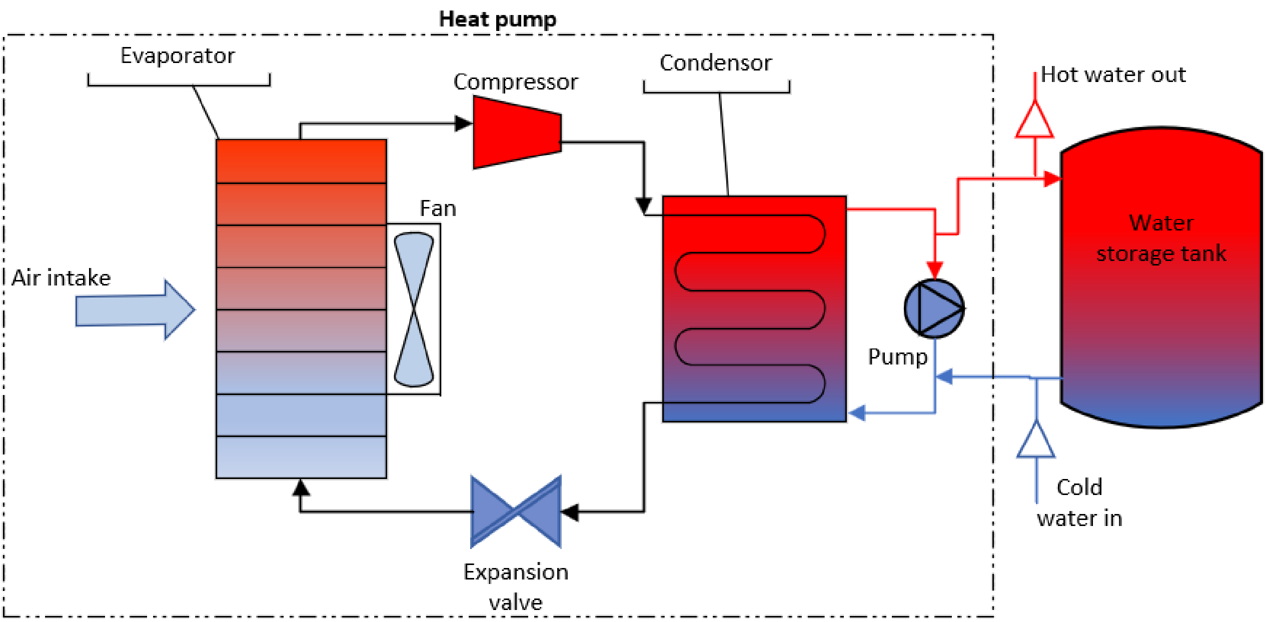

Figure 4.1: HPWH cycle schematic

A heat pump water heater extracts thermal energy from the air in order to heat water (Hohne et al., 2019:7). The thermal energy is transferred by a refrigerant, also known as the working fluid, in a vapour compression refrigeration cycle (Rankin & van Eldik, 2010:3). The evaporator extracts the thermal energy from its surrounding ambient air, transferring it into the refrigerant at low pressure and temperature. The compressor increases the pressure and temperature of the refrigerant before it is circulated through the condenser. The condenser transfers the heat from the high pressure and temperature refrigerant to the cold inlet water, thus heating the water. After the heat exchange the refrigerant travels through the expansion valve, lowering its pressure, before the cycle is repeated (Rankin & van Eldik, 2010:3).

A heat pump water heater can either be a split type or an integrated unit. The dotted line in Figure 4.1 details a split type heat pump water heater, meaning the complete unit is separate from the water storage tank. This study will thus focus on a split type heat pump water heater. Water is pumped through the condenser, heat is absorbed into the water and pumped back into the storage tank (Morrison et al., 2004:148). An integrated type heat pump is when the refrigeration cycle and water storage tank forms one unit. The evaporator and compressor is typically mounted on top of the water storage tank (Morrison et al., 2004:148). The condenser can either be mounted externally, or internally as a wrap-around coil in the vessel shell (Morrison et al., 2004:148). An integrated type heat pump is more efficient than a split type, due to greater parasitic losses in the split type (Tangwe & Simon, 2019:458). The major advantage of a split type heat pump is that is can be retrofitted to an existing water storage tank, whereas installing an integrated type must replace the entire existing system. Service and repairs for a split unit is also easier and less expensive. If a refrigerant leak occurs within the condenser of an integrated unit the vessel also needs replacement

One of the most attractive features of a heat pump water heater is its COP. The COP describes the ratio of useful thermal energy provided from the amount of electrical energy consumed (Hohne et al., 2019:7). A heat pump will typically produce 3 units of heat for every 1 unit of electrical energy consumed (Rankin & van Eldik, 2010:4). The heat pump utilizes electrical energy to power the evaporator, compressor and pump. In domestic application the COP value of a heat pump water heater can range between 2 and 4 (Hohne et al., 2019:7).

4.1.2 Factors affecting the COP of a heat pump water heater

There are several factors that affect the COP, all of which can be categorised into three groups: 1) system specifications, 2) operational and 3) environmental conditions. System specifications refer to the type of heat pump, component design and refrigerant used (Zhang et al., 2007; Peng et al., 2016). While system specifications are important, they will not be focussed on in this study. The system specifications from a previous study done by Ras (2015) will be used.

There are several operational- and environmental conditions that affect the COP, namely: 2a) the volume heated, 2b) inlet- and 2c) outlet temperature of the water, 3a) the ambient temperature and 3b) relative humidity. The performance of a heat pump water heater is mainly dependent on the energy in the atmosphere, making the ambient temperature the primary influencing factor (Ras, 2015:7). The other mentioned conditions are all secondary influencing factors.

In order to accurately rate the performance of a heat pump water heater, Morrison et al. (2004:150) included both the primary and secondary influencing factors. This was achieved by determining the COP in relation to the difference between the water storage tank temperature and the ambient air temperature, while varying the environmental conditions (Morrison et al., 2004:150). Figure 4.2 illustrates the relationship between the COP and the difference in the tank Tt and ambient Ta temperatures.

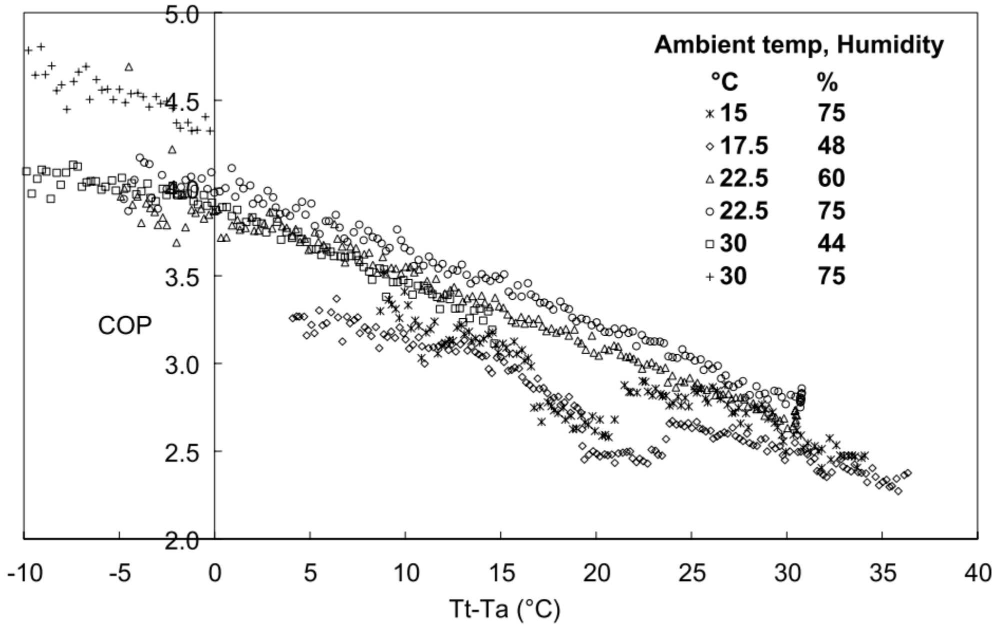

Figure 4.2: Relationship between the COP and the difference between tank and ambient temperature (Morrison et al., 2004)

By including the water storage tank temperature in the relationship, all the influencing factors are considered in the rated performance of a heat pump water heater (Ras, 2015:9).

4.1.3 Actual in-field performance of a heat pump water heater

The rated COP supplied by the manufacturer of a heat pump water heater typically overestimates the actual in-field performance it is capable of. This is due to the fact that the rated COP testing methodology is mainly done in controlled conditions while focussing on the varying effect of ambient temperature, without including all the secondary influencing factors (Ras, 2015:2). Ras (2015) researched and developed an experimental testing method that accurately rates the in-field performance of a residential heat pump water heater in South Africa. Figure 4.3 below shows that Ras (2015) adapted the method of Morrison et al. (2004) and also included all primary and secondary influencing factors by plotting the COP in relation to the temperature difference Tt-Ta.

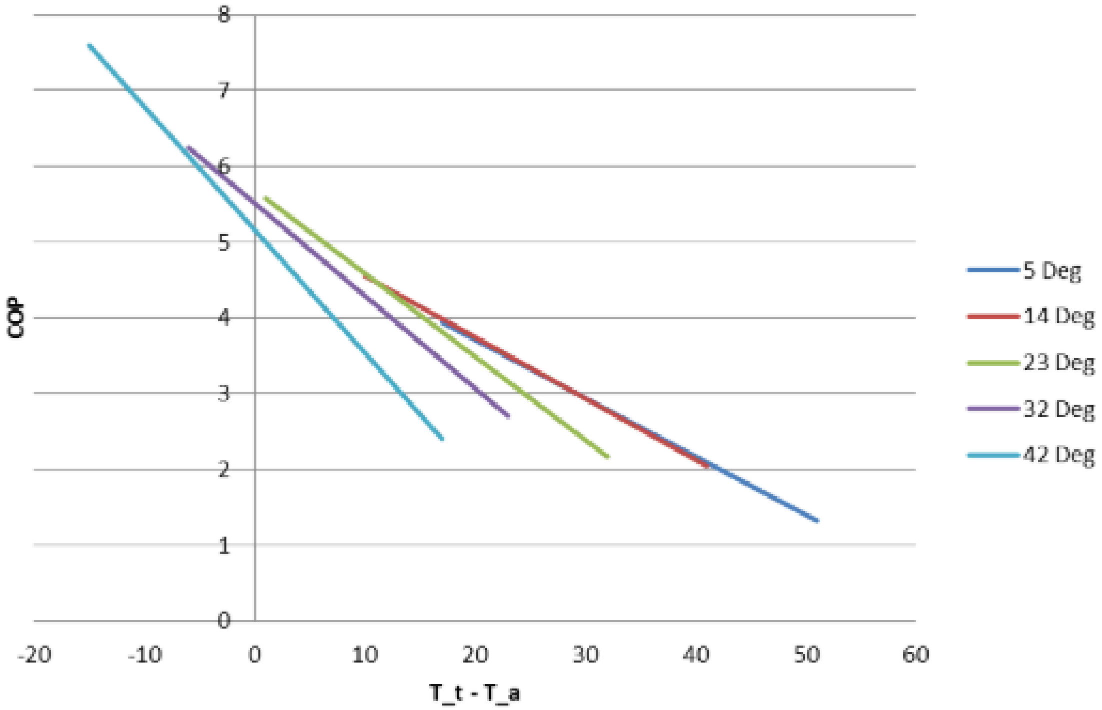

Figure 4.3: Laboratory test results of Ras (2015:47)

Ras (2015:46) experimentally determined the COP for ambient air temperatures of 5°C, 14°C, 23°C, 32°C and 42°C at a relative humidity of 50%. A relative humidity of 50% was chosen as it best represented the average in-field performance of the heater (Ras, 2015:45).

In order to ascertain the average experimental performance curve of the heat pump water heater, Ras (2015:47) determined the linear regression line of the laboratory test results, as presented in Figure 4.4 below.

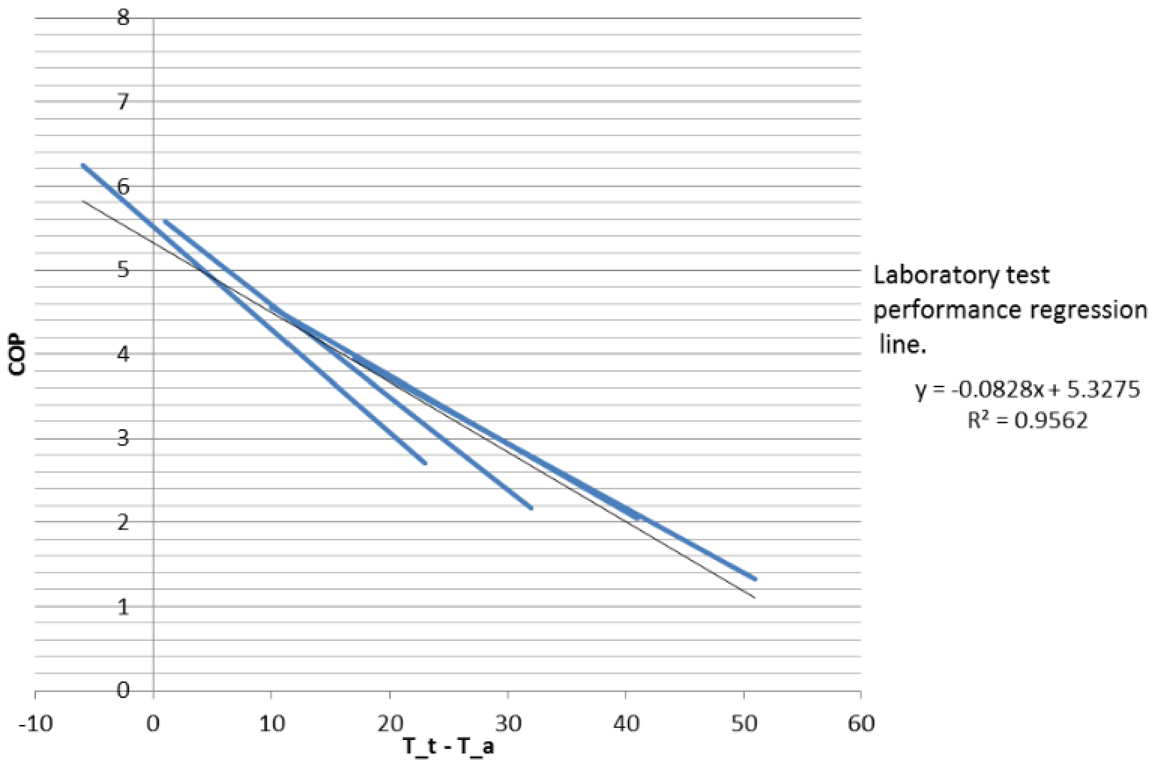

Figure 4.4: Linear regression of laboratory data, Ras (2015:48)

The regression line of Figure 4.4 represents the average performance curve of the heat pump water heater, which will be directly implemented and discussed in the mathematical model development section. Ras (2015:47) did not include the 42°C performance curve in the linear regression. The highest recorded in-field ambient temperature was found to be 36°C and the 42°C curve would negatively affect the in-field prediction accuracy (Ras, 2015:48,49). Ras (2015:50) compared the laboratory performance curve to the in-field, simulated and manufacturer performance curves, as illustrated in Figure 4.5 below.

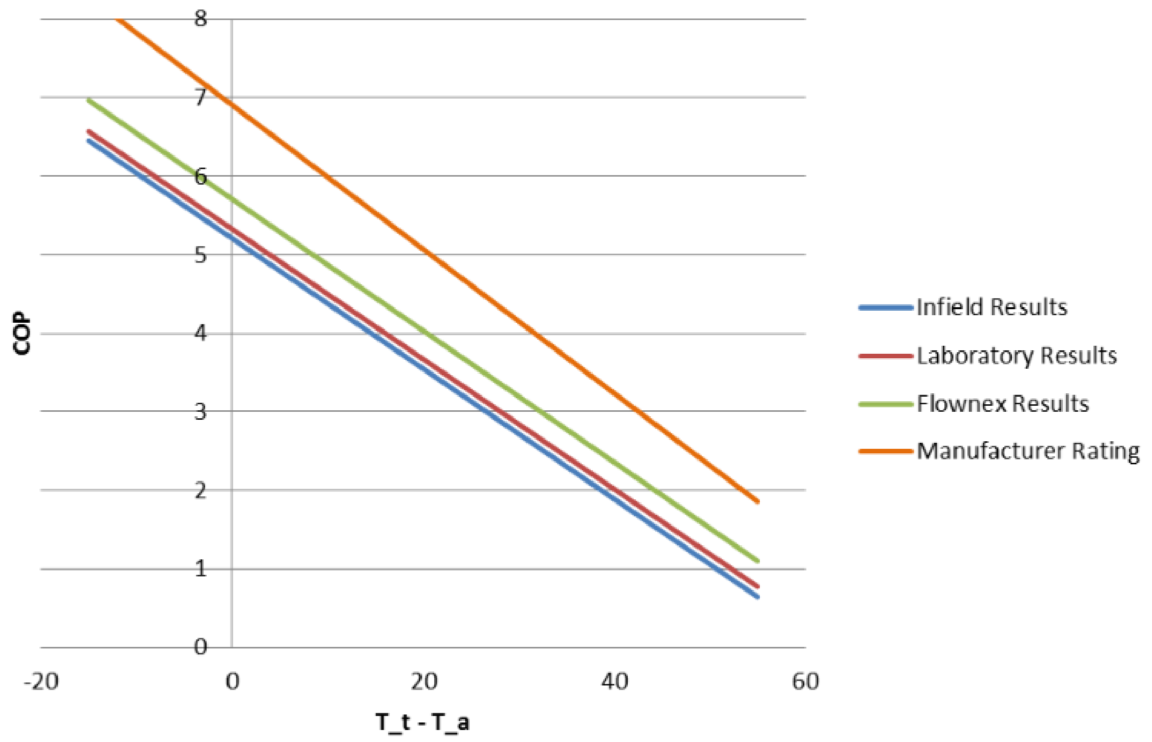

Figure 4.5: Comparison of performance curves (Ras, 2015:51)

The compared results of Ras (2015:51) clearly indicates the difference between the rated COP and the actual in-field performance of a heat pump water heater. The experimental testing methodology developed by Ras (2015:51,52) was validated by a 3% difference between the actual in-field and laboratory performance curve results. In the current study, the laboratory result of Ras (2015) will be used in the mathematical model in order to determine the actual in-field performance of the heat pump water heater. The laboratory results of Ras (2015) will be directly used due to experimental testing of a heat pump water heater not being included in the scope of this study.

4.2 Mathematical model development

This section presents the development of the mathematical model by discussing its setup, assumptions and methodology. The ERHP-SU14E-MS heat pump water heater is modelled in this study (Enerflow, 2020). Note that this is also the heat pump water heater experimentally tested by Ras (2015). The heat pump water heater, its components and the water storage tank are treated as a black-box. The energy balance method is applied on the HPWH system, as illustrated in Figure 4.6 below.

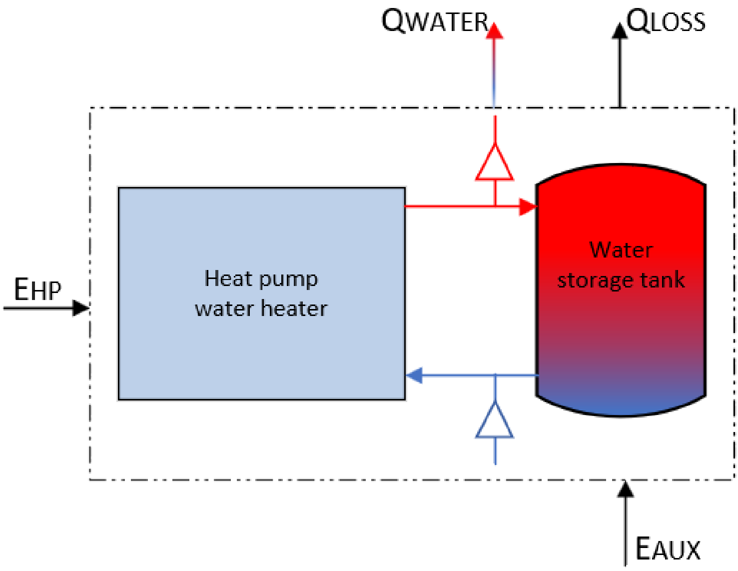

Figure 4.6: HPWH energy balance

The energy balance equates to:

$$U_{i-1} + E_{HP} + E_{AUX} = U_i + Q_{WATER} + Q_{LOSS} \quad (4.1)$$

$U_{i\text{-}1}$ represents the internal energy of the water storage tank at the previous hour i-1. E_{HP} is the total electrical energy utilized by the evaporator fan, compressor and water pump. E_{AUX} is the auxiliary electrical energy utilized by the resistive heating element in the water storage tank. Both E_{HP} and E_{AUX} are supplied by the utility grid. Q_{WATER} represents the change in thermal energy within the water storage tank due to the simultaneous consumption and replenishment of the water storage tank volume. It is thus also the thermal energy required to heat the water. Q_{LOSS} is the standing loss of the water storage tank, indicating the amount of heat lost to the environment surrounding the water storage tank.

The heat pump water heater has a rated heating capacity of 5.6kW (20160kJ/h) and is capable of heating water up to 55°C (Enerflow, 2020). If a higher water temperature is required, the heating element of the water storage tank is activated (Enerflow, 2020). In the case of HPWH, the maximum water temperature setpoints is 55°C. E_{AUX} will thus not be required in the modelling approach of HPWH.

In order to predict the operational costs of HPWH, the amount of electrical energy utilized by the heat pump water heater must be determined. This is done by means of the COP equation:

$$COP = \frac{Q_{WATER} + Q_{LOSS}}{E_{HP}} \quad (4.2)$$

As shown in Equation (4.2) above, E_{HP} is determined by dividing the system output Q_{WATER} + Q_{LOSS} by the COP of the heat pump water heater. The COP of the heat pump water heater is given by Ras (2015:48) as illustrated in Figure 4.4. The COP thus equates to:

$$COP = -0.0828(Tt - Ta) + 5.3275 \quad (4.3)$$

Tt is the average temperature of the water storage tank and Ta the ambient temperature as given by the climatic design year data. When calculating the COP, the average tank temperature is assumed to be 45°C. This assumption is based on the fact that the heat pump water heater modelled is a multiple-pass recirculation type heater (Tangwe & Simon, 2019:3). This means that the inlet water is continuous recirculated through a diverter valve in the heat pump until it reaches the setpoint temperature of the valve (Tangwe & Simon, 2019:3). The operating principle of the diverter valve is illustrated in Figure 4.7 below.

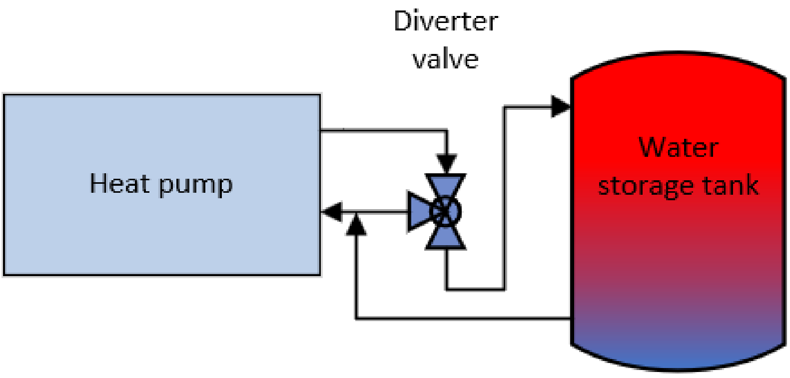

Figure 4.7: Diverter valve schematic

The outlet temperature of the diverter valve is set to 45°C. Water is recirculated through the heat pump in a closed loop until it is heated to a temperature of 45°C. When the average temperature of 45°C is reached within the water storage tank, the diverter valve opens completely and the water in the tank is heated further from 45°C to the setpoint temperature of 55°C. These setpoint temperatures thus also respectively represent the ON and OFF setpoints.

The final terms needed for Equation (4.2) are Q_{WATER} and Q_{LOSS}. As done in Section 2.5, the specific IF conditions and accompanying equation used to determine these terms are given in Annexure B Section B.1. The next section will provide a less technical discussion of the control methodology.

4.2.1 HPWH control methodology

This section will discuss the control methodology of the HPWH mathematical model. The control methodology will discuss the different temperature and energy control methodologies throughout the following points. Lastly, the methodology for the determination of the annual operational costs and simple payback period is discussed.

i. Auxiliary grid input

Unlike PVWH and STWH, HPWH requires no auxiliary electrical grid input for backup heating. A heat pump water heater already utilizes electrical energy supplied by the grid to operate. Also, as mentioned, the heating capacity of the heat pump alone is sufficient to reach the maximum temperature setpoint.

ii. Maximum and minimum setpoint temperatures

The maximum and minimum temperature setpoints of the water storage tank is set to 55°C (Tt_{max}) and 45°C (Tt_{min}) respectively. The water storage tank thus has a temperature buffer of 10°C.

iii. Heat input

In the case of HPWH, changes in the water storage tank temperature are caused solely by consumption $\Delta T_{\dot{m}}$ (Equation(2.18)) and the standing loss ΔT_{LOSS} (Equation(2.19)). The water is only heated to the maximum temperature setpoint when it is equal to the minimum temperature setpoint. The heat pump thus simply maintains the storage tank temperature buffer. The electrical energy utilized by the heat pump (E_{HP}) in order to maintain the temperature buffer (Q_{WATER}) can thus be determined. With Q_{LOSS} already compensated for by ΔT_{LOSS}, Equation (4.2) can be adapted to Equation (4.4) below in order to determine the electrical energy utilized by the heat pump water heater.

$$E_{HP} = \frac{Q_{WATER}}{COP} \tag{4.4}$$

iv. Annual operational costs and simple payback period

The total electrical energy utilized by the heat pump water heater from the grid, in order to provide the thermal energy required to heat the water over the period of an entire year $E_{REQUIRED}$, is determined by Equation

(4.5) below.

$$E_{REQUIRED} = \sum_{1}^{8760} E_{HP} \tag{4.5}$$

The amount of electrical energy required is thus simply the sum of E_{HP} over all 8760 hours of a year. Finally, the annual operational costs R_{HPWH} in R/year is given by Equation (4.6) below.

$$R_{HPWH} = \frac{Q_{REQUIRED}}{3600} \times R_{kWh} \quad (4.6)$$

R_{HPWH} is thus equal to the yearly amount of electrical energy required, divided by 3600 (converting kJ to kWh) and multiplied with the cost of electricity R_{kWh} in R/kWh. Equation (2.22) is again applied to determine the SPP of the heat pump water heater.

The capital cost of a retrofitted system, including the heat pump and installation, lies between R22871 and R23977 (including VAT). Quotations were requested from two different suppliers. ITS Solar quoted their 5kW domestic heat pump. Enerflow heat pumps quoted their 5kW ERHP-SU14-MS residential heat pump.

Given the input parameters of the mathematical model as listed in Table 1.2 and those explained in this section, the model results are determined and discussed in the next section.

4.3 Results and discussion

The final results are listed in Table 4.1 below.

Table 4.1: HPWH cost results

Symbol	Result	Value	Unit
R_{HPWH}	HPWH operational costs	2880	R/year
R_{EWH}	Baseline EWH operational costs	7933	R/year
R_{SAVED}	Annual saving relative to baseline	5054	R/year

The estimated annual operational costs of HPWH per household is R2880. Relative to the baseline R_{EWH} of R7933, the annual savings for HPWH is R5054. An average capital cost of R23424 is used to determine the SPP for the heat pump water heater. The SPP for the heat pump water heater, based on the average capital cost, is 4.64 years. The SPP can also vary between 4.53 and 4.74 years, based in the capital cost of different suppliers.

In terms of performance, Table 4.2 below indicated the amount of energy required from the grid for HPWH and EWH.

Table 4.2: HPWH grid energy required

Symbol	Result	Value	Unit
E_{HPWH}	HPWH auxiliary grid energy required	1308.76	kWh/year
E_{EWH}	Baseline EWH grid energy required	3605.79	kWh/year

The results indicate that HPWH, as applied in this study, saved 63.7% of the utility grid input required for EWH.

This concludes the HPWH chapter, with the focus now moving to gas water heating. The techno-economical comparison of the different water heating technologies will be presented and discussed in the final chapter.

CHAPTER 5 – GAS WATER HEATING

The goal of this chapter is to develop a mathematical model that will accurately predict the performance and operational costs of gas water heating (GWH). The performance, capital and operational costs vary between heaters with different efficiencies. The operational costs of GWH will also vary in accordance with the price of fuel gas. The efficiency of a gas water heater must be experimentally evaluated in order to determine its performance and accurately predict its operational costs.

Chapter 5 will entail: a literature study focussing on the efficiency of a gas water heater; the experimental evaluation of the gas water heater in order to determine its efficiency; the development of the GWH mathematical model and finally a discussion of the model results.

5.1 Literature study

The literature study will discuss the working principles, operational states and factors that affect the efficiency of a gas water heater. Lastly, a method found in literature in order to evaluate the efficiency of a gas water heater is discussed.

5.1.1 Working principle of a gas water heater

A gas water heater can either be a non-condensing or condensing type model. The relevant working principles of these two different models, as shown in Figure 5.1 below, are as follows.

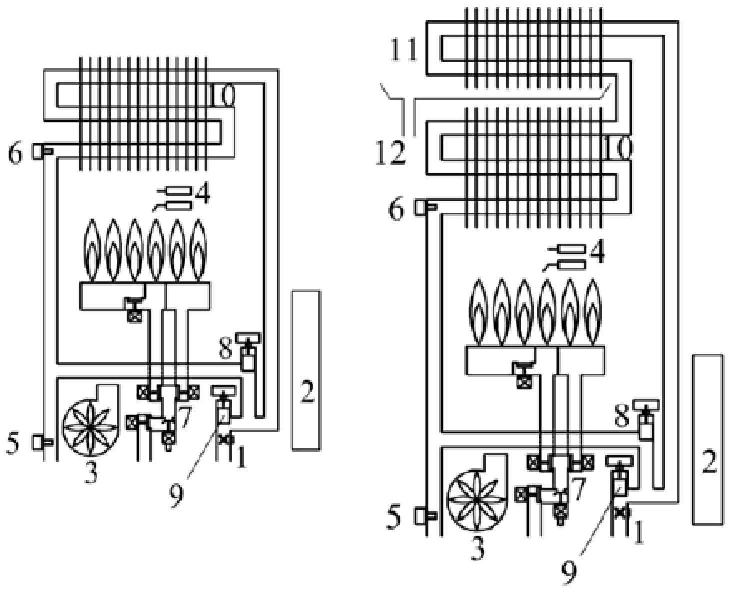

Figure 5.1: Non-condensing (left) and condensing (right) gas water heater (Bourke, 2015)

When there is a demand for hot water, cold water enters the heater via the inlet impellor (1) (Bourke, 2015:11). The rotating magnetic tipped blades of the impellor emits a signal, which is monitored by the microprocessor (2) (Bourke, 2015:11). The microprocessor reads the frequency of rotation, calculates the water flow rate and initiates the heating operation. The volume of fuel gas required to achieve the desired water outlet temperature is determined by the microprocessor. The gas control valve (7) opens and the speed of the air-supply fan (3) is adjusted to supply the correct air-gas mixture (Bourke, 2015:11). The ignition electrodes (4) ignite a spark and a constant flame is maintained (Bourke, 2015:11). The thermal energy produced by the flame heats the heat exchanger (10) fins and the fins in turn exchange the energy to the conductive piping, heating the water (Bourke, 2015:12). The data from the hot water outlet temperature sensor (5) is continuously sent to the microprocessor and the necessary operational adjustment is made to the air supply (Bourke, 2015:12). If the heated water exceeds the desired outlet temperature, the cold-water by-pass valve (8) mixes heated and cold water (Bourke, 2015:12). In a condensing model, the cold water first flows through the latent heat exchanger (11) (Bourke, 2015:13). It also has a condensate drain (12), which collects the water condensate from the latent heat exchanger (Bourke, 2015:13).

5.1.2 Operational states of a gas water heater

A gas water heater has several states of operation that can be summarized as: 1) standby, 2) ramp-up, 3) steady state operation and 4) draw decay (Burch *et al.*, 2008). The different operational states are shown in Figure 5.2 below.

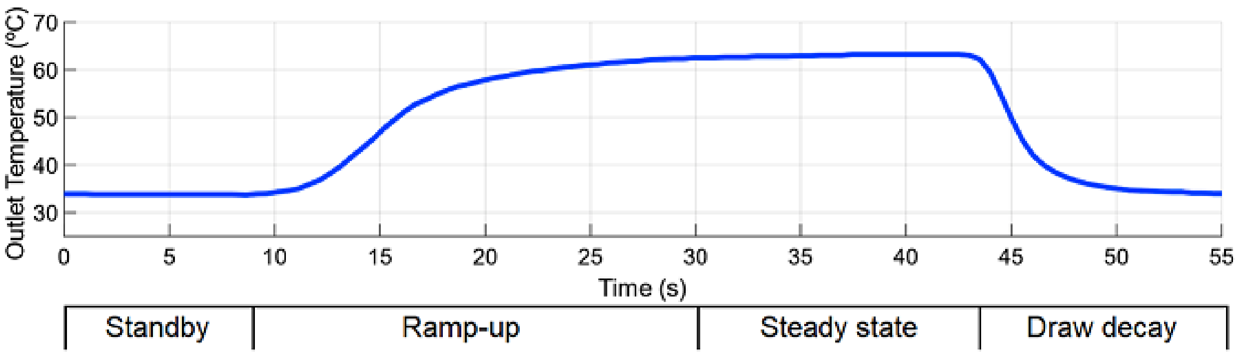

Figure 5.2: Operational states of GWH (adapted from Quintã et al., 2019)

The heater is on standby when there is no demand for hot water or if the water has already been heated to the required temperature and the heater cycled off. Ramp-up operation refers to the time from start of heating until steady state operation is reached. Steady state operation is achieved when the output temperature remains constant (Burch *et al.*, 2008:5). Depending on the demand, steady state operation can either be continues or the heater can cycle off, as is the case in Figure 5.2. After the heater has cycled off, draw decay represents the loss of temperature as the outlet temperature approaches the inlet water temperature (Burch *et al.*, 2008:5). Note that there is also loss of heat to the environment present during all operational states. When the operational states in Figure 5.2 are repeated, a gas water heater is undergoing cyclic operation. If the demand is increased, by increasing the water flow rate, steady state operation will continue until the demand is lessened. Glanville et al. (2013:7) stated that gas water heaters are "best suited for steady-state operation". During steady state operation the heater efficiency is the most dominant parameter and environmental losses are limited during this state (Burch *et al.*, 2008:1). Changes in the internal energy is also minimized (Healy et al., 2011:523).

5.1.3 Factors affecting the efficiency of a gas water heater

Four factors that affect the efficiency of a gas water heater will be discussed: namely, 1) the water consumption profile, which has the most significant impact, 2) the water flow rate, 3) the recovery of latent heat and 4) the composition of the fuel gas.

5.1.3.1 Water consumption profile

The efficiency of a gas water heater is highly dependent on the water consumption profile (Butcher & Schoenbauer, 2011:683). Although the rated efficiency of a heater is given, it significantly differs from the actual performance (Johnson & Beausoleil-Morrison, 2016:741). This is caused by the standard energy factor (EF) test used when a water heater is rated. The EF test consists out of six 40.6 litre consumptions of water over a period of 24 hours, with the hot water output temperature set to 57.2°C (Butcher and Schoenbauer, 2011:683). The water consumption profile employed during the EF test is immensely different from a realistic consumption profile (Butcher & Schoenbauer, 2011:683). Realistic residential hot water consumption varies depending on the type of residence, location, size of the family and occupational behaviour patterns (Healy et al., 2011:522). The difference in profile is clearly indicated by Figure 5.3 below.

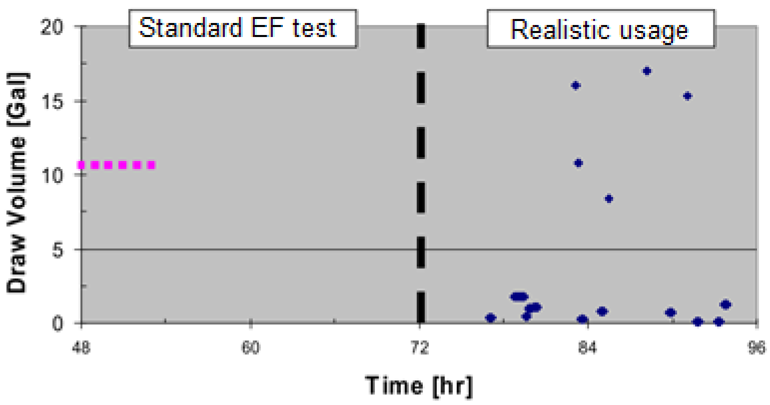

Figure 5.3: Contrast between standard test and realistic consumption patterns (adapted from Burch et al., 2008)

Realistic water consumption profiles are non-uniform in pattern and mostly consists of more regular smaller quantity consumption (Healy et al., 2011:522). Realistic consumption lowers the efficiency of a gas water heater because more energy is diverted towards increasing the temperature of the heat exchanger, rather than actually heating the water (Healy et al.,2011:522). The heat supplied to the heat exchanger is also lost after the burner cycles off, inducing more heat loss than found in the standard EF test (Healy et al., 2011:522). Burch *et al.* (2008:7) and Healy et al., (2011:522) both reported a degradation of about 8% in the standard efficiency rating of a gas water heater.

5.1.3.2 Water flow rate

The unpredictability of water flow rate changes in a realistic consumption profile leads to temporary over- and undershoots in the delivery temperature (Costa et al., 2016:1404). The outlet water temperature depends on the flow rate and temperature of the inlet water, thermal energy released by the heat exchanger, water travel length and the thermal inertia of the heater (Costa et al., 2016:1405). During sudden changes in the hot water demand, the control system must adjust the thermal input via the air supply or by simply limiting the demand (Glanville et al., 2013:2). The feedback control of a heater alone is insufficient to reduce outlet temperature fluctuations to acceptable values and Costa et al. (2016:1405) stated that this is due to the slow dynamics of a heat exchanger. Yuill et al. (2010:677) addressed the same problem and applied several different control approaches. It was found that the combination of a feedback and feed-forward control system achieved an improvement (Yuill et al., 2010:677). The solution proposed by Costa et al. (2016:1405) involved the incorporation of a motorized three way bypass valve, mixing valve and an accumulation tank. Costa et al. (2016:1405) did not specify the size of the vessel, but mentioned that it was not meant as energy storage, only to avoid temperature fluctuations.

5.1.3.3 Latent heat recovery

As explained in the working principles of a gas water heater, there are two different models. A condensing model has a higher efficiency, due to the fact that it recovers the latent heat contained in the off-gas water vapor (Bourke, 2015:13). This is achieved by an additional heat exchanger to recover the latent heat from the water vapor in the off-gas by transferring in to the cold inlet water. A condensing gas water heater is capable of achieving efficiencies equal to or greater than 90% (Barros et al., 2014:66).

5.1.3.4 Fuel gas composition

A gas water heater can either use liquefied petroleum gas (LPG) or natural gas as fuel (Bosch, 2019). A specified operating pressure is the only system requirement when using either of these gases (Bosch, 2019). LPG and natural gas are primarily composed out of propane and methane respectively (Swedish Gas Technology Center Ltd, 2012:7; Afrox, 2015). The effect of fuel gas composition on the efficiency of a gas water heater can be approximated with the amount of thermal energy provided during combustion of a fuel gas. This is indicated by the calorific value (also known as the heating value) of a fuel gas, listed in Table 5.1 below.

Table 5.1: Fuel gas energy specifications (adapted from Engineering Toolbox, 2003)

Fuel gas	Calorific value (MJ/kg)	Density (kg/m^3)	Energy content (MJ/m^3)
Propane	50.4	1.899	95.71
Methane	55.5	0.716	39.74

The amount of thermal energy provided during combustion is however also dependent on the density of a fuel gas. The thermal energy released during combustion can be determined by selecting an arbitrary gas flow rate and calculating the enthalpy of formation for each respective fuel gas, as shown in Figure 5.4 below (Borgnakke & Sonntag, 2009:627).

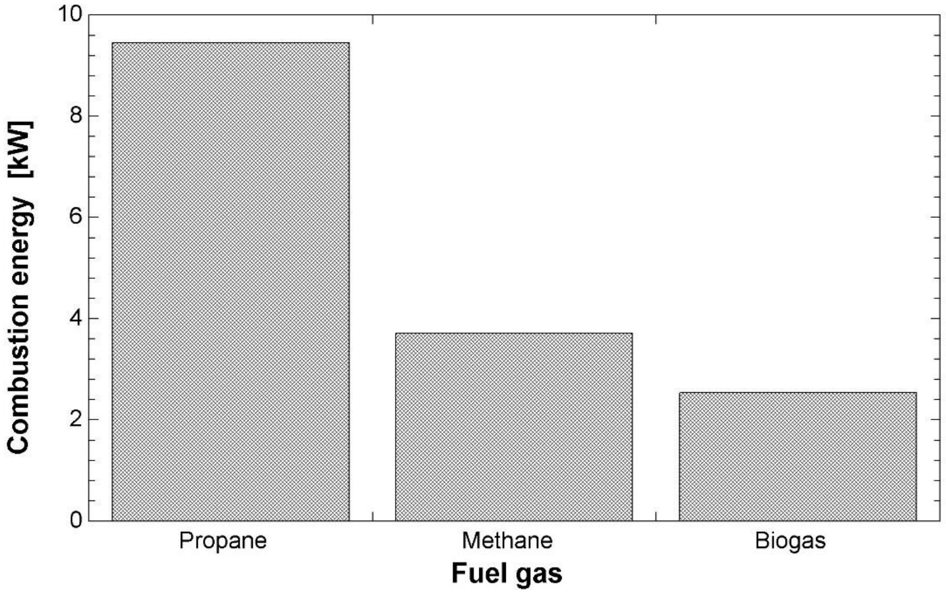

Figure 5.4: Combustion energy released by respective fuel gas

Although propane has a lower calorific value than methane per kg as observed in Table 5.1, Figure 5.4 clearly shows that propane releases more energy during combustion, due to its greater density. Figure 5.4 also indicates the amount of energy released during combustion when using biogas. Biogas comprises of methane (±65%), carbon dioxide (±35%) and small traces of hydrogen, hydrogen sulphide and ammonia (Greben & Oelofse, 2009:678). The exact composition, as well as the energy content of biogas, is dependent on the type of biomass used to produce it (Okudoh *et al.*, 2014:1037). According to Msibi & Kornelius (2017:3), biogas has a calorific value of about 20MJ/kg and due to its low energy content is mainly used for cooking purposes in rural areas of South Africa (Mutungwazi et al., 2018:174). A brief look at the implementation of biogas in South Africa is further presented in Annexure C Section C.1.

5.1.4 Evaluating the efficiency of a gas water heater

The method used to evaluate the efficiency of a gas water heater is commonly referred to in literature as the input-output method (Healy et al., 2011:521). There exists a clear linear relationship between the thermal energy released during combustion and the sensible heat used by a gas water heater, as shown in Figure 5.5 below (Healy et al., 2011:527).

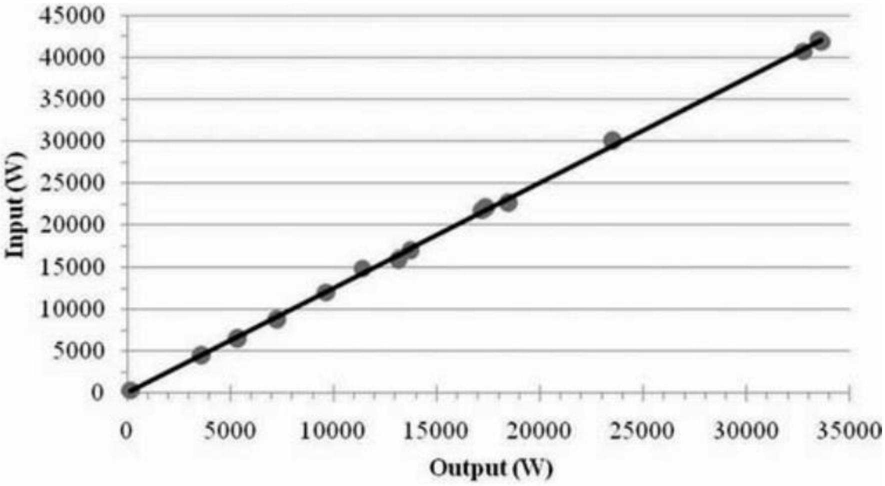

Figure 5.5: Example of the linear energy relationship of a gas water heater (Healy et al., 2011)

The input-output method utilizes the linear energy relationship of a gas water heater in order to (1) determine its efficiency and (2) predict the heater performance under arbitrary conditions (Healy et al., 2011:521). The input-output method is comprised out of a series of quick laboratory experiments, which provides essential data for drafting the linear relationship curve of a heater (Glanville et al., 2013:3). An advantage of the input-output method is that a single set of measurements can be used to evaluate the efficiency under any arbitrary consumption profile (Butcher & Schoenbauer, 2011). In theory only two test points are necessary, the minimum and maximum capability points (Healy et al., 2011:523). Investigation of the relationship however requires midpoint testing, which is determined by the variation of standby time, consumption volume, water flow rate and the target outlet temperature during tests (Healy et al., 2011:524).

It is made clear by the literature study that in order to develop a GWH model, the efficiency of a gas water heater is required. The next section will discuss the experimental evaluation of the gas water heater in order to determine its efficiency.

5.2 Experimental evaluation of the efficiency

The GWH experimental evaluation section will firstly discuss the experimental setup, apparatus and procedure. The mathematically methodology used to process the experimental data will then be discussed in detail. Finally, the results of the efficiency evaluation will be given and discussed.

5.2.1 Setup, apparatus and procedure

The Bosch 26Lt Optiflow Professional LPG / Natural gas geyser (Bosch, 2019) was used in the GWH experiment. The experimental process flow diagram is shown in Figure 5.6 below.

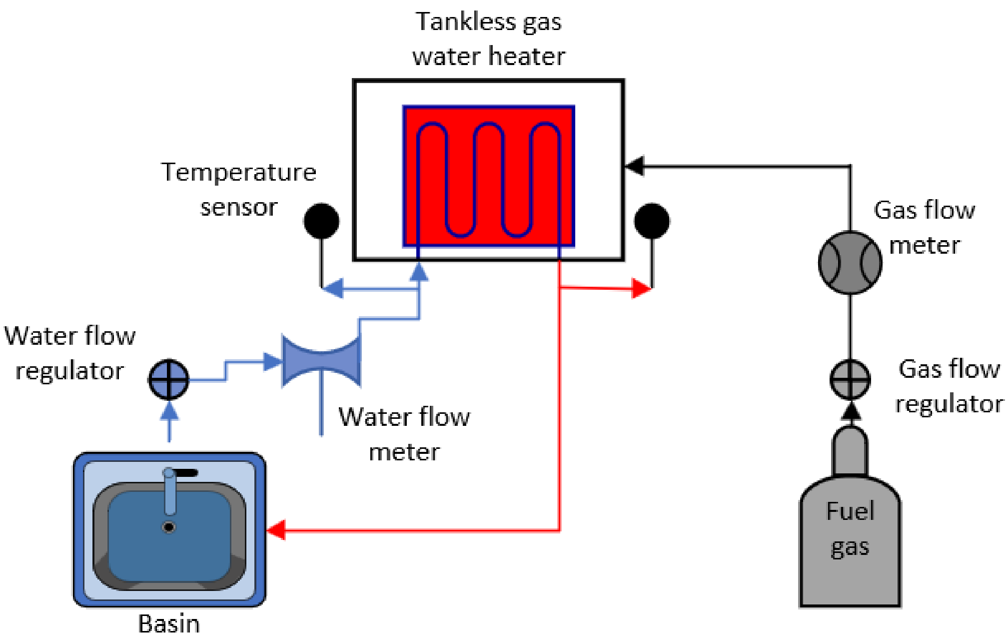

Figure 5.6: GWH experimental process flow diagram

A water rotameter (MODEL FP-1-27-G-10/83 + 1-GSVGT-64, DN2043) was used to measure the rate at which water was supplied to the heater. The water flow meter was installed between the water supply tap and the cold-water inlet connection of the heater. The hot water from the heater outlet flowed back into the basin and directly into the drain.

An ONSET HOBO 4-channel analog logger was used to measure the inlet and outlet water temperatures. Figure 5.7 below shows the temperature sensors installed in fittings connecting the inlet and outlet water connections of the heater.

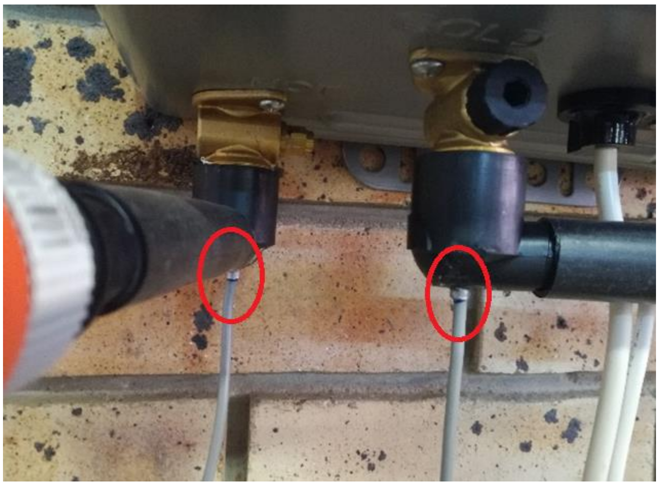

Figure 5.7: Installed temperature sensors

As liquefied petroleum gas is a mixture of mostly propane, butane and small amounts of other hydrocarbons, it was decided to simply use propane in the experiment (Afrox, 2015). The propane was fed to the geyser using a 2.8kPa gas regulator and standard gas hose. A Fischer & Porter gas flow meter was used to measure the amount of gas used by the heater (Model 10A6132M/B10 – ¼" NPTF, Tube FP-1/4-25-G-5/81dt/df, Float CD-14, Black glass ball).

The following paragraph details the procedure of the experiment.

The user-controlled experimental variables are the flow rate and outlet temperature of the water. The heater controls the air-supply fan speed and the continuous or intermittent flow of gas, depending on the demand. Continuous flow of gas is required for steady state operation and the required operating conditions must first be determined. This was done by selecting an outlet temperature and increasing the water flow rate from zero until continuous gas flow was observed. Once continuous gas flow was observed, the water flow rate was recorded and again increased in order to record all the possible water flow rates at which gas flowed continuously for the selected outlet temperature. The water flow rated was increased until the selected outlet temperature was not reached. A new outlet temperature was selected and the process reiterated. By repeating this process, the water flow rates required for continuous gas flow was ascertained. Finally, a short series of tests were done in randomized fashion across the known steady state operational conditions. The continuous gas flow operating condition results and the experimental data recorded are summarized in Table C.1 and Table C.2 of Annexure C Section C.2 respectively.

5.2.2 Data processing

In order to evaluate the efficiency of the gas water heater, the energy balance method was applied to the experimental setup. The experimental data was processed using Engineering Equation

Solver (EES). Only the main equations of the mathematical methodology will be discussed. Refer to Annexure C Section C.3 for all experimental evaluation calculations and results. The experimental energy balance of the gas water heater is shown in Figure 5.8 below. Note that the experimental methodology and the methodology of the mathematical model will be very similar. As to not confuse these methodologies, the symbol for thermal energy will be assigned as E in this experimental section and as Q in the development of the mathematical model.

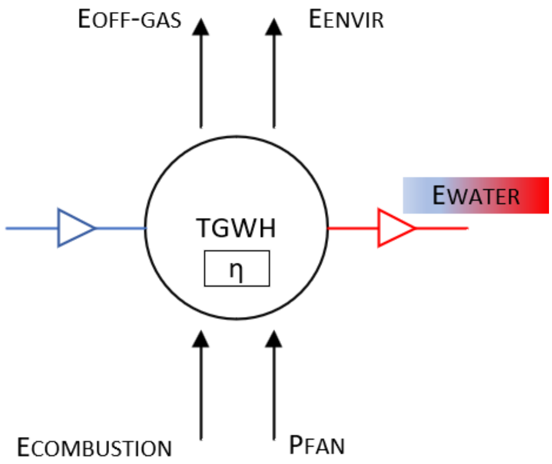

Figure 5.8: GWH experimental energy balance

$E_{COMBUSTION}$ is the thermal energy generated by the combustion of the fuel gas. P_{FAN} is the power used by the air-supply fan. E_{WATER} is the energy transferred to the water. $E_{OFF\text{-}GAS}$ is the heat lost in the off-gas of the combustion process and E_{ENVIR} is the heat lost to the environment surrounding the gas water heater. The experimental energy balance thus equates to:

$$E_{COMBUSTION} + P_{FAN} = E_{WATER} + E_{OFF-GAS} + E_{ENVIR} \tag{5.1}$$

The efficiency η of the heater is determined by dividing the system's thermal output energy by the input energy and fan work:

$$\eta = \frac{E_{WATER}}{E_{COMBUSTION} + P_{FAN}} \times 100 \tag{5.2}$$

The thermal energy transferred into the water, E_{WATER}, is determined by Equation (5.3) below.

$$E_{WATER} = \dot{m} c_p \Delta T \tag{5.3}$$

$\dot{m}$ is the water flow rate recorded per test, c_p is the fixed specific heat value of water and ΔT the increase in water temperature. The energy released by the combustion of the fuel gas, $E_{COMBUSTION}$, is the difference between the enthalpy of the products (H_P) and reactants (H_R) (Borgnakke and Sonntag, 2009:627). The heat lost in the off-gas is incorporated in H_P.

$$E_{COMBUSTION} = H_P - H_R \quad (5.4)$$

The power supplied to the air-supply fan, P_{FAN}, is given by Equation (5.5) below.

$$P_{FAN} = V_{AC} \times I_{AC} \quad (5.5)$$

V_{AC} is the single-phase utility voltage and I_{AC} the current drawn. The power supplied to the fan was measured once and assumed constant. The assumption is deemed valid as there is little variation and the fan power is but a small fraction of the total energy input. The assumption was also made by Burch *et al.* (2008:4). E_{ENVIR} represents the heat lost to the environment. An equivalent energy balance across the system was assumed to approximate the environmental heat loss by simply subtracting the total amount of energy going out of the system from the total amount of energy going into the system. The reason for the approximation is that the heat-loss coefficient of the gas water heater must be measured when heated water flows through a disabled heater (Johnson and Beausoleil-Morrison, 2016:747). This was not done during the experimental phase. Burch *et al.* (2008:4) also stated that during steady state operation, the burner efficiency is dominant and that the heat-loss coefficient may be estimated or simply neglected. As supported by literature, the approximation was thus deemed adequate. Changes in the internal energy of the system was also neglected, as they are minimized during steady state operation (Healy et al., 2011:523).

5.2.3 Results and discussion

An average efficiency of 85% was determined for the Bosch 26Lt Optiflow Professional. The linear energy relationship of the gas water heater is shown by Figure 5.9 below.

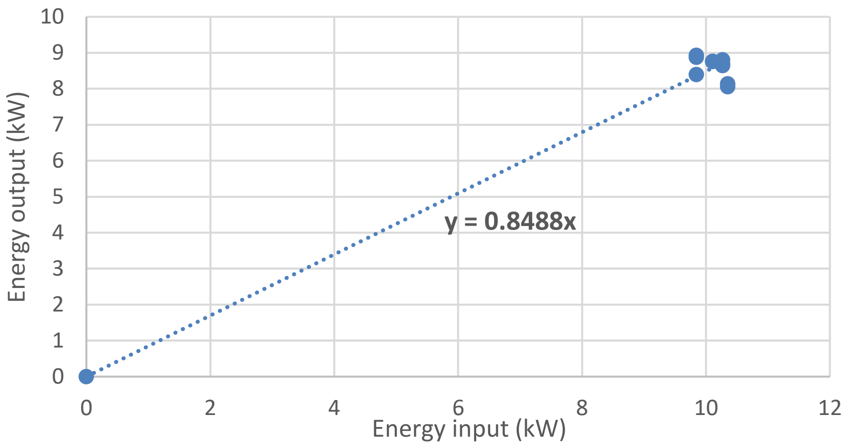

Figure 5.9: Linear energy relationship of the Bosch Optiflow

The efficiency of the gas water heater is given by the gradient of the linear energy relationship. A combustion efficiency of 85% is well in agreeance with several other GWH studies. The efficiencies of 78.8% by Healy et al. (2011:525), 87% by Butcher and Schoenbauer (2011:688), 85.9% by Glanville et al. (2013:5) and a thermal efficiency range of 87.9% – 94.1% was given by Johnson and Beausoleil-Morrison (2016:746), each for the respective gas tankless water heaters used. The primary performance relationship observed during testing was between the water flow rate and delivery temperature, as shown in Figure 5.10 below.

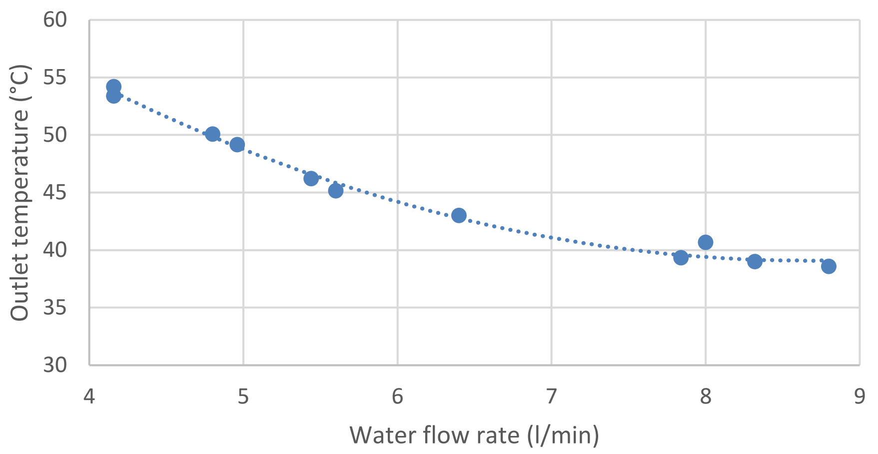

Figure 5.10: Relationship between water flow rate and delivery temperature

An indirect equivalent relationship exists between the water flow rate and delivery temperature. This is simply because the heat exchanger has more time to transfer heat into the slower flowing water. It is also clear that the amount of heat supplied by combustion is directly equivalent to the amount of gas combusted, as shown by Figure 5.11 below.

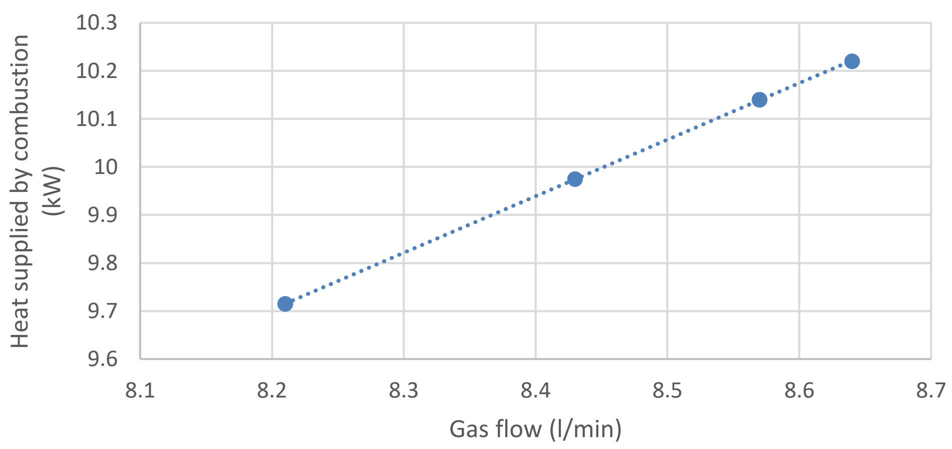

Figure 5.11: Relationship between gas flow rate and combustion energy

The effect of natural gas and biogas on the heater efficiency was also experimentally approximated with the use of methane. It was found that the efficiency lowered to 80% when using methane. Further details of the methane experimentation are provided in Annexure C

Section C.1. With the heater efficiency known, the GWH mathematical model can be developed, as is discussed in the next section.

5.3 Mathematical model development

This section presents the development of the mathematical model by discussing its setup, assumptions and methodology. As in the experiment, the Bosch 26Lt Optiflow Professional is modelled in this study (Bosch, 2019). The gas water heater and water storage tank are treated as a black-box. Figure 5.12 below represents the mathematical model setup and energy balance.

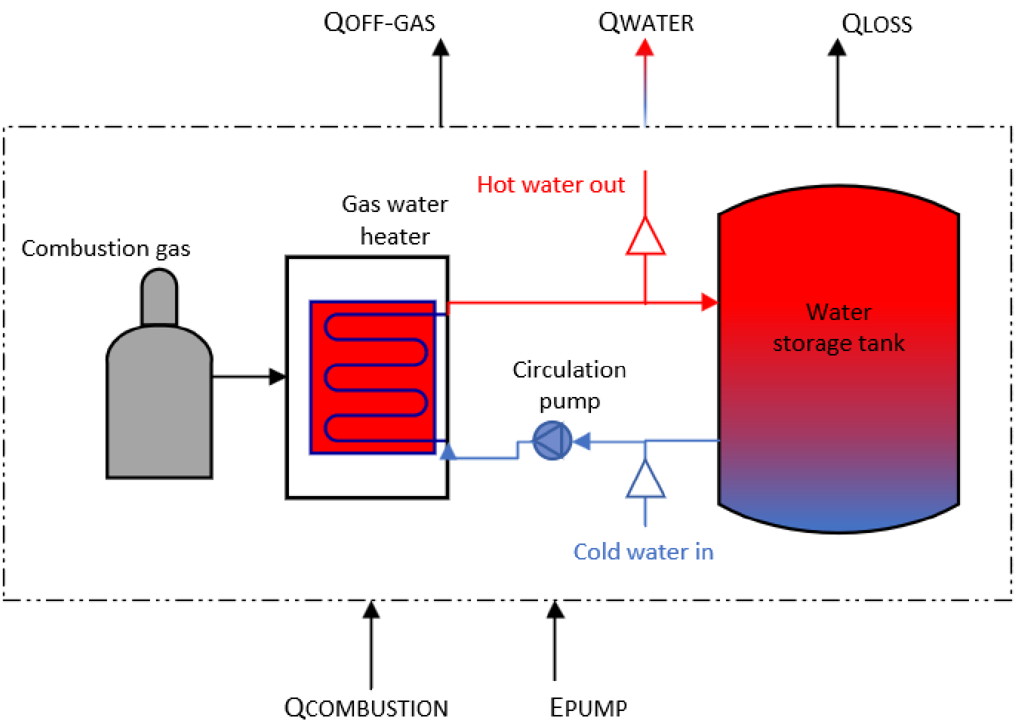

Figure 5.12: GWH mathematical model energy balance

As seen in Figure 5.12 above, cold water enters the water storage tank and is circulated through the gas water heater via a circulation pump. The work normally done by the resistive heating element of an electric water heater is thus instead done by the gas water heater. Although a storage-type gas water heater is not available in the South African market, the storage element introduced during modelling is necessary for more than just an equivalent comparison, as it also ensures the accurate prediction of GWH energy losses. As discussed in Section 5.1.3.1, the efficiency of a gas water heater is dependent on the water consumption profile. While the efficiency prediction of the heater is most accurate during steady-state operation, most consumptions in a realistic water consumption profile are of an unsteady nature. The introduction of the water storage tank thus allows for the modelling of steady-state operation and supplies a constant daily energy loss value, ensuring the accuracy of the GWH model prediction.

The energy balance equates to:

$$U_{i-1} + Q_{COMBUSTION} + E_{PUMP} = U_i + Q_{WATER} + Q_{LOSS} \quad \textbf{(5.6)}$$

U_{i-1} represents the internal energy of the water storage tank at the previous hour i-1. $Q_{COMBUSTION}$ is the thermal energy generated by the combustion of the fuel gas. E_{PUMP} is the electrical energy utilized by the circulation pump. Q_{WATER} represents the change in thermal energy within the water storage tank due to the simultaneous consumption and replenishment of the water storage tank volume. It is thus also the thermal energy required to heat the water. Q_{LOSS} is the standing loss of the water storage tank, indicating the amount of heat lost to the environment surrounding the water storage tank. $Q_{OFF\text{-}GAS}$, shown in Figure 5.12 above, is the heat lost in the off-gas of the combustion process and is not included in Equation (5.6) as it is already represented by the efficiency of the gas water heater.

In order to predict the cost of GWH, the amount of fuel gas m_{gas} and the electrical energy utilized by the circulation pump must be determined. m_{gas} is determined by Equation (5.7) below.

$$Q_{INPUT} = m_{gas} LHV \quad \textbf{(5.7)}$$

LHV is the lower heating value of LPG and equal to 45.5MJ/kg (Borgnakke and Sonntag, 2009). The LHV is used when working with a non-condensing heater, as the water vapour is simply released into the atmosphere. Q_{INPUT} represents the amount of thermal combustion energy that must be delivered in order to heat the water and compensate for the standing loss of the water storage tank. Q_{INPUT} is thus the sum of the energies required divided by the efficiency η of the heater:

$$Q_{INPUT} = \frac{Q_{WATER} + Q_{LOSS}}{\eta} \quad \textbf{(5.8)}$$

The efficiency of the heater was determined in the experimental section and equal to 85%. In order to determine the amount of thermal energy required by the water, the GWH control methodology must be defined. Note that the control methodology of the GWH mathematical model is identical to the HPWH model discussed in Section 4.2. The exact same IF conditions and accompanying equations are applied and can be referred to in Annexure B Section B.1. In order to determine the electrical energy utilized by the circulation pump E_{PUMP} for GWH, the same 12V DC pump used in STWH is modelled (GeyserWise, 2020). E_{PUMP} is again determined using Equation (3.10) and is operational only when the water in the storage tank is being heated from its minimum to maximum setpoint temperature.

The yearly sum of combustion energy delivered by the gas water heater in order to provide the thermal energy required to heat the water $Q_{REQUIRED}$ and electrical energy utilized by the circulation pump $E_{REQUIRED}$ is respectively given by Equations (5.9) and (5.10) below.

$$Q_{REQUIRED} = \sum_{1}^{8760} Q_{INPUT} \tag{5.9}$$

$$E_{REQUIRED} = \sum_{1}^{8760} E_{PUMP} \tag{5.10}$$

The amount of energy required is thus simply the sum of Q_{INPUT} and E_{PUMP} over all 8760 hours of a year. Q_{INPUT} of Equation (5.7) is thus simply replaced with $Q_{REQUIRED}$ in order to determine the yearly sum of m_{gas} required. Finally, the annual operational costs R_{GWH} in R/year is given by Equation (5.11) below.

$$R_{GWH} = \left(m_{gas} \times R_{LPG}\right) + \left(\frac{E_{REQUIRED}}{3600} \times R_{kWh}\right) \tag{5.11}$$

R_{GWH} is thus equal to the yearly amount of m_{gas} in kg required multiplied by the price of LPG in R/kg, plus the electrical energy required by the pump divided by 3600 (converting kJ to kWh) and multiplied with the cost of electricity R_{kWh} in R/kWh. The South African Department of Mineral Resources and Energy determines and updates the retail price of LPG per month. Taken in July 2020, the average zonal price of LPG is R25.78/kg (Department of Mineral Resources and Energy, 2020).

Given the input parameters of the mathematical model as listed in Table 1.2 and those explained in this section, the model results are determined and discussed in the next section.

5.4 Results and discussion

The final results are listed in Table 5.2 below.

Table 5.2: GWH cost results

Symbol	Result	Value	Unit
R_{GWH}	GWH operational costs	8674	R/year
R_{EWH}	Baseline EWH operational costs	7933	R/year
R_{SAVED}	Annual savings relative to the baseline	-741	R/year

The estimated annual operational costs of GWH per household is R8674. GWH, as approached in this study, is predicted to be more expensive to operate than the baseline electric resistance water heater at R7933. This results in a negative annual savings of -R741. There is thus no SPP with a negative annual savings. The capital cost of a Bosch 16Lt Optiflow Professional gas water heater, including VAT, installation and the circulation pump needed for the applied approach, is estimated at R16127.

In terms of performance, Table 5.3 below indicated the amount of energy required from the grid for GWH and EWH.

Table 5.3: GWH grid energy required

Symbol	Result	Value	Unit
E_{GWH}	GWH auxiliary grid energy required	10.65	kWh/year
E_{EWH}	EWH grid energy required	3605.79	kWh/year

Generally, no grid input would be required for GWH. However, due to the application of GWH in this study, it requires grid energy in order to operate the water circulation pump. The amount required can however be considered negligible when compared to the requirements of the previously discussed technologies.

The results thus indicate that GWH, as applied in this study, saved 99.7% of the utility grid input required for EWH.

The techno-economical comparison of the different water heating technologies follows in the next chapter.

CHAPTER 6 – TECHNO-ECONOMICAL COMPARISON

This chapter concludes the study by presenting a side-by-side techno-economical comparison and discussion of the results found in the previous chapters. The conclusion of the study will aim to address the problem statement and purpose of the study by discussing the approach of the study, the findings and the effect of certain input parameters and modelling uncertainties on the findings. Finally, recommendations for future studies will be given.

6.1 Comparison of the water heating technologies

This section compares the following results from each chapter: i) SPP (capital cost divided by annual savings), ii) annual operational costs and annual savings, iii) capital cost and iv) performance results of the water heating technologies. For each comparison the technologies will be arranged by a best-worst scaling for the considered result.

i. Simple payback period

Figure 6.1 below shows the comparative SPP of the water heating technologies.

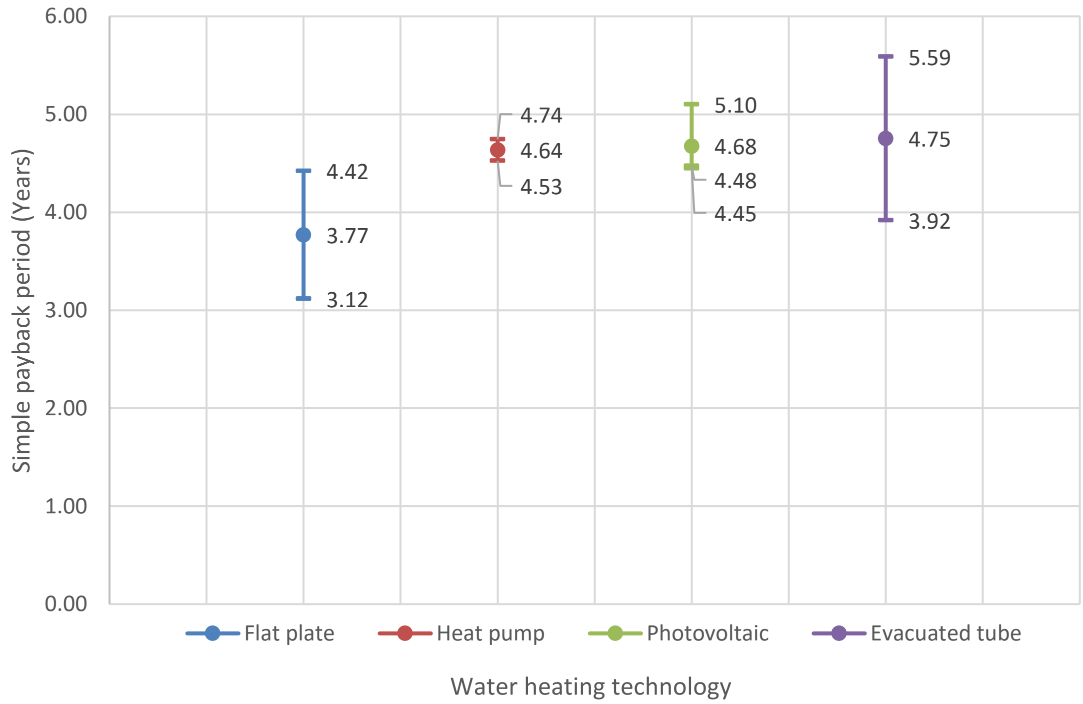

Figure 6.1: Comparison of the SPP

The flat plate solar thermal heater has the shortest SPP of 3.77 years, followed by the heat pump at 4.64 years. The SPP of evacuated tube solar thermal and solar photovoltaic are respectively 4.68 and 4.75 years respectively. The large range observed between the minimum and maximum

SPP of the evacuated tube solar thermal water heater may indicate a significant difference in quality between suppliers. A smaller range is observed between solar photovoltaic suppliers, whereas there is almost no range between the SPP of different heat pump suppliers. The SPP of gas water heating is not given as gas water heating generated a negative annual savings, to be discussed below.

ii. Annual operational costs and savings

Figure 6.2 below shows the comparison of the annual operational costs and savings of the water heating technologies, against the baseline electric resistance water heater.

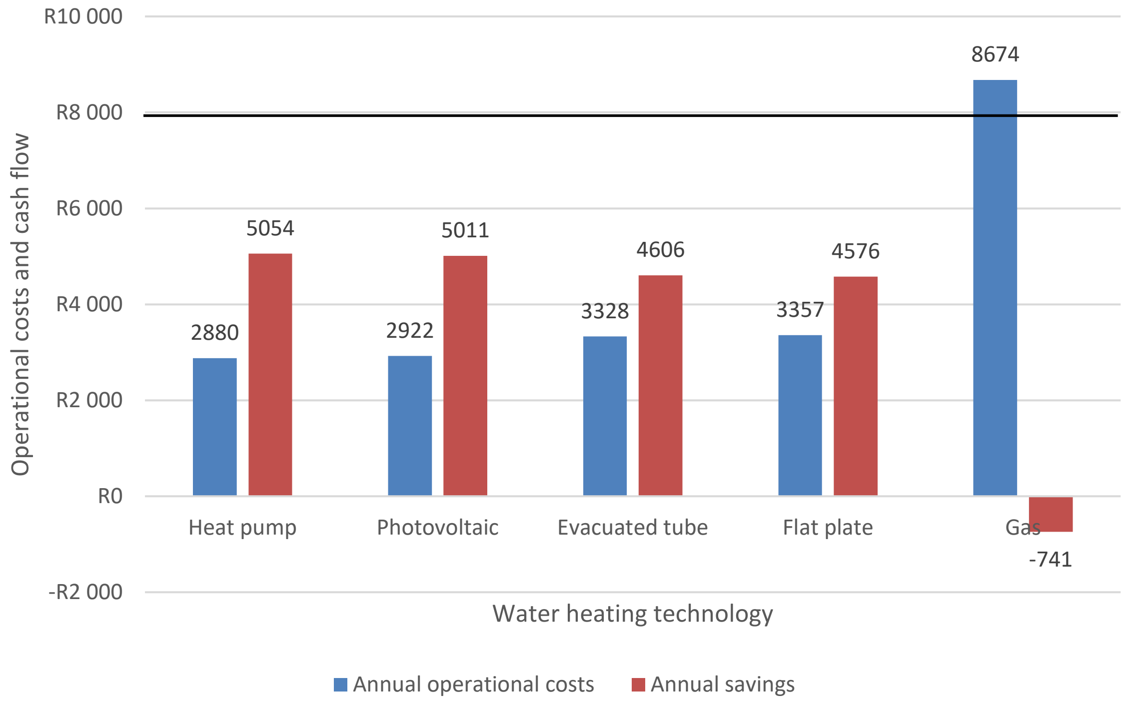

Figure 6.2: Comparison of the annual operational costs and savings

The straight line in Figure 6.2 indicates the annual operational costs of electric water heating at R7933. The operational costs of the solar technologies are based on the backup power required. The operational costs of the heat pump are for the electrical grid energy required and for gas water heating, it is based on the price of LPG. The lower the annual operational costs of the water heating technology, the higher the annual savings. The heat pump generated the highest annual savings of R5054, closely followed by the solar photovoltaic system at R5011. The evacuated tube and flat plate solar thermal water heaters were also very close at R4606 and R4576 respectively. Gas water heating was more expensive to operate than the electric water heater baseline and generated a negative savings of -R741. Although gas water heating is very expensive, with the price of LPG fluctuating according to the oil price, it has the lowest capital cost and generally requires no grid as will be discussed below.

iii. Capital cost

Figure 6.3 below shows the capital cost (including installation and VAT) of each water heating technology.

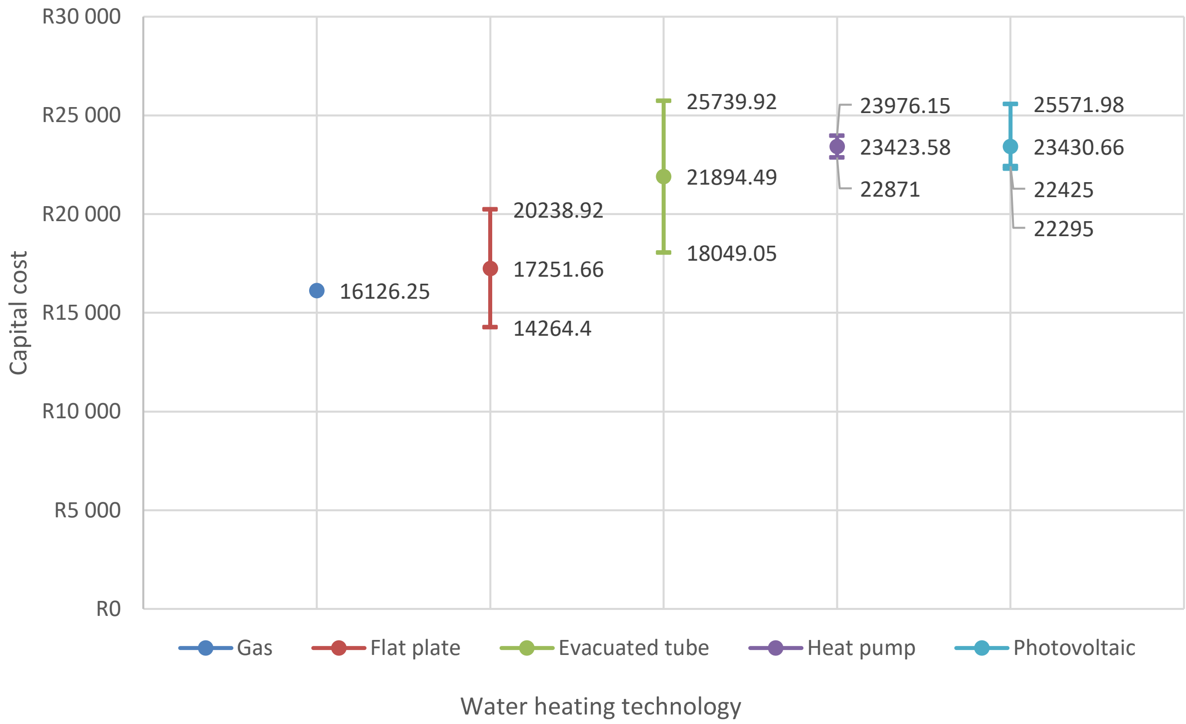

Figure 6.3: Comparison of the capital cost

The capital cost of the gas water heater and flat plate solar thermal water heater are the least expensive at R16127 and R17252 respectively. The evacuated tube solar thermal water heater is R21895 and also has the highest capital cost given by a single supplier. With a negligible difference, the capital cost of the heat pump and solar photovoltaic system are the most expensive at R23424 and R23431 respectively.

iv. Performance

Figure 6.4 below shows the comparison in terms of the percentage grid input energy each water heating technology saved.

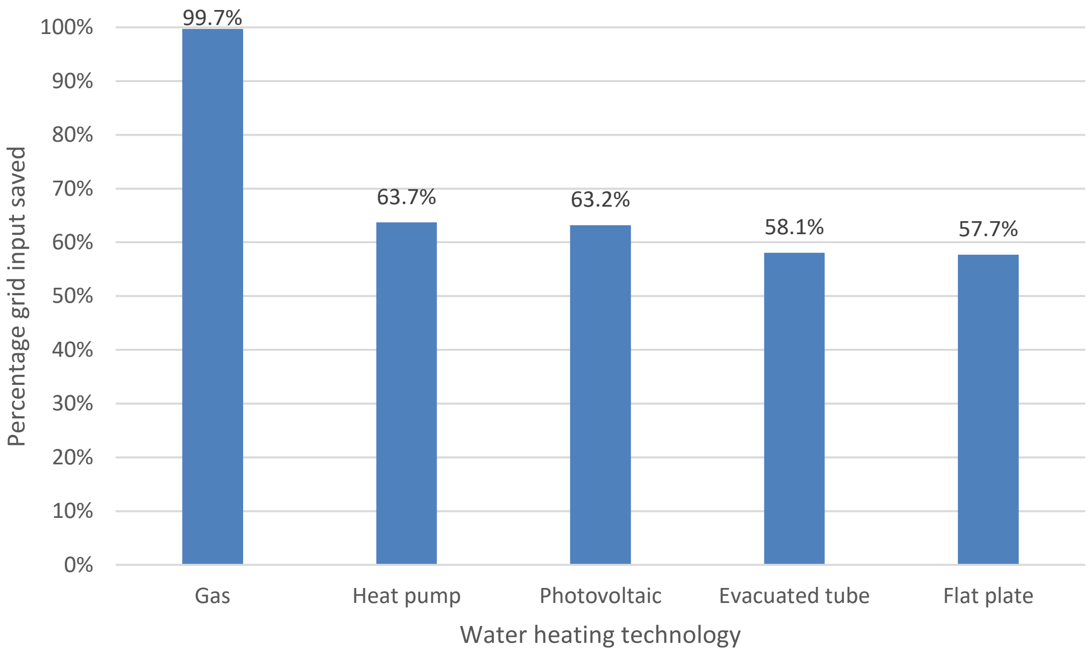

Figure 6.4: Comparison of the grid input saved

As stated, gas water heating generally requires no grid input. However, due to the modelling approach of gas water heating in this study, an insignificant amount of grid energy is required in order to operate the water circulation pump. Gas water heating thus outperformed the other water heating technologies in terms of the amount of grid input saved, relative to that required by the electric resistance water heater baseline, at 99.7%. The heat pump performed second best at 63.7% saved, followed closely by the solar photovoltaic system at 63.2%. Evacuated tube and flat plate solar thermal respectively saved 58.1% and 57.7% grid input. Considering that the modelling approach ensured the adequate supply of hot water during peak consumption using auxiliary grid input, all water heating technologies saved greater than 50% of the grid input required relative to the electric water heater baseline.

In terms of the ability of each water heating technology to provide hot water, the solar driven technologies alone cannot provide hot water during early morning hours. The hot water availability of a heat pump water heater equals that of the conventional electric water heater, although both are grid dependent. Lastly, gas water heating can supply hot water at all times, but at a cost.

The tabled results of Figures 6.1 to 6.4 are given by Table D.1 of Annexure D Section D.1. To summarize, Table 6.1 below rate the water heating technologies from best to worst in terms of their simple payback period, annual operational costs and performance in terms of the percentage grid input saved.

Table 6.1: Ranking of the water heating technologies

Ranking	Simple payback period	Annual operational costs	Grid input saved
1.	Flat plate solar thermal water heater	Heat pump water heater	Gas water heating
2.	Heat pump water heater	Solar photovoltaic water heating system	Heat pump water heater
3.	Solar photovoltaic water heating system	Evacuated tube solar thermal water heater	Solar photovoltaic water heating system
4.	Evacuated tube solar thermal water heater	Flat plate solar thermal water heater	Evacuated tube solar thermal water heater
5.	Gas water heating	Gas water heating	Flat plate solar thermal water heater

Three different conclusions can be drawn when considering the ranking of Table 6.1 above. Firstly, if the lowest initial capital investment is the decisive factor, a flat plate solar thermal water heater is the best solution. Flat plate solar thermal is also the best solution if the shortest payback period is the decisive factor. Secondly, if the annual operational costs of water heating are considered the decisive factor, a heat pump water heater is the best solution, followed very closely by a solar photovoltaic system. Both of these water heating technologies delivered the lowest annual operational costs, generating the highest annual savings relative to the baseline. Lastly, gas water heating saved the greatest percentage of grid input required by the baseline. The most effective grid independent water heating solution would however be the conventional tankless application of gas water heating.

6.2 Conclusion

In this study, four different renewable and alternative domestic water heating technologies were evaluated, namely: (a) solar photovoltaic, (b) solar thermal, (c) heat pump and (d) gas water heating. These water heating technologies were compared, against the baseline electric resistance water heater, in terms of their cost effectiveness over a typical climatic year in Johannesburg, South Africa, for a grid connected household of four people.

A literature study was conducted on each water heating technology in order to determine two main aspects. Firstly, to determine the working principles of the water heating technology as applied in this study and secondly, to determine the factors affecting the efficiency of the water heating technology. It was found that the environmental and operational conditions affected the efficiency of all the water heating technologies. Environmental conditions mainly referred to the solar irradiation and ambient temperature, whereas operational conditions mainly referred to the water consumption profile and various operating temperatures. A system level mathematical model was created for each water heating technology, which included these factors as the main input parameters. Climatic design year data provided hourly values of the total horizontal radiation and ambient temperature. A ratio to determine the radiation on a tilted surface to that of a horizontal surface was also applied, as the PV panels and solar collectors were modelled at an optimal tilt angle. A normalised hot water consumption profile was also applied to the daily amount of hot water consumed per household. Each water heating technology was modelled as if retrofitted to an existing electric water heater, also referred to as the water storage tank. The electric water heater primarily acted as an auxiliary unit, ensuring that hot water was provided as required by drawing power from the utility grid. Secondly, it acted as a water storage unit, ensuring that system losses were equal in each water heating system. The normalised hot water consumption profile and water storage tank aided to compare the technologies on an equal footing. Furthermore, the solar photovoltaic mathematical model incorporated a simulation model in order to determine the power generated by the PV system from the solar radiation profile. The simulation model was also experimentally verified. Gas water heating also included an experimental section in order to determine its water heater efficiency, used in its mathematical model. The solar thermal and heat pump water heating mathematical models incorporated system specification provided by reputable suppliers. Heat pump water heating also incorporated the findings of a previous study by Ras (2015).

The mathematical models determined the yearly amount of auxiliary electrical energy required from the utility grid, to provide hot water when required. This was done by mainly assessing the hourly temperature of the water in the storage tank. The temperature of the water in the storage tank was mainly dependent on the consumption profile, water setpoint temperatures, the heat input from the water heating technology and auxiliary and finally, on the standing loss of the water storage tank. The yearly amount of auxiliary energy required from the utility grid was used to determine the annual operational costs of each water heating technology. It was also used to determine the amount of grid input each water heating technology saved. The annual savings was determined for each water heating technology against that of the baseline electric water heater. Quotations were requested from reputable South African suppliers in order to determine the capital cost of each retrofitted water heating system. With the capital cost and annual savings, a simple payback period was determined. Finally, the water heating technologies were compared and ranked in terms of their simple payback period, annual operational costs and savings, capital costs and performance in terms of the percentage grid input saved.

The results found the flat plate solar thermal water heater had the shortest payback period. The less expensive capital cost of the flat plate solar collector contributed significantly to this result. The heat pump water heater was ranked second best in terms of the simple payback period. It was also found that in terms of annual operational costs and annual savings, the heat pump water heater ranked first, with the solar photovoltaic water heating system second. Although the heat pump water heating system is one of the most expensive solutions, it ranked second in terms of the simple payback period as it generated the highest annual savings. In terms of the simple payback period, annual operational costs and savings, gas water heating ranked last. Gas water heating was the most expensive water heating system to operate and generated a negative annual savings. Lastly, the results found that gas water heating saved the greatest percentage of grid input. Heat pump and solar photovoltaic water heating respectively ranked second and third in this regard. This result indicated that if total grid independency is required, coupled with the immediate availability of hot water, gas water heating is the only solution. A solar photovoltaic water heating system is however assumed to be the best grid independent solution if hot water is not immediately required.

The study by Buckley *et al.* (2020), mention in the introduction of Chapter 2, also experimentally evaluated and compared a residential solar photovoltaic and flat plate solar thermal water heating system in Stellenbosch, South Africa. Buckley *et al.* (2020) found that solar thermal water heating produced a better thermal energy yield. This study however found that solar photovoltaic water heating performed better. The difference in findings may be contributed to the following factors. While both Buckley *et al.* (2020) and this study used a 2.4m^2 flat plate solar collector, Buckley *et al.* (2020) used a 1.56kW solar photovoltaic system. This study used a 1.8kW solar photovoltaic system. As was shown in Figure 1.1, Johannesburg also experiences a higher average daily global horizontal irradiation level that Stellenbosch. There may also be a difference in system efficiencies. Similar to this study, Buckley *et al.* (2020) did however find that the flat plate solar thermal water heating system had a shorter payback period than the solar photovoltaic water heating system. Buckley *et al.* (2020) found a flat plate solar thermal water heating payback period of 6 years, compared to 4.57 years found in this study.

It is difficult to conclude which water heating technology is best overall, due to varying decisive factors and because not all variations of the different water heating systems were evaluated. These results thus only apply to the specific systems evaluated in this study and not to the water heating methods as a whole. It can be concluded that although solar driven systems have low operational costs, they alone have the disadvantage of only delivering hot water during sufficient solar hours. Gas water heating alone can supply hot water at all times, independent from the grid, but comes at a cost. The results may also vary if each system was optimized before being compared. Optimization was however not included in the scope of this study. Applying the optimal size of each system and determining the optimal consumption profile for each water heating system may have a significant impact on the results. The annual savings will most likely also be affected when optimizing the consumption profile, as greater consumption will lead to greater savings in the case of renewables.

6.3 Recommendations

The recommendations for further studies firstly entail improving upon the assumptions made in this study. It was assumed that the temperature distribution within the water storage tank was uniform, neglecting stratification. The effect of stratification can be considered in a future study. The hourly standing loss of the water storage tank was assumed constant at its rated loss. The effect of the ambient temperature surrounding the water storage tank on the standing losses can be modelled in more detail.

Secondly, the respective water heating technologies can be modelled in more detail. Maximum power point tracking could be included for the solar photovoltaic water heating system. A two-diode photovoltaic simulation model can also be considered. It was however found that the accuracy of the single-diode model proved adequate during the experimental evaluation. The experimental evaluation of the gas water heater can also be improved by determining its heat-loss coefficient. The off-gas produced by the gas water heater can also be analysed in order to determine the amount of excess oxygen in the combustion process.

In this study, the water heating technologies were mathematically modelled on a system level. A component level simulation model of the water heating technologies could be considered in future studies. A component level simulation model would also allow an in-depth parametric study in order to optimize each water heating technology.

It is recommended that an optimization study focuses on the hot water consumption profile. The consumption profile greatly affects all results found in this study. Different findings could be assumed if the consumption profile were to be optimized for each respective water heating technology. Finally, the financial analysis can also be expanded upon to include maintenance cost and the changing tariffs of electricity and gas. It could also include net present value, internal rate of return and the levelized cost of water heating.

REFERENCE LIST

Aeidapu, M. (2015) *Simulation of one diode model of PV Cell using MATLAB/Simulink*. Available at: https://www.youtube.com/watch?v=uuKOu7vpteo&ab_channel=MaheshAeidapu (Accessed: 29 July 2019).

Afrox (2015) ‘Product Reference Manual - Section 5 - Liquefied Petroleum Gas’, p. 10. doi: 10.1039/c0nr00444h.

Alberto, P. and Ferrer, F. (2017) ‘Average economic performance of solar water heaters for low density dwellings across South Africa’, *Renewable and Sustainable Energy Reviews*. Elsevier Ltd, 76(May 2016), pp. 507–515. doi: 10.1016/j.rser.2017.03.074.

Ayodele, T. R., Ogunjuyigbe, A. S. O. and Ekoh, E. E. (2016) ‘Evaluation of numerical algorithms used in extracting the parameters of a single-diode photovoltaic model’, *Sustainable Energy Technologies and Assessments*. Elsevier Ltd, 13, pp. 51–59. doi: 10.1016/j.seta.2015.11.003.

Ayompe, L. M. *et al.* (2011) ‘Comparative field performance study of flat plate and heat pipe evacuated tube collectors (ETCs) for domestic water heating systems in a temperate climate’, *Energy*. Elsevier Ltd, 36(5), pp. 3370–3378. doi: 10.1016/j.energy.2011.03.034.

ayyanaraz (2014) *PV parameter extraction example TSM290*. Available at: https://www.youtube.com/watch?v=wNg4e6_QASw&ab_channel=ayyanaraz (Accessed: 29 July 2019).

Barros, J. P., Azevedo, J. L. T. and Monteiro, L. (2014) ‘Effect of relative humidity in the efficiency of condensing gas water heater appliance’, *Applied Thermal Engineering*. Elsevier Ltd, 65(1–2), pp. 66–73. doi: 10.1016/j.applthermaleng.2013.12.073.

Borgnakke, C. and Sonntag, R. E. (2009) *Fundamentals of Thermodynamics*. Seventh ed, *Journal of Chemical Information and Modeling*. Seventh ed. Edited by N. Repasky and M. McDonald. Michigan: Don Fowley. doi: 10.1017/CBO9781107415324.004.

Bosch (2019) *Bosch OptiFlow Professional*. Available at: https://hotwaterprofessionals.com.au/sites/default/files/optiflow_professional_au_1.pdf (Accessed: 24 October 2019).

Bouraiou, A. *et al.* (2015) ‘Modeling and Simulation of Photovoltaic Module and Array Based on One and Two Diode Model Using Matlab/Simulink’, *Energy Procedia*. Elsevier B.V., 74, pp. 864–877. doi: 10.1016/j.egypro.2015.07.822.

Bourke, G. (2015) *Integration of gas instantaneous auxiliaries with renewable energy residential water heaters*. Available at: http://hdl.handle.net/2292/26953.

Lo Brano, V. *et al.* (2010) 'An improved five-parameter model for photovoltaic modules', *Solar Energy Materials and Solar Cells*. Elsevier, 94(8), pp. 1358–1370. doi: 10.1016/j.solmat.2010.04.003.

Buckley, A. I. *et al.* (2020) 'Comparison of Photovoltaic and Solar Thermal Hot Water Systems in the South African Context'. Available at: https://mcusercontent.com/fb863ec402c2feeef15192072/files/6dec30b8-95d3-426b-bcc7-92984c1e7844/solar_electric_vs_solar_thermal_full_paper.pdf.

Burch, J. *et al.* (2008) 'Preliminary Modeling, Testing, and Analysis of a Gas Tankless Water Heater', in *SOLAR 2008*, pp. 1–8. Available at: https://digital.library.unt.edu/ark:/67531/metadc893927/.

Butcher, T. A. and Schoenbauer, B. (2011) 'Application of a linear input/output model to tankless water heaters', *ASHRAE Transactions*, 117(PART 1), pp. 683–689. Available at: https://www.researchgate.net/publication/255001743_Application_of_a_Linear_InputOutput_Model_to_Tankless_Water_Heaters.

Chromagen (2020) *Chromangen Product Catalog*. Available at: https://chromagen.com/wp-content/uploads/2020/03/Chromagen_Product-Catalog_2020_Website.pdf (Accessed: 8 September 2020).

Costa, V., Ferreira, J. and Guilherme, D. (2016) 'Modeling and simulation of tankless gas water heaters to reduce temperature overshoots and undershoots', *12th International Conference on Heat Transfer, Fluid Mechanics and Thermodynamics (HEFAT 2016)*, pp. 1404–1409. Available at: https://repository.up.ac.za/handle/2263/61870.

Cotfas, D. T., Cotfas, P. A. and Kaplanis, S. (2013) 'Methods to determine the dc parameters of solar cells: A critical review', *Renewable and Sustainable Energy Reviews*. Elsevier, 28, pp. 588–596. doi: 10.1016/j.rser.2013.08.017.

dataTaker (2017) *DT80W Series 4 Data Logger*. Available at: https://www.dataloggerinc.com/wp-content/uploads/2017/06/dataTaker_DT80W.pdf (Accessed: 13 August 2019).

Deloitte Consulting Pty (Ltd) (2017) *An overview of electricity consumption and pricing in South Africa*. Available at: http://www.eskom.co.za/Documents/EcoOverviewElectricitySA-2017.pdf.

Department of Mineral Resources and Energy (2020) *Petroleum products act, 1977*. Available at: http://www.energy.gov.za/files/esources/petroleum/July2020/LPG-Regulations.pdf.

Department of Renewable Energy (2020) *Solar-Power*. Available at: http://www.energy.gov.za/files/esources/renewables/r_solar.html.

Diez, F. J. *et al.* (2019) 'Modelling of a flat-plate solar collector using artificial neural networks for different working fluid (water) flow rates', *Solar Energy*. Elsevier, 188(April), pp. 1320–1331. doi: 10.1016/j.solener.2019.07.022.

Dintchev, O. *et al.* (2018) 'Potential of Photovoltaics for Water Heating in South Africa', *Strategic Planning for Energy and the Environment*, 37(4), pp. 22–38. doi: 10.1080/10485236.2018.12002424.

Dobriyal, R. *et al.* (2020) 'A brief review on solar flat plate collector by incorporating the effect of nanofluid', *Materials Today: Proceedings*. Elsevier Ltd., 21, pp. 1653–1658. doi: 10.1016/j.matpr.2019.11.294.

Duffie, J. A. and Beckman, W. A. (2013) *Solar Engineering of Thermal Processes*. Fourth ed. John Wiley & Sons, Inc. doi: 10.1119/1.14178.

Electrolux SA (2019) *KWIKOT superline 400 DUAL electric water heaters*. Available at: https://www.kwikot.com/kwikot/brochures/Superline-Dual-Electric-Water-Heaters-July-2019.pdf (Accessed: 27 May 2020).

Enerflow (2020) *Residential heat pumps*. Available at: https://www.enerflow.co.za/images/pdfs/technical_specs/2 RHP-specsheet_digital_rev1.pdf (Accessed: 30 June 2020).

Engineering Toolbox. (2011) *Mixing Fluids*. Available at: https://www.engineeringtoolbox.com/mixing-fluids-temperature-mass-d_1785.html (Accessed: 29 July 2019).

Fanney, A. H. and Dougherty, B. P. (1997) 'A Photovoltaic Solar Water Heating System', *Journal of Solar Energy Engineering*, 119(2), pp. 126–133. doi: 10.1115/1.2887891.

Fanney, A. H. and Dougherty, B. P. (2001) 'Experiences With Using Solar Photovoltaics to Heat Domestic Water', *Journal of Solar Energy Engineering*, pp. 1–13. doi: 10.1115/1.1562635.

Farahat, S., Sarhaddi, F. and Ajam, H. (2009) 'Exergetic optimization of flat plate solar collectors', *Renewable Energy*. Elsevier Ltd, 34(4), pp. 1169–1174. doi: 10.1016/j.renene.2008.06.014.

Ge, Z. *et al.* (2014) ‘Exergy analysis of flat plate solar collectors’, *Entropy*, 16(5), pp. 2549–2567. doi: 10.3390/e16052549.

GeyserRobot (2015) *GeyserRobot*. Available at: http://www.geyserrobot.co.za/?fbclid=IwAR0itPdq75y8iRhZTAg6LqcSWw0hfrNif89i6b3ohs6tGKJUd8O39eR6AzU (Accessed: 13 August 2019).

GeyserWise (2020) *Brushless DC Pump*. Available at: https://cdn.shopify.com/s/files/1/0004/6143/9027/files/GeyserWise-Manual-Brushless-DC-Pump-12V1_18f5815d-d73b-4171-aeaf-0aafa45dbe58.pdf?5956 (Accessed: 8 September 2020).

Glanville, P., Kosar, D. and Stair, J. (2013) ‘Short-term performance of gas-fired tankless water heaters: Laboratory characterization’, *ASHRAE Transactions*, 119(PART 1), pp. 1–22. Available at: https://www.researchgate.net/publication/281699574_Short-term_performance_of_gas-fired_tankless_water_heaters_Laboratory_characterization.

Greben, H. A. and Oelofse, S. H. H. (2009) ‘Unlocking the resource potential of organic waste: A South African perspective’, *Waste Management and Research*, 27(7), pp. 676–684. doi: 10.1177/0734242X09103817.

Healy, W. M., Ullah, T. and Roller, J. (2011) ‘Input-output approach to predicting the energy efficiency of residential water heaters - Testing of gas tankless and electric storage water heaters’, *ASHRAE Transactions*, 117(PART 2), pp. 521–532. Available at: https://www.researchgate.net/publication/299506823_Input-Output_Approach_to_Predicting_the_Energy_Efficiency_of_Residential_Water_Heaters--Testing_of_Gas_Tankless_and_Electric_Storage_Water_Heaters.

Hohne, P. A., Kusakana, K. and Numbi, B. P. (2019a) ‘A review of water heating technologies: An application to the South African context’, *Energy Reports*. Elsevier Ltd, 5, pp. 1–19. doi: 10.1016/j.egyr.2018.10.013.

Hohne, P. A., Kusakana, K. and Numbi, B. P. (2019b) ‘Optimal energy management and economic analysis of a grid-connected hybrid solar water heating system: A case of Bloemfontein, South Africa’, *Sustainable Energy Technologies and Assessments*. Elsevier, 31(December 2018), pp. 273–291. doi: 10.1016/j.seta.2018.12.027.

Humada, A. M. *et al.* (2016) ‘Solar cell parameters extraction based on single and double-diode models: A review’, *Renewable and Sustainable Energy Reviews*. Elsevier Ltd, 56, pp. 494–509. doi: 10.1016/j.rser.2015.11.051.

Ibrahim, H. and Anani, N. (2017) ‘Evaluation of Analytical Methods for Parameter Extraction of PV modules’, *Energy Procedia*. Elsevier B.V., 134, pp. 69–78. doi: 10.1016/j.egypro.2017.09.601.

Ishaque, K. *et al.* (2011) ‘Modeling and simulation of photovoltaic (PV) system during partial shading based on a two-diode model’, *Simulation Modelling Practice and Theory*. Elsevier B.V., 19(7), pp. 1613–1626. doi: 10.1016/j.simpat.2011.04.005.

Ishaque, K., Salam, Z. and Taheri, H. (2011) ‘Simple, fast and accurate two-diode model for photovoltaic modules’, *Solar Energy Materials and Solar Cells*. Elsevier, 95(2), pp. 586–594. doi: 10.1016/j.solmat.2010.09.023.

ITS Solar (2020) *ITS 58/1800 Power output per collector unit*. Available at: https://www.itssolar.co.za/its-product-its-58-1800-10-tube-collectors-55 (Accessed: 8 September 2020).

Jafarkazemi, F. and Ahmadifard, E. (2013) ‘Energetic and exergetic evaluation of flat plate solar collectors’, *Renewable Energy*. Elsevier Ltd, 56, pp. 55–63. doi: 10.1016/j.renene.2012.10.031.

Jain, S. and Jain, P. K. (2017) ‘The rise of Renewable Energy implementation in South Africa’, *Energy Procedia*. Elsevier B.V., 143, pp. 721–726. doi: 10.1016/j.egypro.2017.12.752.

JB Marks Local Municipality (2019) *Schedule of tariffs for the supply of electricity*. Available at: https://jbmarks.co.za/sites/default/files/2019-08 documents/scheduleofTariffsElectricity.pdf (Accessed: 27 July 2020).

Johnson, G. and Beausoleil-Morrison, I. (2016) ‘The calibration and validation of a model for predicting the performance of gas-fired tankless water heaters in domestic hot water applications’, *Applied Energy*. Elsevier Ltd, 177, pp. 740–750. doi: 10.1016/j.apenergy.2016.05.130.

Kakaza, M. and Folly, K. A. (2015) ‘Effect of solar water heating system in reducing household energy consumption’, *IFAC-PapersOnLine*. Elsevier B.V., 48(30), pp. 468–472. doi: 10.1016/j.ifacol.2015.12.423.

Kicsiny, R. (2014) ‘Multiple linear regression based model for solar collectors’, *Solar Energy*, 110, pp. 496–506. doi: 10.1016/j.solener.2014.10.003.

Kritzinger, K. (2017) *Policy Brief : Solar Photovoltaic Technologies*. Available at: https://www.crses.sun.ac.za/files/research/publications/popular-media-and-policy-brief/PV Policy Brief Dec 2017.pdf.

Laudani, A., Riganti Fulginei, F. and Salvini, A. (2014) ‘Identification of the one-diode model for photovoltaic modules from datasheet values', *Solar Energy*. Elsevier Ltd, 108, pp. 432–446. doi: 10.1016/j.solener.2014.07.024.

Lee, K. H. and Baek, N. C. (2014) 'A modified efficiency equation of solar collectors', *Energy Procedia*. Elsevier B.V., 48, pp. 145–149. doi: 10.1016/j.egypro.2014.02.018.

Maleki, S. A. M., Hizam, H. and Gomes, C. (2017) 'Estimation of hourly, daily and monthly global solar radiation on inclined surfaces: Models re-visited', *Energies*, 10(134), pp. 1–28. doi: 10.3390/en10010134.

Mangal, D. *et al.* (2010) 'Acknowledgement Of Evacuated Tube Solar Water Heater Over Flat Plate Solar Water Heater', *International Journal of Engineering*, 4(4), pp. 279–284. Available at: http://citeseerx.ist.psu.edu/viewdoc/download?doi=10.1.1.301.9890&rep=rep1&type=pdf.

Mares, O., Paulescu, M. and Badescu, V. (2015) 'A simple but accurate procedure for solving the five-parameter model', *Energy Conversion and Management*. Elsevier Ltd, 105, pp. 139–148. doi: 10.1016/j.enconman.2015.07.046.

Morrison, G. L., Anderson, T. and Behnia, M. (2004) 'Seasonal performance rating of heat pump water heaters', *Solar Energy*, 76(1–3), pp. 147–152. doi: 10.1016/j.solener.2003.08.007.

Msibi, S. S. and Kornelius, G. (2017) 'Potential for domestic biogas as household energy supply in South Africa', *Journal of Energy in Southern Africa*, 28(2), pp. 1–13. doi: 10.17159/2413-3051/2017/v28i2a1754.

Mukumba, P., Makaka, G. and Mamphweli, S. (2016) 'Biogas Technology in South Africa, Problems, Challenges and Solutions', *International Journal of Sustainable Energy and Environmental Research*, 5(4), pp. 58–69. doi: 10.18488/journal.13/2016.5.4/13.4.58.69.

Mutungwazi, A., Mukumba, P. and Makaka, G. (2018) 'Biogas digester types installed in South Africa: A review', *Renewable and Sustainable Energy Reviews*. Elsevier Ltd, 81(July 2017), pp. 172–180. doi: 10.1016/j.rser.2017.07.051.

NERSA (2008) *Inquiry into the national electricity supply shortage and load shedding*. Available at: https://static.pmg.org.za/docs/080528nersa.pdf.

Okudoh, V. *et al.* (2014) 'The potential of cassava biomass and applicable technologies for sustainable biogas production in South Africa: A review', *Renewable and Sustainable Energy Reviews*. Elsevier, 39, pp. 1035–1052. doi: 10.1016/j.rser.2014.07.142.

Page-Shipp, R. J. (1980) 'The basic principles of solar water heating', in *Solar Press Conference*.

Pretoria: NATIONAL BUILDING RESEARCH INSTITUTE OF THE CSIR, pp. 1–7. Available at: https://researchspace.csir.co.za/dspace/bitstream/handle/10204/3596/Paige-Shipp_1980.pdf?sequence=1.

Peng, J. W., Li, H. and Zhang, C. L. (2016) 'Performance comparison of air-source heat pump water heater with different expansion devices', *Applied Thermal Engineering*. Elsevier Ltd, 99, pp. 1190–1200. doi: 10.1016/j.applthermaleng.2016.01.113.

Ranjith, P. V. and Karim, A. A. (2016) 'A Comparative Study on the Experimental and Computational Analysis of Solar Flat Plate Collector Using an Alternate Working Fluid', *Procedia Technology*. Elsevier B.V., 24, pp. 546–553. doi: 10.1016/j.protcy.2016.05.098.

Rankin, R. and van Eldik, M. (2010) 'An investigation into the energy savings and economic viability of heat pump water heaters applied in the residential sector - A comparison with solar water heating systems', pp. 1–10. Available at: https://www.enerflow.co.za/images/pdfs/case_studies/1 Heat pumps vs solar heating.pdf.

Ras, M. N. (2015) *A method for the seasonal performance rating of a residential water heating heat pump*. Potchefstroom. Available at: https://repository.nwu.ac.za/bitstream/handle/10394/20595/Ras_MN_2015.pdf?sequence=1.

Rasimphi, T. E. and Tinarwo, D. (2020) 'Relevance of biogas technology to Vhembe district of the Limpopo province in South Africa', *Biotechnology Reports*. Elsevier B.V., 25, pp. 1–5. doi: 10.1016/j.btre.2019.e00412.

ReneSola (2014) *ReneSola Virtus ® II Module 300W, 305W, 310W*. Available at: http://www.renesola.com/file/Global/product/pdf/Virtus II 300-310(4035) En 1405 TUV 3BB.pdf (Accessed: 13 August 2019).

Salilih, E. M. and Birhane, Y. T. (2019) 'Modeling and Analysis of Photo-Voltaic Solar Panel under Constant Electric Load', *Journal of Renewable Energy*, 2019, pp. 1–10. doi: 10.1155/2019/9639480.

Seco-Nicolás, M., Alarcón García, M. and Luna-Abad, J. P. (2020) 'Experimental calculation of the mean temperature of flat plate thermal solar collectors', *Results in Engineering*, 5(September 2019), pp. 1–7. doi: 10.1016/j.rineng.2020.100095.

Shukla, R. *et al.* (2013) 'Recent advances in the solar water heating systems: A review', *Renewable and Sustainable Energy Reviews*. Elsevier, 19, pp. 173–190. doi: 10.1016/j.rser.2012.10.048.

Smith, M. T., Schroenn Goebel, J. and Blignaut, J. N. (2014) 'The financial and economic feasibility of rural household biodigesters for poor communities in South Africa', *Waste Management*. Elsevier Ltd, 34(2), pp. 352–362. doi: 10.1016/j.wasman.2013.10.042.

Solargis (2019) *South Africa Global Horizontal Irradiation solar resource map*. Available at: https://solargis.com/maps-and-gis-data/download/south-africa (Accessed: 29 July 2019).

Struckmann, F. (2008) *Analysis of a Flat-Plate Solar Collector*. Sweden. Available at: http://www.lth.se/fileadmin/ht/Kurser/MVK160/Project_08/Fabio.pdf.

Swedish Gas Technology Center Ltd (2012) *Basic Data on Biogas*. Available at: http://www.sgc.se/ckfinder/userfiles/files/BasicDataonBiogas2012.pdf.

Tangwe, S. loh and Simon, M. (2019) 'Quantification of the viability of residential air source heat pump water heaters as potential replacement for geysers in South Africa', *Journal of Engineering, Design and Technology*, 17(2), pp. 1–15. doi: 10.1108/JEDT-05-2017-0042.

Tangwe, S., Simon, M. and Meyer, E. (2014) 'Mathematical modeling and simulation application to visualize the performance of retrofit heat pump water heater under first hour heating rating', *Renewable Energy*. Elsevier Ltd, 72, pp. 203–211. doi: 10.1016/j.renene.2014.07.011.

van Deventer, E. N. (1971) *Climatic and other design data for evaluating heating and cooling requirements of buildings (CSIR research report)*. Available at: https://www.amazon.com/Climatic-evaluating-requirements-buildings-research/dp/B0007AG60Q.

Villalva, M. G., Gazoli, J. R. and Filho, E. R. (2009) 'Comprehensive Approach to Modeling and Simulation of Photovoltaic Arrays', *IEEE TRANSACTIONS ON POWER ELECTRONICS*, 24(5), pp. 1198–1207. doi: 10.1039/c4dt03820g.

Widén, J. and Munkhammar, J. (2019) *Solar Radiation Theory*, *Solar Radiation Theory*. doi: 10.33063/diva-381852.

Yuill, D. P., Coward, A. H. and Henze, G. P. (2010) 'Performance comparison of control methods for tankless water heaters', *HVAC and R Research*, 16(5), pp. 677–690. doi: 10.1080/10789669.2010.10390927.

Zhang, J., Wang, R. Z. and Wu, J. Y. (2007) 'System optimization and experimental research on air source heat pump water heater', *Applied Thermal Engineering*, 27(5–6), pp. 1029–1035. doi: 10.1016/j.applthermaleng.2006.07.031.

ANNEXURE A

A.1 Characteristic parameter derivations

1. Photogenerated current

Assume short circuit conditions: $I = I_{SC}$ and $V = 0$. As the value of R_S is small, the diode voltage $V_D = V + IR_S$ is also small. As V_D is then relatively small compared to the thermal voltage V_T, it follows that:

$$\exp\left(\frac{V_D}{V_T}\right) - 1 \approx 0$$

Under the same argument, the value of the shunt current $I_{RS} \approx 0$. The exponential term is also multiplied with the reverse saturation current I_0 which has a nano ranged value. This proves that under short circuit condition the diode and shunt currents are negligible and reduces equation 2.2 to:

$$I = I_{PV} - I_0\left[\exp\left(\frac{q(V + IR_S)}{aN_s kT}\right) - 1\right] - \frac{V + IR_S}{R_{SH}}$$

Resulting in $I_{PV} = I_{SC}$.

2. Shunt resistance

The relationship between the shunt resistance R_{SH} and the slope of the curve at short circuit condition is applied by taking the derivative of the current with respect to the voltage:

$$\frac{dI}{dV} = -\frac{I_0}{V_T}\left[\exp\left(\frac{V + IR_S}{V_T}\right)\left(1 + R_S\frac{dI}{dV}\right)\right] - \frac{1}{R_{SH}} - \frac{R_S}{R_{SH}}\frac{dI}{dV}$$

Factoring the $\frac{dI}{dV}$ terms:

$$\frac{dI}{dV}\left[1 + \frac{R_S}{R_{SH}} + \frac{I_0 R_S}{V_T}\exp\left(\frac{V + IR_S}{V_T}\right)\right] = -\frac{I_0}{V_T}\exp\left(\frac{V + IR_S}{V_T}\right) - \frac{1}{R_{SH}}$$

A few simplifications can be made to this expression due to the short circuit condition. As $I = I_{SC}$, $V = 0$ and the value of R_S is small, the diode voltage V_D is also small compared to the thermal voltage V_T and multiplied with the nano-value of I_0, making the exponential terms in the expression:

$$I_0 \exp\left(\frac{V + IR_S}{V_T}\right) = I_0 \exp\left(\frac{I_{SC} R_S}{V_T}\right) \approx 0$$

It is also known that R_S is much smaller that R_{SH} and thus:

$$R_S << R_{SH} \rightarrow \frac{R_S}{R_{SH}} \approx 0$$

It follows then that the following terms can be eliminated:

$$\frac{dI}{dV}\left[1 + \cancel{\frac{R_S}{R_{SH}}} + \cancel{\frac{I_0 R_S}{V_T} \exp\left(\frac{V + IR_S}{V_T}\right)}\right] = -\cancel{\frac{I_0}{V_T} \exp\left(\frac{V + IR_S}{V_T}\right)} - \frac{1}{R_{SH}}$$

3. Series resistance

The derivation $\frac{dI}{dV}$ is a general expression and valid under any condition. To determine the series resistance R_S, $\frac{dI}{dV}$ is subjected to the open circuit conditions. Looking specifically at the diode current term $I_0 \exp\left(\frac{V + IR_s}{V_T}\right)$, the external current is zero making the diode voltage equal to the open current voltage $I_0 \exp\left(\frac{V_{OC}}{V_T}\right)$. There is no external current, therefore the entire photocurrent is equal to the short circuit current $I_{PV} = I_{SC}$, meaning that the entire diode current is equal to the short circuit current. Another approximation is with the small current flowing through the shunt resistance, but because the resistance is so large it is neglected. The derived expression is simplified to:

$$\frac{dI}{dV}\left[1 + R_S\left(\frac{1}{R_{SH}} + \frac{I_{SC}}{V_T}\right)\right] = -\left(\frac{1}{R_{SH}} + \frac{I_{SC}}{V_T}\right)$$

The expression for R_S is thus:

$$R_S = -\frac{dV}{dI} - \frac{1}{\left(\frac{1}{R_{SH}} + \frac{I_{SC}}{V_T}\right)}$$

As R_{SH} is very large, $\frac{1}{R_{SH}} << \frac{I_{SC}}{V_T}$, the expression is further simplified to express the series resistance.

4. System of non-linear equation

$$F_1 = I_0\left[\exp\left(\frac{qV_{OC}}{nN_skT}\right) - 1\right] - I_{SC} + \frac{V_{OC}}{R_{SH}} \tag{A.1}$$

$$F_2 = R_s + \frac{dV}{dI_{OC}} + \frac{1}{\frac{qI_0}{nN_skT}\exp\left(\frac{qV_{OC}}{nN_skT}\right)} \tag{A.2}$$

$$F_3 = I_0\left[\exp\left(\frac{q\left(V_{MP} + I_{MP}R_S\right)}{nN_skT}\right) - 1\right] + \frac{V_{MP} + I_{MP}R_S}{R_{SH}} + I_{MP} - I_{SC} \tag{A.3}$$

A.2 Operating cell temperature assessment

The values of the temperature coefficients of the Virtus II module are given in Table A.1 below (ReneSola, 2014).

Table A.1: Virtus II temperature coefficients

Temperature coefficient of V_{OC}	-0.3% /°C
Temperature coefficient of I_{SC}	0.04% /°C

The current temperature coefficient of most PV modules is generally low and has little to almost no effect on the photogenerated current at variating temperatures. When comparing the voltage coefficient of the Virtus II to PV modules used in other studies, like the Kyocera KC200GT solar module by Villalva et al. (2009), the Kyocera KC175GHT-2 module used by Lo Brano *et al.* (2010) or the Isofoton 75 panel used by Bouraiou *et al.* (2015), its voltage coefficient is significantly lower. This is assumed to be due to component level differences between the different brands.

Equation (A.4) below describes the influence of the voltage temperature coefficient on the open circuit voltage.

$$V_{OC} = V_{OC\_STC} + nT\ln\left(\frac{G}{G_{NOM}}\right) + K_V \Delta T \quad \text{(A.4)}$$

As the effect is studied at 1000W/m^2, making $\ln 1 = 0$, Equation (A.4) can be simplified to:

$$V_{OC} = V_{OC,STC} + K_V \left(T - T_{NOM}\right) \quad \text{(A.5)}$$

V_{OC_STC} is the open circuit voltage at STC. The extracted parameters n, I_0 and R_S are dependent of V_{OC} and must be recalculated by solving the system of non-linear equations. The operating temperatures 10°C, 50°C and 70°C were chosen to be evaluated against the standard 25°C.

The calculated values of the extracted parameters are listed in Table A.2 below.

Table A.2: Extracted parameters at different temperatures: Kv = -0.3%/°C

Operating cell temperature	Open circuit voltage, Voc [V]	Reverse saturation current, I_0 [A]	Diode ideality factor (n)	Series resistance, Rs [Ω]
10°C	44.845	9.53E-08	1.394938	0.060099
25°C	44.8	1.77E-08	1.212065	0.189366
50°C	44.725	7.98E-08	1.207316	0.004287
70°C	44.665	8.98E-08	1.142666	0.017231

The resulting IV and PV curves are plotted in Figure A.1 and Figure A.2 respectively below.

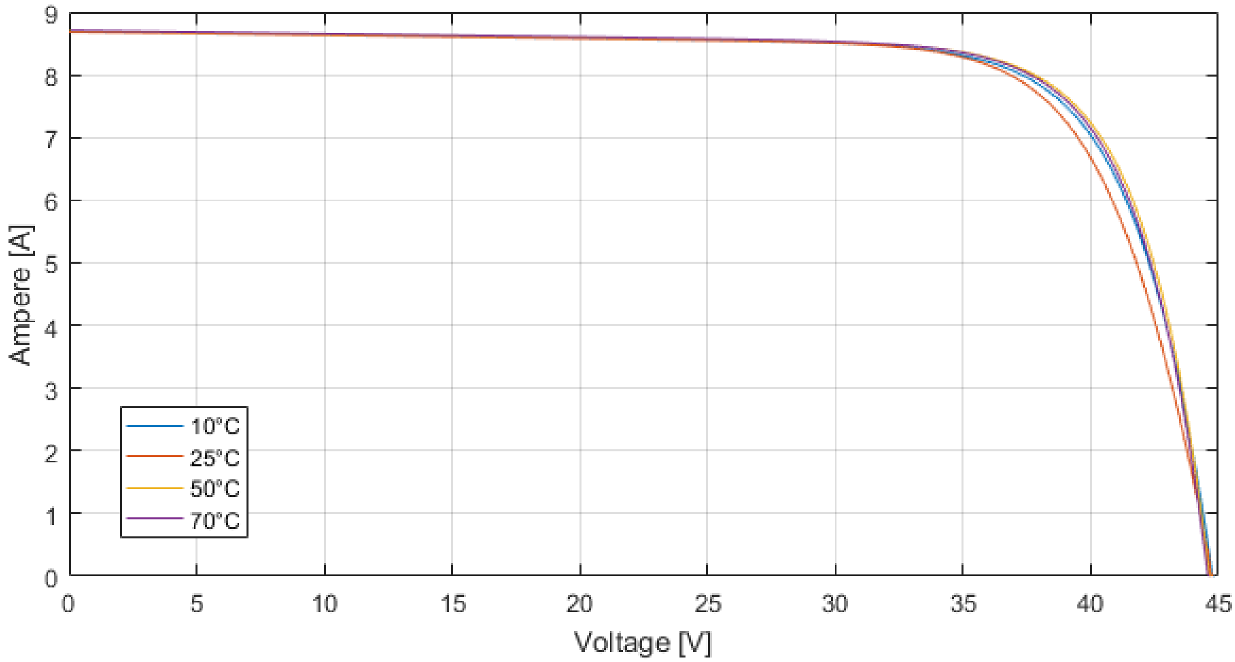

Figure A.1: Effect of temperature coefficient Kv = -0.3%/°C on IV curves

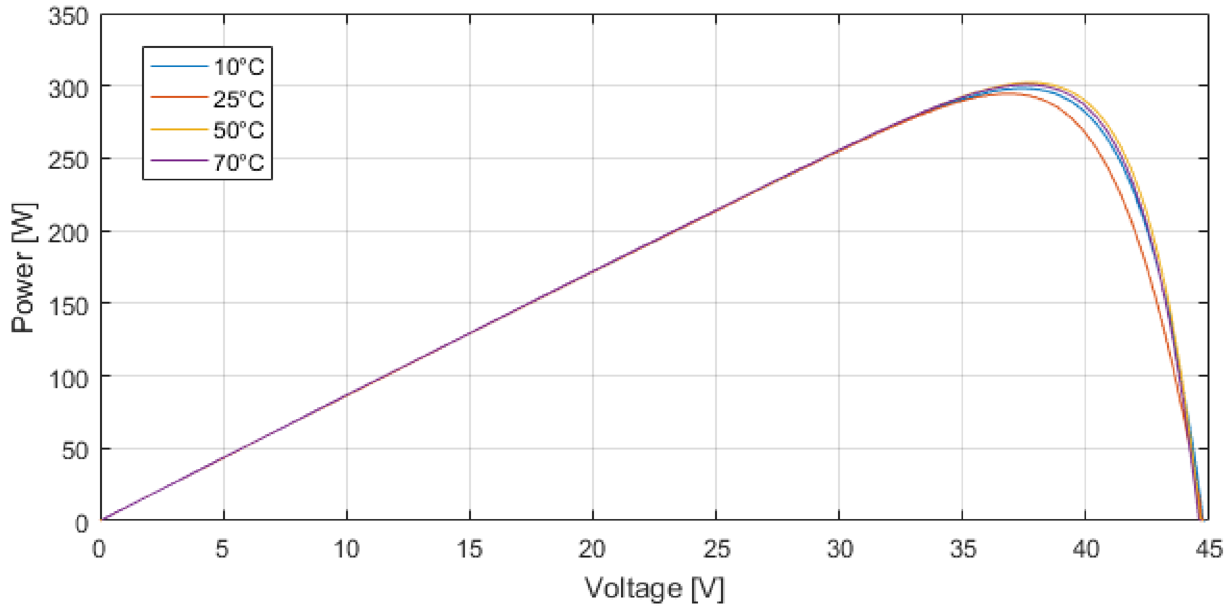

Figure A.2: Effect of temperature coefficient Kv = -0.3%/°C on PV curves

As found in literature, it is expected to see a clear difference in the IV curves of Figure A.1 as well as in the maximum power points indicated by Figure A.2 at different temperature. The reason for so little difference in the curves can be due to the significantly small value of K_V, which in turn then has a rather insignificant influence on V_{OC}. To prove this, the value of K_V is increased and the new values of V_{OC} are calculated and used to again extract the parameters, as listed in Table A.3 below.

Table A.3: Extracted parameters at different temperatures: Kv = -12.3%/°C

Operating cell temperature	Open circuit voltage, Voc [V]	Reverse saturation current, I_0 [A]	Diode ideality factor (n)	Series resistance, Rs [Ω]
10°C	46.645	2.88E-09	1.217916	0.187447
25°C	44.8	1.77E-08	1.212065	0.189366
50°C	41.725	0.000000149	1.165819	-0.073463
70°C	39.265	0.000000369	1.090233	-0.135170

The IV and PV curves subjected to a higher K_V value of -0.123ΔT, equal to that of a KC200GT module used by Villalva et al. (2009), are given in Figure A.3 and Figure A.4 respectively below.

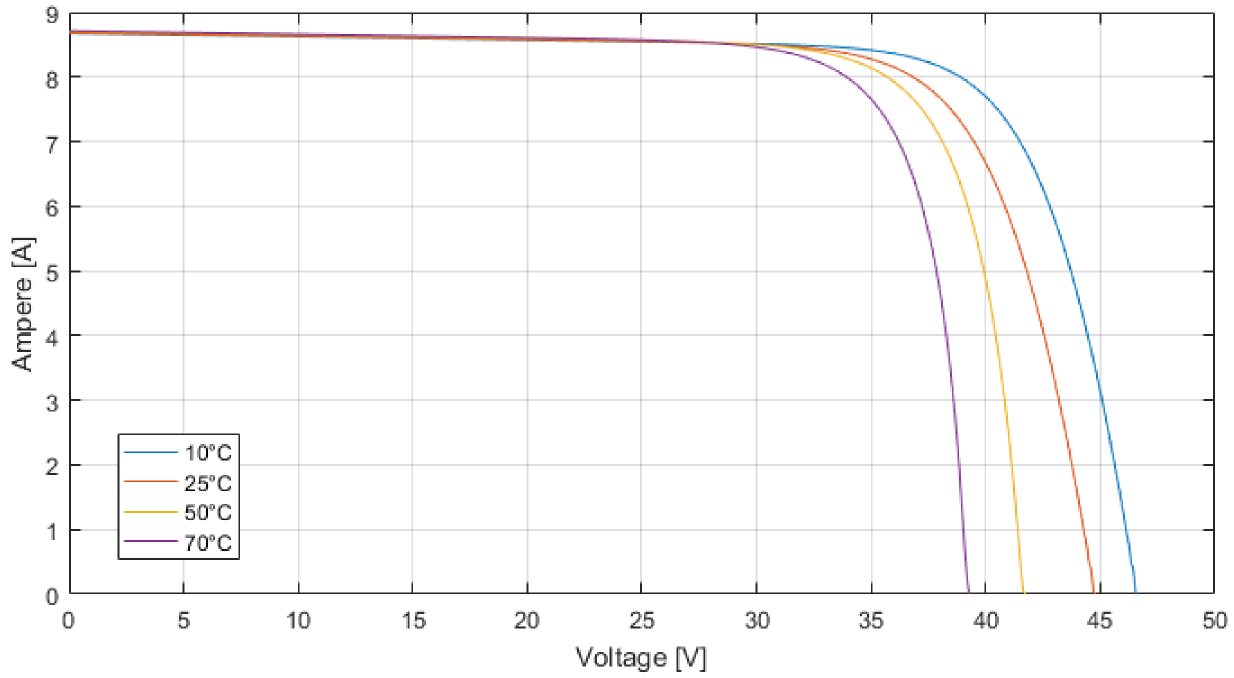

Figure A.3: Effect of temperature coefficient Kv = -12.3%/°C on IV curves

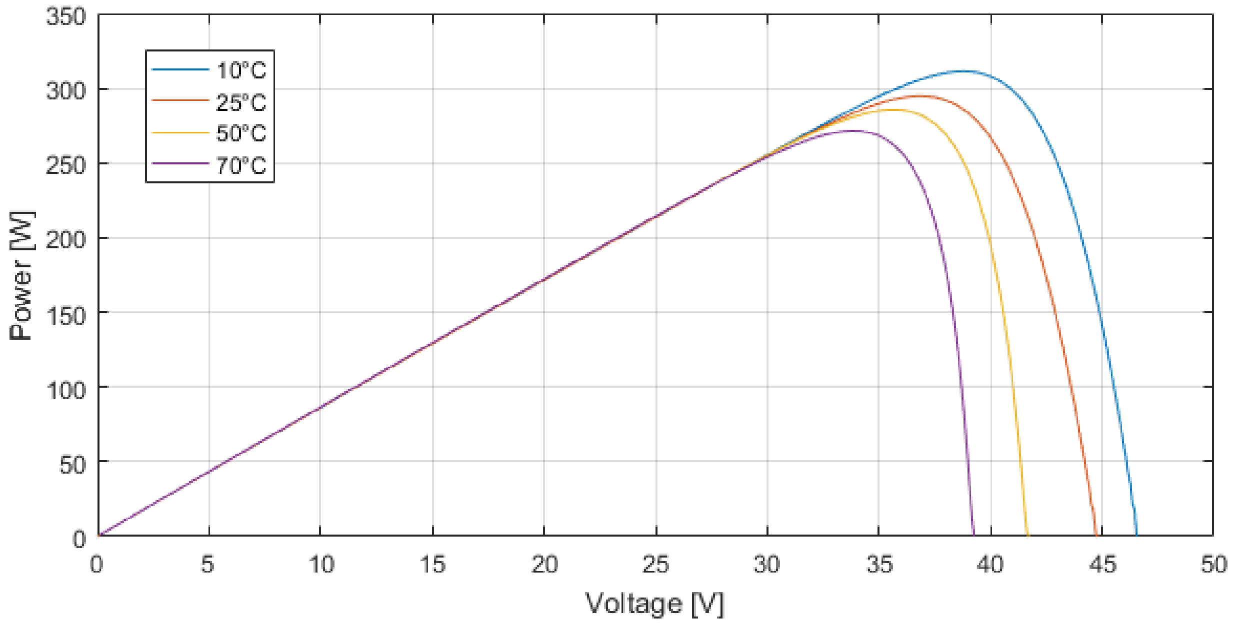

Figure A.4: Effect of temperature coefficient Kv = -12.3%/°C on PV curves

As the value of K_V is significantly larger, a clear difference in the value of V_{OC} and the plotted curves of Figure A.3 and Figure A.4 are observed. This proves that a sufficiently small voltage temperature coefficient has very little effect on the resulting IV characteristics, a fact rather obvious when considering its mathematical expression and similar prior statements of the current temperature coefficient. Although obvious, it proved that a possible simulation code error is not at fault for the insignificant differences in Figure A.1 and Figure A.2. The operating cell temperature assessment also validates the accuracy of the simulation model without considering the temperature coefficients.

A.3 PV simulation model procedure in Excel

The following example is given to explain the procedure of the simulation model in order to calculated the PV system power output per input irradiance. Firstly, a reference table is created for the data table function. The reference table equates the input solar irradiance to the variating irradiance G_{VAR} and the output intersect power P_{INT} calculated by the model.

Table A.4: Variable reference table

Data table variables	
Input - Solar Irradiance	= G_{VAR}
Output - Intercept power	= P_{INT}

The reference table is not entirely necessary as the input and output variables can simply be selected from the simulation model cells during the initiation of the data table function. It does however organize and simplify the selection process when working on multiple sheets in Excel. The data table on which the What-If Analysis will be done is then created and given by Table A.5 below.

Table A.5: What-If Analysis data table

		Column 1	Column 2
Row 1		Power per irradiance:	Output = Intercept power = P_{INT}
Row 2	Arbitrary irradiance 1:	235 W/m^2	
Row 3	Arbitrary irradiance 2:	482 W/m^2	
Row 4	Arbitrary irradiance 3:	679 W/m^2	

To generate the data, column 1 and 2 of the table is highlighted (as done in grey) and the data table function is selected. As the initial value of column 2 is P_{INT}, the data table function automatically knows that for each given input, P_{INT} must be calculated. After selecting the data table function, one must either provide a row or column input value. As the irradiance data expands down column 1, the column input value is equated to G_{VAR}. The What-If Analysis is done instantaneously and the output P_{INT} per irradiance is entered into column 2 by the analysis. The explanation will however give each P_{INT} value separately to explain how the simulation model is used by the analysis to calculated each P_{INT}.

The analysis takes the first arbitrary irradiance value of 235W/m^2 and enters it into the G_{VAR} cell of the simulation program. The program then generates the following IV and load curve, shown in Figure A.5 below.

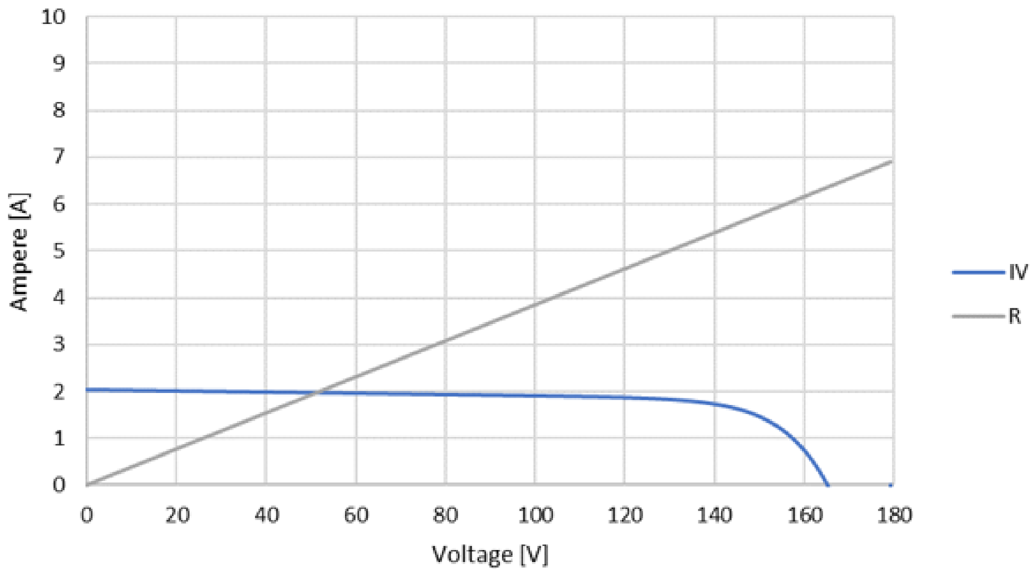

Figure A.5: IV & R curves at 235W/m^2

The intersect point of the curves is then determined and the voltage and current given as (51.2V; 1.9736A). The output power at the operating point is then calculated as 101.05W, and the P_{INT} cell of the program is updated to this value. The analysis then takes the P_{INT} value and enters it in column 2, next to the corresponding irradiance. With the first output entered by the analysis, Table A.5 is updated to:

		Column 1	Column 2
Row 1		Power per irradiance:	Output = Intercept power = P_{INT}
Row 2	Arbitrary irradiance 1:	235 W/m^2	101.05W
Row 3	Arbitrary irradiance 2:	482 W/m^2	
Row 4	Arbitrary irradiance 3:	679 W/m^2	

The analysis reiterated this procedure with the simulation program for each of the arbitrary irradiances inserted to column 1. The IV and load curves of 482W/m^2 and 679W/m^2 are given by Figure A.6 and Figure A.7 below respectively.

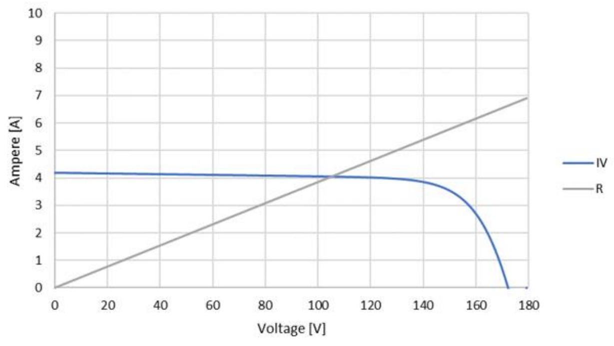

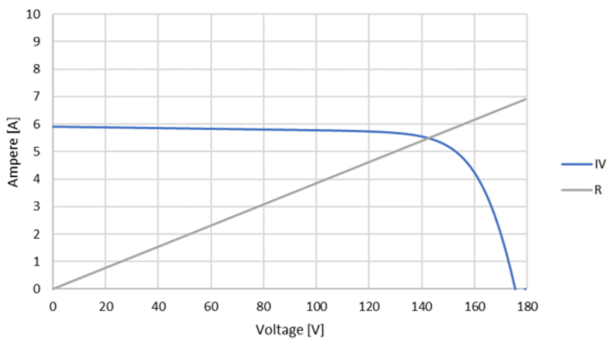

Figure A.6: IV & R curves at 482W/m^2

Figure A.7: IV & R curves at 679W/m^2

As each intersect point is determined and P_{INT} updated, the output values are entered into the data table to give:

		Column 1	Column 2
Row 1		Power per irradiance:	Output = Intercept power = P_{INT}
Row 2	Arbitrary irradiance 1:	235 W/m^2	101.05W
Row 3	Arbitrary irradiance 2:	482 W/m^2	425.54W
Row 4	Arbitrary irradiance 3:	679 W/m^2	780.34W

This concludes the example of the PV simulation model procedure in Excel.

A.4 PV cycle data of lowest and highest prediction error

- Lowest error – 0.02%

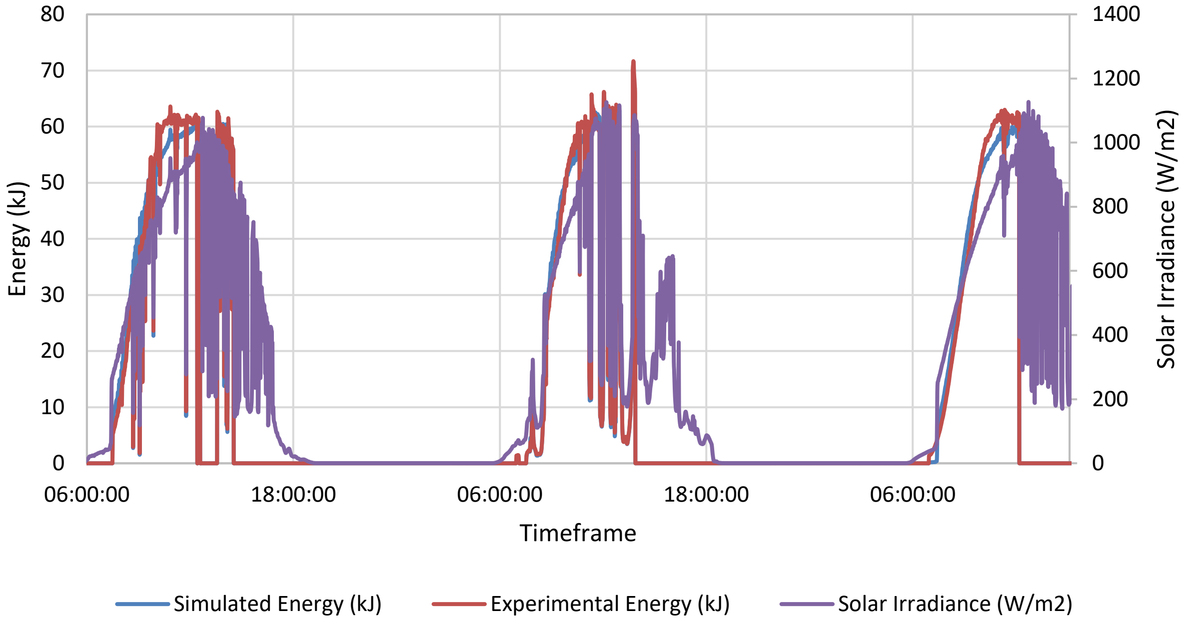

Figure A.8: PV simulation vs experimental results, 9 - 12 February

- Highest error – 4.08%

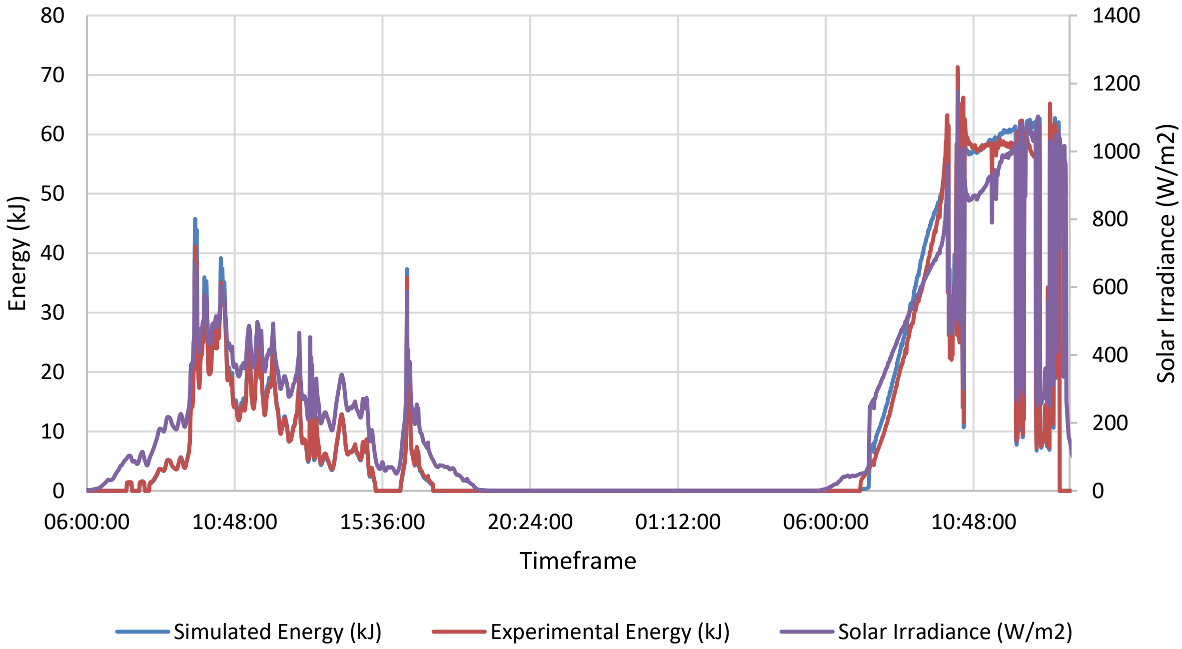

Figure A.9: PV simulation vs experimental results, 20 - 22 February

A.5 Prediction of PV simulation model

Figure A.10 below illustrates the actual energy delivered by the PV array.

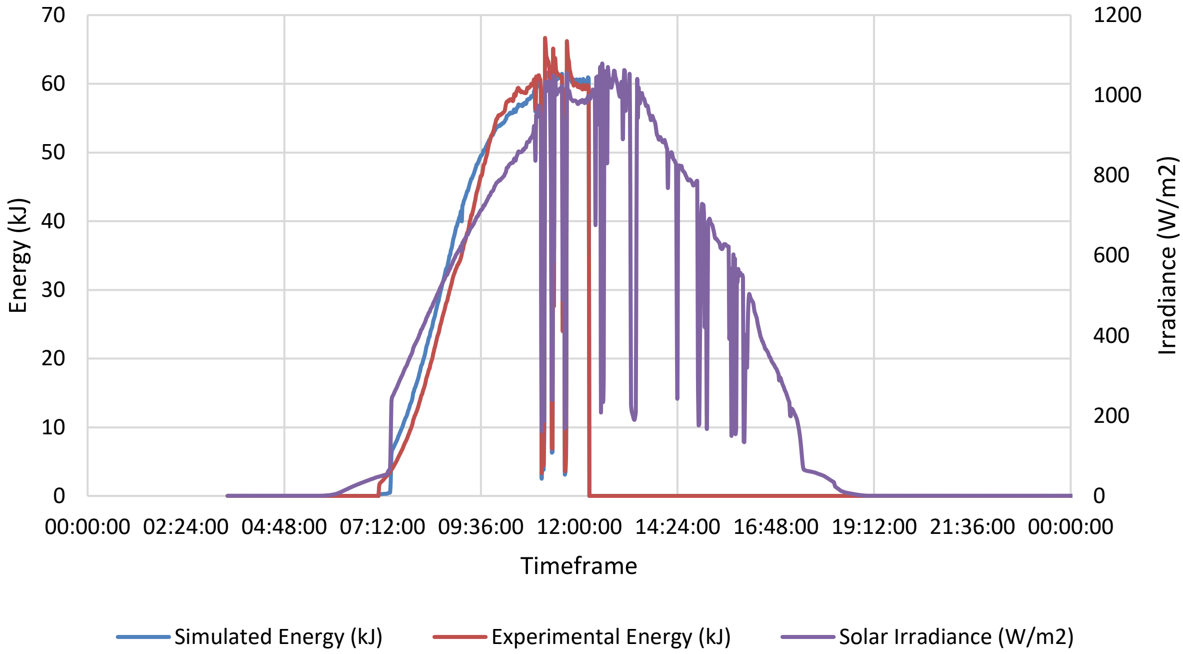

Figure A.10: PV simulation vs experimental results, 26 - 27 February

The focus for Figure A.10 is on the solar irradiance profile of the respective cycle. The profile reveals a sunny day with the irradiance level rising steadily as the sun rose, up to almost 900W/m^2 at approximately 11h00. It seems that partial shading took place, indicated by the sudden drop in irradiance, as the level ultimately rose to 1000W/m^2. After 13h00 a steady decline in irradiance is observed as the afternoon went by. The irradiance profile thus proved ample for PV energy generation.

Figure A.11 below is identical, only zoomed in to provide a detailed comparison of the experimental and simulated energies.

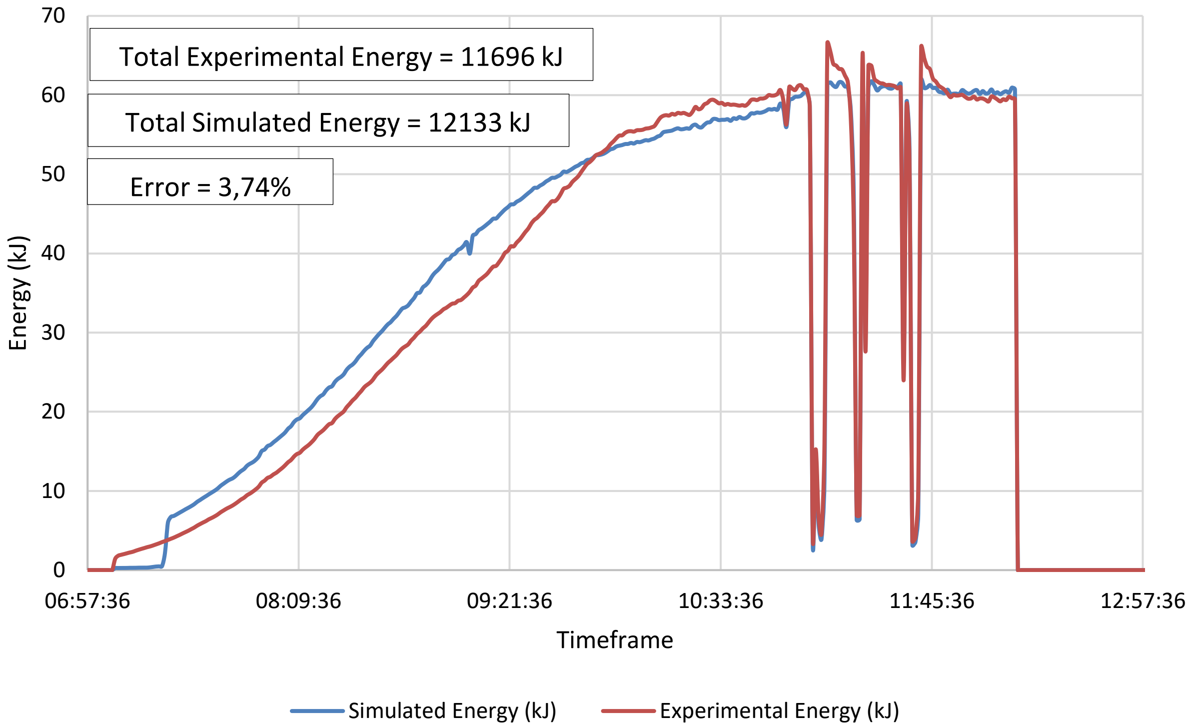

Figure A.11: PV simulation vs experimental results, 26 - 27 February, zoomed

Figure A.11 above illustrates the time period within the interval over which the water was heated. It is observed that the simulation model initially slightly overpredicted the energy generated by the PV system, however became more accurate as the solar irradiance increased. This was to be expected, as noted from the literature section, that the accuracy of the single diode model is linearly dependent on solar irradiance (Lo Brano *et al.*, 2010). The model could accurately deal with the sharp fluctuations observed in the experimental energy delivered, due to the fluctuation of irradiance. From 12h15 it is observed that no energy is delivered into the geyser, simply because the geyser reached its setpoint temperature. Over the cycle of the 26th – 27th February, 11696 kJ of energy was supplied to the geyser by the PV system. The simulation modelled an amount of 12133 kJ of energy over the cycle, resulting in an error of 3.74%. The error for this particular cycle is higher than the average simulation error over all the cycles.

A.6 PVWH control methodology

The different IF conditions and accompanying equations for the determination of the tank water temperature are as follows. Equation (A.6) below gives the standard current tank temperature.

$$Tt_i = Tt_{i-1} - \Delta T_{\dot{m}} + \Delta T_{PV} - \Delta T_{LOSS} \quad \text{(A.6)}$$

Without any conditions, the current tank temperature Tt_i is equal to the previous tank temperature Tt_{i-1} after being subjected to changes in temperature caused by the consumption, the heat input from the PV generated energy and the standing loss respectively.

Temperature condition 1: if the tank temperature is below the auxiliary setpoint temperature during any of the timed grid input hours:

$$Tt_i = Tt_{i-1} - \Delta T_{\dot{m}} - \Delta T_{LOSS} + \Delta T_{AUX} \quad \text{(A.7)}$$

Under this condition, ΔT_{PV} is removed and ΔT_{AUX} is added to form Equation (A.7 above. ΔT_{PV} is removed as there is no PV input during grid input hours. With the electric element having a maximum heating capacity of 14400kJ/h, the maximum increase in temperature for the 200L tank is 17.2°C. The conditions thus state that during the timed grid input hours, where the maximum capability of the heating element is insufficient to heat the water in the storage tank to 55°C, the temperature of the tank below 55° is determined.

Temperature condition 2: if the tank temperature is greater than the auxiliary setpoint temperature during any of the timed grid input hours:

$$Tt_i = Tt_{max\,AUX} \quad \text{(A.8)}$$

The condition states that if during the timed grid input hours, the maximum capability of the heating element is sufficient to heat the water in the storage tank to 55°C, the tank temperature is simply set equal to 55°C. The actual increase in temperature that the heating element supplied will be determined when determining the amount of auxiliary energy utilized from the grid, which will be discussed hereafter.

The final tank temperature condition is: if the tank temperature is greater or equal to the PV setpoint temperature:

$$Tt_i = Tt_{maxPV} \quad \text{(A.9)}$$

This condition states that if the heat input of the PV generated energy is sufficient to heat the water in the storage tank equal to or greater than 65°C during solar time, that the water is simply heated to 65°C.

With the temperature of the water in the storage tank known for the given conditions, the amount of auxiliary energy utilized in order to provide the thermal energy required to heat the water Q_{WATER} can be determined. The thermal energy required is also determined by IF statements.

Firstly, if the previous tank temperature plus the change in temperature due to the auxiliary energy input is below the auxiliary setpoint temperature, at either first hour of the timed morning and evening grid input hours:

$$Q_{WATER} = 14400kJ \tag{A.10}$$

The condition for Equation (A.10) states that if, during the first of the timed morning and evening grid input hours, the difference between Tt_i and Tt_{i-1} is greater than ΔT_{AUX}, the maximum heating capacity of the electric water heater was utilized for the whole hour. Secondly:

Energy condition 2: if the tank temperature is equal to the auxiliary setpoint temperature during any of the timed grid input hours:

$$Q_{WATER} = Vt \times c_p \times \left(Tt_{max\,Aux} - \left(Tt_{max\,Aux} - \Delta T_{\dot{m}} - \Delta T_{LOSS}\right)\right) \tag{A.11}$$

The second condition states that if the tank temperature is equal to 55°C during any of the of timed grid input hours, the amount of thermal energy required is determined by the difference in temperature due to the consumption and standing loss of the current hour. Lastly, if the tank temperature is greater than the auxiliary setpoint temperature during the timed evening grid input hours:

$$Q_{WATER} = 0kJ \tag{A.12}$$

The final condition applies if the PV generated energy was more than sufficient in heating the water during solar time and no auxiliary grid input during either of the timed evening hours is required. If all three conditions are false, no auxiliary energy was utilized.

ANNEXURE B

B.1 HPWH control methodology

In the case of HPWH, the tank temperature is only dependent on the change in temperature due to consumption $\Delta T_{\dot{m}}$ and the change in temperature due to the standing loss ΔT_{LOSS}, given by Equations (2.18) and (2.19) respectively. The different IF conditions and accompanying equations for the determination of the tank water temperature are as follows. Equation (B.1) below gives the standard tank temperature.

$$Tt_i = Tt_{i-1} - \Delta T_{\dot{m}} - \Delta T_{LOSS} \quad \text{(B.1)}$$

Without any IF conditions, the current tank temperature Tt_i is equal to the previous tank temperature Tt_{i-1} after being subjected to changes in temperature caused solely by the consumption and standing loss respectively. There is only one IF condition in the determination of the tank temperature for HPWH. If the tank temperature is below or equal to its minimum setpoint temperature ($Tti <= Tt_{min}$), then:

$$Tt_i = Tt_{max} \quad \text{(B.2)}$$

The accompanying Equation (B.2) of the condition above states that if the tank temperature Tt_i reaches the minimum temperature setpoint, it is set to the maximum temperature setpoint. The amount of thermal energy required to heat the water between its two setpoints is similar to Equation (A.11) and again given by the IF condition of Equation (B.3) below.

If the tank temperature is equal to its maximum setpoint temperature:

$$Q_{WATER} = Vt \times c_p \times \left(Tt_{max} - \left(Tt_{max} - \Delta T_{\dot{m}} - \Delta T_{LOSS}\right)\right) \quad \text{(B.3)}$$

The amount of thermal energy required is thus determined by the difference in temperature due to the consumption and standing loss, multiplied by the volume of the tank Vt and specific heat of the water c_p. The values of Vt and c_p have been listed and explained in Table 1.2. If the IF condition for Equation (B.3) is false, Q_{WATER} is simply 0.

ANNEXURE C

C.1 Biogas

Biogas is produced through the process of anaerobic digestion in a biodigester. Anaerobic digestion is the natural decomposition of organic material in the absence of oxygen (Greben & Oelofse, 2009:678). Organic material generally refer to either human waste, livestock dung or food waste (Msibi & Kornelius, 2017:1). The amount of biogas yield is dependent on the composition of the organic material (Okudoh *et al.*, 2014:1037). Biogas comprises of methane, carbon dioxide and small traces of hydrogen, hydrogen sulphide and ammonia (Greben & Oelofse, 2009:678). Methane is the most sought after component in biogas and accounts for more than 60% thereof (Okudoh *et al.*, 2014:1036). Biogas has a calorific value of 20 MJ/m^3 and efficiency of 55% (Msibi & Kornelius, 2017:3). Roughly 1m^3 of biogas is required to produce 6kWh units of energy (Mutungwazi et al., 2018:173).

Although South Africa has potential for the implementation of biogas as a source of renewable energy, it is lacking in comparison to the rest of the world (Mukumbaet al., 2016:59). The high capital cost of a biodigester (ZAR 22,743.00 as stated by Smith et al. in 2014:354) is only one of the challenges facing the implementation of biogas (Mukumba et al., 2016:61). Other challenges are summarized as ignorance of operation, lack of construction skills and the availability of organic material (Mutungwazi et al., 2018:174). Research of biogas technology in the South African context is also scant (Rasimphi & Tinarwo, 2020:2). Biogas in South Africa is mainly used for cooking and heating purposes in rural areas (Greben & Oelofse, 2009:679; Smith et al., 2014:352; Mukumba et al., 2016:59; Mutungwazi et al., 2018:172; Rasimphi & Tinarwo, 2020:2).

Out of a matter of interest, the efficiency of biogas and natural gas for water heating was experimentally approximated. Methane was utilized as a substitute for natural gas and biogas, as it represents 90% and 65% of the total gas volumes respectively (Swedish Gas Technology Center Ltd, 2012:7). The effect of methane on the heater efficiency was also determined. The linear energy relationship of the gas water heater, using methane, is presented in Figure C.1 below.

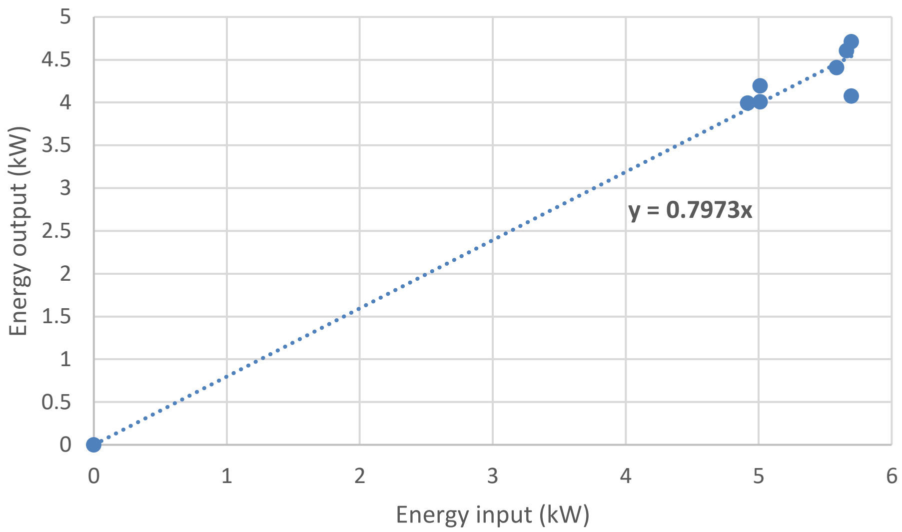

Figure C.1: Linear energy relationship of the Bosch Optiflow (methane)

An efficiency of 80% was achieved with the use of methane, 5% lower than with propane gas. Figure C.2 below illustrated the relationship between the amount of heat supplied and the flow rate of methane.

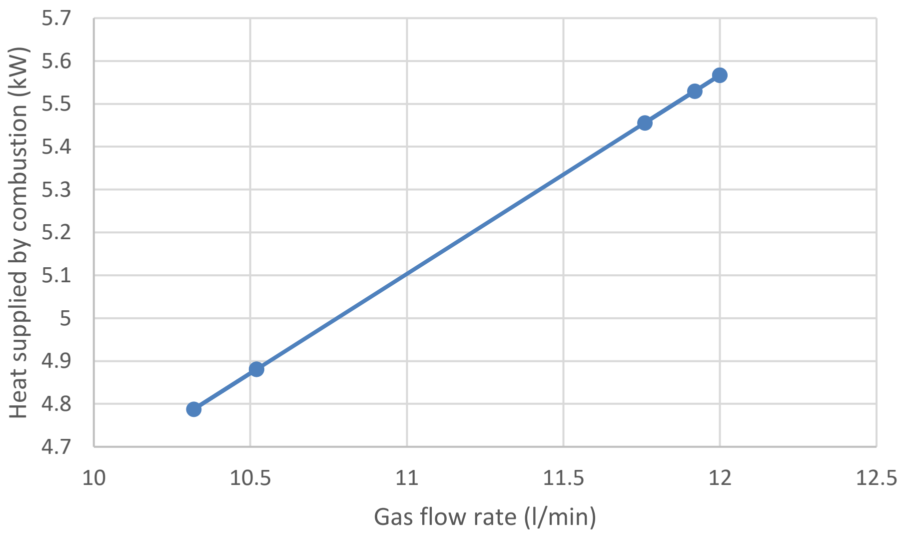

Figure C.2: Relationship between gas flow rate and combustion energy (methane)

A comparison between the gas flow rate required for the amount of heat supplied by combustion between propane and methane is presented in Figure C.3 below.

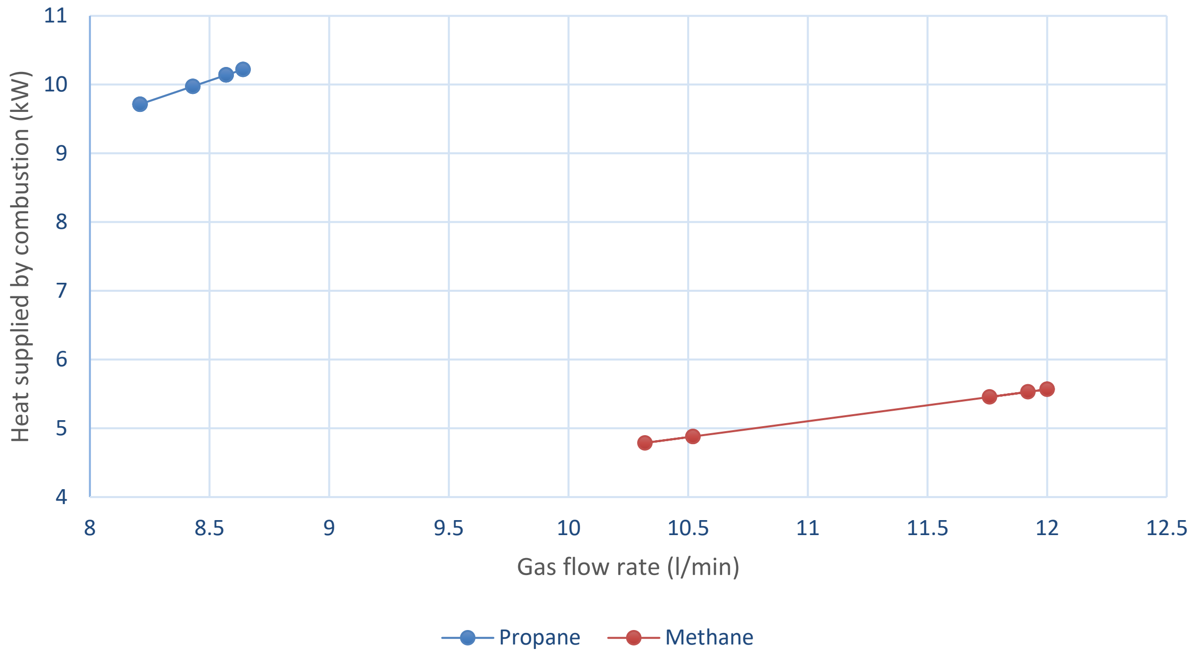

Figure C.3: Comparison of GWH with propane and methane gas

Roughly 30% more methane is required to deliver about half the amount of heat supplied by propane. The effectiveness of domestic water heating using biogas is thus questionable as it has an even lower energy content than methane.

C.2 GWH experimental procedure data

Table C.1: Steady state operational points of the Optiflow geyser

		Water outlet temperature [°C]			
		40	45	50	55
Water flow rate [l/min]	3,2				
	4				✗
	4,8			✗	
	5,6		✗		
	6,4		✗		
	7,2				
	8	✗			
	8,8	✗			
	9,6				

Table C.2: GWH test data

Test	Water flow rate (l/min)	Propane flow rate (l/min)	Inlet temperature (°C)	Outlet temperature (°C)
1	8	8.64	26.21	40.65
2	5.6	8.64	24.29	45.13
3	4.16	8.43	24.01	54.2
4	4.8	8.43	23.91	50.08
5	6.4	8.21	24.2	43
6	8.8	8.21	24.04	38.58
7	4.96	8.57	23.68	49.14
8	8.32	8.21	23.69	38.99
9	4.16	8.57	23.58	53.38
10	7.84	8.57	23.39	39.33
11	5.44	8.57	23.35	46.2

C.3 GWH experimental evaluation

EES code:

Constant

$Cp_{water} = 4,184$ Specific heat of water J/gK

$R_{gas} = 8,314$ Universal gas constant J/molK

Pressure

$P_{prop} = 87$ Propane pressure measured kPa

$P_{conv} = 101,3$ Propane pressure on chart for conversion kPa

Temperature

$T_{prop} = 25 + 273,15$ Propane temperature measured K

$T_{conv} = 20 + 273,15$ Propane temperature on chart for conversion K

$$T_{CO2} = \frac{31 + 273,15 + 78 + 273,15}{2}$$ Combustion product temperature measured K

$T_{N2} = T_{CO2}$ K

$T_{H2O} = T_{CO2}$ K

Density

$\rho_{prop} = \rho\left(Propane ; T = T_{prop} ; P = P_{prop}\right)$ Density of propane kg/m^3

$\rho_{conv} = \rho\left(Propane ; T = T_{conv} ; P = P_{conv}\right)$ Density of propane on chart for conversion kg/m^3

Enthalpy

$h_{C3H8} = \mathbf{h}\left(C3H8 ; T = T_{prop}\right)$ Enthalpy of propane kJ/kg

$h_{CO2} = \mathbf{h}\left(CO2 ; T = T_{CO2}\right)$ Enthalpy of carbon dioxide kJ/kg

$h_{H2O} = \mathbf{h}\left(h2o ; T = T_{H2O}\right)$ Enthalpy of water$_g$ kJ/kg

$h_{N2} = \mathbf{h}\left(N2 ; T = T_{N2}\right)$ Enthalpy of nitrogen kJ/kg

Molar mass

m_{C3H8} = **MolarMass** (C3H8) Molar mass of propane g/mol

m_{CO2} = **MolarMass** (CO2) Molar mass of carbon dioxide g/mol

m_{H2O} = **MolarMass** (h2o) Molar mass of water$_g$ g/mol

m_{N2} = **MolarMass** (N2) Molar mass of nitrogen g/mol

..............................ENERGY IN.............................

..........POWER USED BY GEYSER COMBUSTION FAN - P_fan..........

$V_{ac} = 230$ V

$A_{ac} = 0{,}565$ A

$$P_{fan} = \frac{V_{ac} \cdot A_{ac}}{1000} \quad \text{kW}$$

..........HEAT SUPPLIED BY PROPANE GAS - Q_comb..........

Lookup gas flow rate from input data table and convert units

$$\dot{V}_{prop;i} = \frac{\textbf{Lookup}\,(\text{'Data'};\ i;\ \text{'Flow}_{gas}\text{'})}{1000 \cdot 60} \qquad (\text{for } i = 1 \text{ to } 11) \quad m^3/s$$

Convert gas flow rate from measuring chart to actual value

$$\dot{V}_{conv;i} = \dot{V}_{prop;i} \cdot \sqrt{\frac{\rho_{conv}}{\rho_{prop}} \cdot \frac{P_{prop}}{P_{conv}} \cdot \frac{T_{conv}}{T_{prop}}} \qquad (\text{for } i = 1 \text{ to } 11)$$

Determine mole of gas used from gas flow rate

$$n_{prop;i} = \frac{P_{prop} \cdot \dot{V}_{conv;i}}{R_{gas} \cdot T_{prop}} \qquad (\text{for } i = 1 \text{ to } 11)$$

ASSUME COMPLETE COMBUSTION

C3H8 + 5O2 + (395/21)N2 --> 3CO2 + 4H2O + (395/21)N2

$n_{C3H8;i} = n_{prop;i}$ (for i = 1 to 11)

$n_{CO2;i} = 3 \cdot n_{C3H8;i}$ (for i = 1 to 11)

$n_{H2O;i} = 4 \cdot n_{C3H8;i}$ (for i = 1 to 11)

$$n_{N2;i} = \frac{395}{21} \cdot n_{C3H8;i} \qquad (\text{for } i = 1 \text{ to } 11)$$

ENTHALPY OF FORMATION

$$HR_i = HP_i + Q_{comb;i} \quad \text{(for } i = 1 \text{ to } 11\text{)}$$

Enthalpy of the reactant

$$HR_i = n_{C3H8;i} \cdot h_{C3H8} \cdot m_{C3H8} \quad \text{(for } i = 1 \text{ to } 11\text{)}$$

Enthalply of the products

$$HP_i = n_{CO2;i} \cdot h_{CO2} \cdot m_{CO2} + n_{H2O;i} \cdot h_{H2O} \cdot m_{H2O} + n_{N2;i} \cdot h_{N2} \cdot m_{N2} \quad \text{(for } i = 1 \text{ to } 11\text{)}$$

..............................ENERGY OUT..............................

..........HEAT TRANSFERRED INTO WATER - Q_water..........

Lookup water flow rate from input data table and convert units

$$\dot{m}_{water;i} = \frac{\textbf{Lookup}\left('Data';\ i;\ 'Flow_{water}'\right)}{60} \quad \text{(for } i = 1 \text{ to } 11\text{)} \quad \text{kg/s}$$

Lookup water inlet temperature from input data table

$$T_{water;in;i} = \textbf{Lookup}\left('Data';\ i;\ 'T_{water;in}'\right) \quad \text{(for } i = 1 \text{ to } 11\text{)}$$

Lookup water outlet temperature from input data table

$$T_{water;out;i} = \textbf{Lookup}\left('Data';\ i;\ 'T_{water;out}'\right) \quad \text{(for } i = 1 \text{ to } 11\text{)}$$

$$Q_{water;i} = \dot{m}_{water;i} \cdot Cp_{water} \cdot \left(T_{water;out;i} - T_{water;in;i}\right) \quad \text{(for } i = 1 \text{ to } 11\text{)}$$

..............................CONSERVATION OF ENERGY..............................

Combustion of gas + combustion fan = heat supplied to water + heat lost

$$Energy_{in;i} = P_{fan} + Q_{comb;i} \quad \text{(for } i = 1 \text{ to } 11\text{)}$$

$$Energy_{out;i} = Q_{water;i} \quad \text{(for } i = 1 \text{ to } 11\text{)}$$

$$Loss_i = Energy_{in;i} - Energy_{out;i} \quad \text{(for } i = 1 \text{ to } 11\text{)}$$

..............................COMBUSTION EFFICIENCY..............................

$$\eta_i = \frac{Energy_{out;i}}{Energy_{in;i}} \cdot 100 \quad \text{(for } i = 1 \text{ to } 11\text{)}$$

EES results

Density			
ρ_{prop}	Density of propane at measured T&P	0.8089	kg/m^3
ρ_{conv}	Density of propane at conversion T&P	0.9505	kg/m^3
Enthalpy			
h_{C3H8}	Enthalpy of propane	-1751	kJ/kg
h_{CO2}	Enthalpy of carbon dioxide	-8646	kJ/kg
h_{H2O}	Enthalpy of water$_g$	-12838	kJ/kg
h_{N2}	Enthalpy of nitrogen	318.6	kJ/kg
Molar mass			
M_{C3H8}	Molar mass of propane	44.1	g/mole
M_{CO2}	Molar mass of carbon dioxide	44.01	g/mole
M_{H2O}	Molar mass of water$_g$	18.02	g/mole
M_{N2}	Molar mass of nitrogen	28.01	g/mole

..............................ENERGY IN..............................

..........POWER USED BY GEYSER COMBUSTION FAN - P_fan..........

Power used by geyser combustion fan			
P_{fan}	Fan power	129.95	W

..........HEAT SUPPLIED BY PROPANE GAS - Q_comb..........

Test	$\dot{V}_{propane}$ - Volumetric flow rate of propane (m^3/s)	$\dot{n}_{propane}$ - Molar flow rate of propane (mole/s)	HR - Enthalpy of reactant
1	0.0001442	0.000005062	-0.5299
2	0.0001442	0.000005062	-0.5299
3	0.0001407	0.000004939	-0.517
4	0.0001407	0.000004939	-0.517
5	0.0001371	0.00000481	-0.5035
6	0.0001371	0.00000481	-0.5035
7	0.0001431	0.000005021	-0.5256
8	0.0001371	0.00000481	-0.5035
9	0.0001431	0.000005021	-0.5256
10	0.0001431	0.000005021	-0.5256
11	0.0001431	0.000005021	-0.5256

Test	$\dot{n}_{CO2}$ - Molar flow rate of carbon dioxide (mole/s)	$\dot{n}_{H2O}$ - Molar flow rate of water$_g$ (mole/s)	$\dot{n}_{N2}$ - Molar flow rate of nitrogen (mole/s)	HP - Enthalpy of products
1	0.00001519	0.00002025	0.00009522	-10.75
2	0.00001519	0.00002025	0.00009522	-10.75
3	0.00001482	0.00001976	0.0000929	-10.49
4	0.00001482	0.00001976	0.0000929	-10.49
5	0.00001443	0.00001924	0.00009048	-10.22
6	0.00001443	0.00001924	0.00009048	-10.22
7	0.00001506	0.00002008	0.00009445	-10.67
8	0.00001443	0.00001924	0.00009048	-10.22
9	0.00001506	0.00002008	0.00009445	-10.67
10	0.00001506	0.00002008	0.00009445	-10.67
11	0.00001506	0.00002008	0.00009445	-10.67

Test	$\dot{Q}_{comb}$ - Heat supplied by propane (kW)	E_{in} - Total energy into system (kW)
1	10.22	10.35
2	10.22	10.35
3	9.975	10.11
4	9.975	10.11
5	9.715	9.845
6	9.715	9.845
7	10.14	10.27
8	9.715	9.845
9	10.14	10.27
10	10.14	10.27
11	10.14	10.27

..............................ENERGY OUT..............................

..........HEAT TRANSFERRED INTO WATER - Q_water..........

Test	$\dot{m}_{water}$ - Mass flow rate of water (kg/s)	Q_{water} - Heat transferred into water (kW)	E_{out} - Total energy out of system (kW)	E_{loss} - Energy lost (kW)
1	0.1333	8.056	8.056	2.298
2	0.09333	8.138	8.138	2.215
3	0.06933	8.758	8.758	1.347
4	0.08	8.76	8.76	1.345
5	0.1067	8.39	8.39	1.454
6	0.1467	8.923	8.923	0.9223
7	0.08267	8.806	8.806	1.456
8	0.1387	8.877	8.877	0.968
9	0.06933	8.645	8.645	1.626
10	0.1307	8.715	8.715	1.556
11	0.09067	8.668	8.668	1.603

..............................COMBUSTION EFFICIENCY..............................

Test	η - Combustion efficiency of the heater (%)
1	77.8
2	78.6
3	86.67
4	86.69
5	85.23
6	90.63
7	85.74
8	90.17
9	84.17
10	84.85
11	84.4

ANNEXURE D

D.1 Techno-economical comparison

The results of the respective chapters are listed in Table D.1 below.

Table D.1: Comparison of results

Water heating technology	Captical cost (VAT & Inst incl)			Average capital cost	Annual operational costs	Annual savings	Payback period (Years)	kWh/year required from grid	Grid input saved
	Supplier A	Supplier B	Supplier C						
Photovoltaic	R22 295.00	R22 425.00	R25 571.98	R23 430.66	R 2 921.86	R 5 010.88	4.68	1328.12	63.17%
Flat plate	R14 264.40	R20 238.92		R17 251.66	R 3 356.81	R 4 575.93	3.77	1525.82	57.68%
Evacuated tubes	R18 049.05	R25 739.92		R21 894.49	R 3 327.28	R 4 605.46	4.75	1512.40	58.06%
Heat pump	R22 871.00	R23 976.15		R23 423.58	R 2 879.27	R 5 053.47	4.64	1308.76	63.70%
Gas	R16 126.25			R16 126.25	R 8 673.55	-R 740.81	-	10.65	99.70%
Baseline electric resistance					R 7 932.74			3605.79	0.00%